2021-06-21

Bottom-Up Fabrication and Characterization of DNA Origami-Templated Electronic Nanomaterials

Basu Ram Aryal
Brigham Young University

Bottom-Up Fabrication and Characterization of DNA Origami-Templated Electronic Nanomaterials

Basu Ram Aryal

A thesis submitted to the faculty of
Brigham Young University
in partial fulfillment of the requirements for the degree of

Doctor of Philosophy

Adam T. Woolley, Chair
John N. Harb
Robert C. Davis
Brian F. Woodfield

Department of Chemistry and Biochemistry
Brigham Young University

ABSTRACT

Bottom-Up Fabrication and Characterization of DNA Origami-Templated Electronic Nanomaterials

Basu Ram Aryal
Department of Chemistry and Biochemistry, BYU
Doctor of Philosophy

This work presents the bottom-up fabrication of DNA origami-assembled metal nanowires and metal-semiconductor junctions, and their electrical characterization. Integration of metal and semiconductor nanomaterials into prescribed sites on self-assembled DNA origami has facilitated the fabrication of electronic nanomaterials, whereas use of conventional tools in their characterization combines bottom-up and top-down technologies. To expand the contemporary DNA-based nanofabrication into nanoelectronics, I performed site-specific metallization of DNA origami to create arbitrarily arranged gold nanostructures. I reported improved yields and conductivity measurements for Au nanowires created on DNA origami tile substrates. I measured the conductivity of C-shaped Au nanowires created on DNA tiles (~130 nm long, 10 nm diameter, and 40 nm spacing between measurement points) with a four-point measurement technique which revealed the resistivity of the gold nanowires was as low as 4.24×10^{-5} Ω m. Next, I fabricated DNA origami-templated metal-semiconductor junctions and performed electrical characterization. Au and Te nanorods were attached to DNA origami in an alternating fashion. Electroless gold plating was used to create nanoscale metal—semiconductor interfaces by filling the gaps between Au and Te nanorods. Two-point electrical characterization indicated that the Au—Te—Au junctions were electrically connected, with non-linear current—voltage curves. Finally, I formed metal-semiconductor nanowires on DNA origami by annealing polymer-encased nanorods. Polymer-coated Au and Te nanorods pre-attached to ribbon-shaped DNA origami were annealed at 170 °C for 2 min. Gold migration occurred onto Te nanorods during annealing and established electrically continuous interfaces to give Au/Te nanowires. Electrical characterization of these Au/Te/Au assemblies revealed both nonlinear current-voltage curves and linear plots that are explained. The creation of electronic nanomaterials such as metal nanowires and metal-semiconductor junctions on DNA origami with multiple techniques advances DNA nanofabrication as a promising path toward future bottom-up fabrication of nanoelectronics.

Keywords: DNA origami, nanowires, metal-semiconductor junctions, electrical characterization

ACKNOWLEDGMENTS

I would like to express my deep appreciation to my advisor, Prof. Adam T Woolley for his continuous inspiration and support to accomplish my academic goals. Without his persistent guidance and encouragement, this dissertation would be impossible. I am grateful to my committee members, Prof. John N Harb, Prof. Robert C Davis, and Prof. Brian F Woodfield for their invaluable guidance and suggestions on my research work. I never forget loving Janet Fonoimoana, Graduate Coordinator–Chemistry Department, BYU, for her immense guidance in the Ph.D. enrollment process. I would like to thank the National Science Foundation (NSF) for providing funding to me and my work. Also, I acknowledge the BYU Department of Chemistry and Biochemistry for a Roland K. Robins Graduate Research Fellowship.

I want to express my gratitude to my family members for their uninterrupted support regardless of my family's ups and downs. My mother, Kanchhi Maya Aryal, father, Badri Bahadur Aryal, and wife, Sarita Neupane Aryal, dreamed of me having a high level of education. I believe that I have made them proud. My older brothers, including Raghunath, Raj Kumar, Bishnu, Jayaram, Prashuram, Kalpana, and others always supported my academic career.

Finally, my fellow friends, including Dr. Shyam Raj Pokhrel, Dr. Umesh Chiluwal, and Dr. Raju Baral inspired me to join the Ph.D. program. I express my gratitude to them.

TABLE OF CONTENTS

LIST OF TABLES

LIST OF FIGURES

CHAPTER 1: INTRODUCTION*

1.1 NANOFABRICATION APPROACHES

Nanofabrication follows two completely opposite pathways to construct nanostructures. The most widely used one is a top-down process in which bulky materials are miniaturized into nanofeatures by using technologies such as photolithography, thin film growth, and etching. In contrast, the emerging bottom-up approach assembles atoms and molecules to create structures with nanoscale dimensions. For example, the growth of all living creatures and the formation of some nonliving materials under controlled conditions occur through the self-arrangement of multiple atoms or biomolecules. Some nanofabrication methods highlight combinations of both top-down and bottom-up processes.

1.1.1 Top-down Nanofabrication

Top-down methods transform approximately centimeter-sized materials into nanostructures using advanced technologies. Contemporary nanofabrication heavily depends on top-down technologies. For example, lithographic nanopatterning techniques are employed to fabricate integrated circuits. Particularly, photolithography uses short-wavelength light sources to transfer desired patterns onto substrates. To obtain high-resolution structures, short-wavelength optical lithography with extreme ultraviolet or X-rays is used.[1] Other lithographic printing techniques such as electron beam lithography and mechanical printing techniques (stamping and imprinting) are also able to manufacture structures at sub-100 nm levels.[2, 3] Despite some critical

* Sections 1.6, 1.7 and 1.9 of this chapter are adapted with permission from Pang, C.; Aryal, B. R.; Ranasinghe, D. R.; Westover, W. R.; Ehlert, A. E. F.; Harb, J. N.; Davis, R. C.; Woolley, A. T. Bottom-up Fabrication of DNA-templated Nanomaterials and Their Characterization. *Nanomaterials* **2021** (submitted).

limitations, top-down techniques are currently the most reliable methods in manufacturing functional nanoscale devices.

1.1.2 Bottom-up Nanofabrication

The bottom-up approach utilizes chemical or physical driving forces working at the nanometer-regime to assemble atoms, molecules or other basic units into larger shapes. Different methods have been utilized in bottom-up nanofabrication to perform self-assembly of individual units. For example, solution-based nanoparticle or nanorod synthesis utilizes chemical reduction to convert precursor units such as ions or nuclei into a geometric shape. DNA-assisted nanofabrication is growing as an alternative bottom-up method which is expected to emerge as a high resolution, cost effective and minimum material consumption technology due to unique characteristics of DNA.

1.1.3 Benefits of Bottom-up Nanotechnology

Top-down nanofabrication depends on tools that are expensive and complex, and follows complicated procedures which demand highly skilled human resources to operate.[1] Furthermore, the process is associated with critical technological challenges at sub-10 nm levels, along with heavy investment including money and machinery.[1, 4] The fabrication process also takes a long time to complete, and the working environment must be extremely clean. On the other hand, bottom-up nanofabrication relies on self-assembly properties of the constructing materials (atoms, molecules, or molecular blocks) and reduces the use of costly tools in fabrication. The self-assembly properties are governed by intermolecular interactions such as electrostatic and Van der Waals forces.[4, 5] The self-assembly approach for nanofabrication can be simple, cheap and fast relative to conventional methods. Nanofabrication involving DNA, protein, and other biomolecules is gaining popularity because of their potential strengths to mitigate challenges

pertaining to top-down technology; however, the bottom-up approach still needs significant improvements in the areas such as defect reduction, precision, and alignment to be used in industrial manufacturing in the future.

1.2 NANOMATERIALS

Nanomaterials are the basis of nanoscience. The widely accepted definition of nanoparticles states that nanoparticles possess a size range between 1 nm and 100 nm.[6, 7] The only legal definition of nanoparticles, developed by the European Commission, is size-based and states that the particle size of more than 50% of the particles (in their number size distribution) must be 100 nm or lower.[6, 8] A weight-based approach has also been proposed for size distribution, because genuinely quantifying nanoscale materials is difficult. Nanomaterials are created naturally through various phenomena taking place in the environment, and they are also intentionally fabricated for functional purposes. These nanoscale materials are found in various forms such as nanoparticles, nanorods, nanowires and nanotubes (**Figure 1.1**).

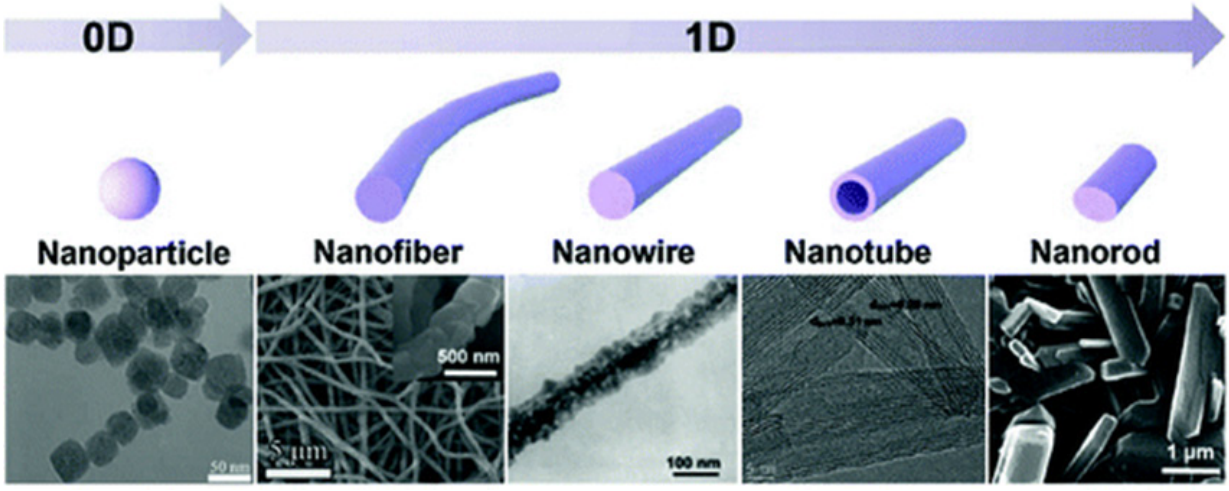

Figure 1.1 Various forms of nanomaterials.[9] Reprinted with permission from Springer International. Copyright 2016

1.2.1 Nanoparticles, Nanorods, Nanowires and Nanotubes

As previously stated, nanoparticles refer to nanoscopic particles with at least one of the dimensions less than 100 nm.[6] Various forms of nanoparticles include clusters, crystals, and powders whose surface area to volume ratio is very high. Particles at the nanoscale demonstrate unique electrical, magnetic, and optical properties compared to bulk materials. Elongated nanostructures such as nanorods, nanowires, nanofibers and nanotubes are considered 1D materials.[7] Nanorods typically have lengths between 10 nm to 120 nm.[10] The diameter of nanowires is typically a few tens of nanometers, without specifying a length. Nanotubes are similar to nanowires but have a hollow inside. Nanoplates and nanosheets are 2D structures. Many forms of nanomaterials are of great interest in the nano-technological world. Some applications of nanomaterials are in medicine, electronics, catalysis, sensors, cosmetics, fuel cells, and batteries.[10]

1.2.2 Semiconductors

Electrical properties of semiconductors lie between metals and insulators because the band gap, the energy spacing between the valence band and the conduction band, is small (**Figure 1.2**). In semiconductors, the small band gap allows electrons to jump from the valence band into the conduction band when excited with modest amounts of energy. The movement of electrons results in electrical conduction.[11] The intermediate electrical conductivity of semiconductor materials is exploited in the manufacturing of diverse electronic devices such as diodes, transistors, and complex integrated circuits with micro- and nanoscale dimensions. These devices are manufacturable and capable of controlling a wide range of current and voltages. Electronic devices rely on semiconductor components in which electrons or holes are responsible for carrying charge.[11, 12] The charge carriers can be manipulated by external factors such as temperature or light. Increasing temperature or shining radiation on intrinsic semiconductors can increase their

conductance. Electrical behavior of semiconductors can also be changed through other factors such as magnetic fields or impuritities.[11, 12] The impurities used to alter semiconductor electrical properties are called dopants.

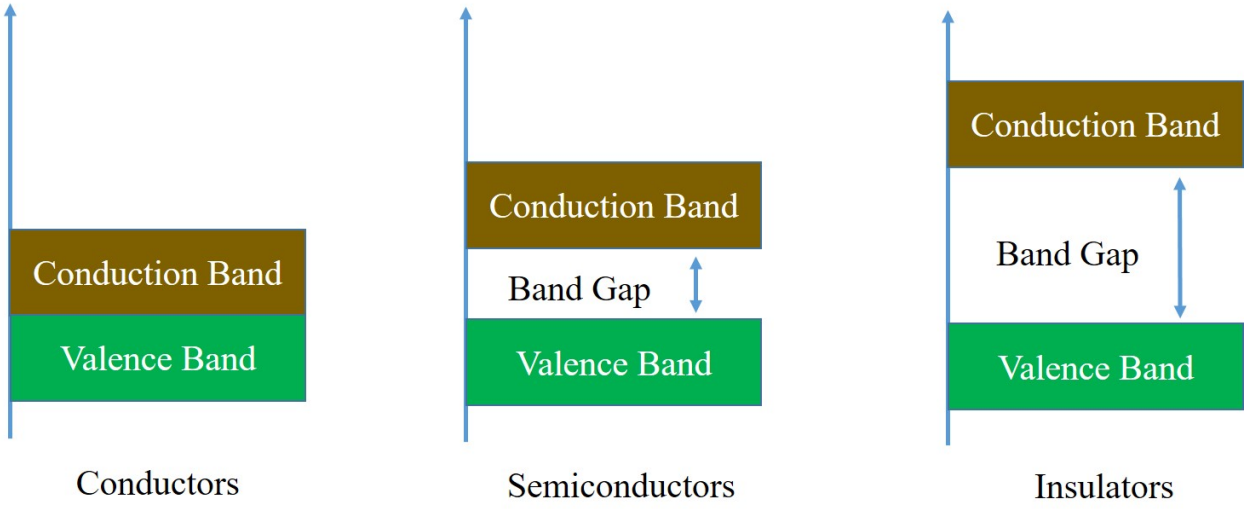

Figure 1.2 Energy bands of solids.

Metallic conductors have high conductivity (10^4 to 10^6 S/cm), while insulators possess high resistivity (10^{-18} to 10^{-10} Ω-cm).[13] Properties of semiconductors fall between these two ranges. Elemental semiconductors consist of only one kind of atom in their structure. A few examples of elemental semiconductors are silicon, germanium, selenium, and tellurium. The combination of two or more elements can give semiconductor materials, called compound semiconductors. Cadmium sulfide and gallium arsenide are examples of compound semiconductors, which are used in numerous electronic devices.

1.2.3 Metal-Semiconductor Junctions

Metal-semiconductor (M-S) junctions are critical components of semiconductor devices because electrical properties of devices are guided by semiconductors, which ultimately define the

device functionality.[14, 15] Based on the work function of semiconductors relative to that of metals, Schottky or Ohmic junctions are formed. The theory of an ideal metal-semiconductor assumes pure metal and semiconductor at the interface without any interaction and undesired interfacial layer. Practically, chemical reaction or interface states, also called localized electron levels, between the metal and the semiconductor impact the formation of ideal metal-semiconductor junctions. However, a general trend has been observed. In general, formation of Schottky interfaces occurs if semiconductors have lower work function values than the metal, but the creation of Ohmic contacts occurs if semiconductors have a higher work function than the metal.

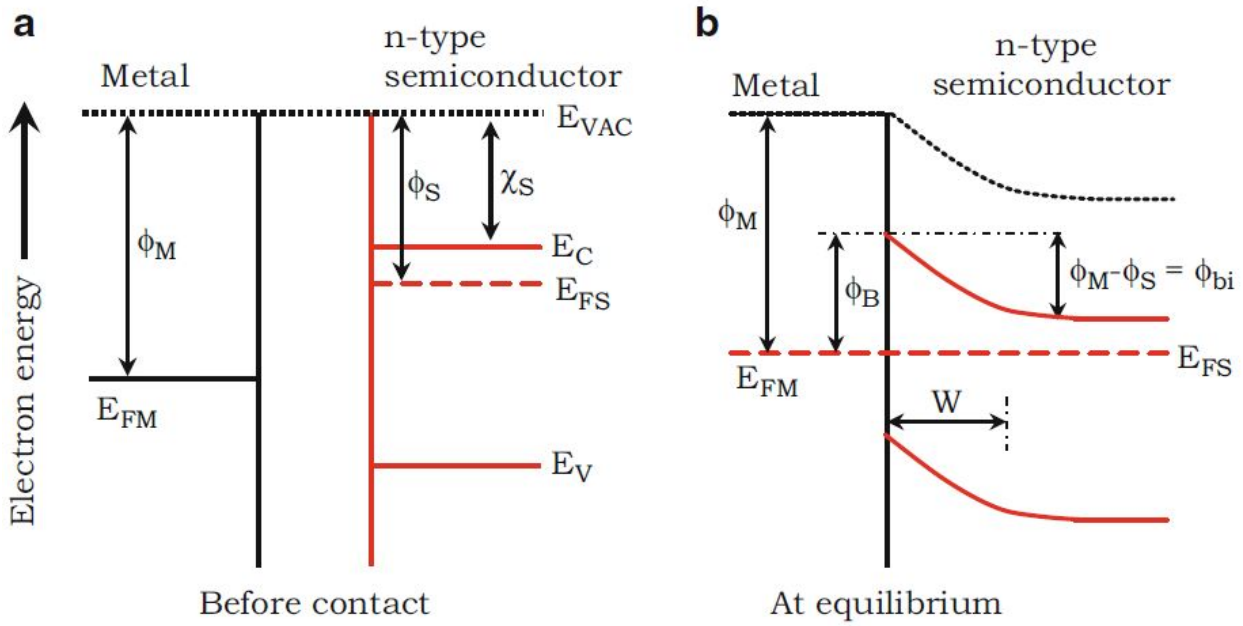

Figure 1.3 Energy band diagram for a metal-semiconductor contact. (a) Band diagram prior to contact, and (b) after contact at equilibrium.[16] Reprinted with the permission from Springer New York. Copyright 2014

Figure 1.3 illustrates a contact between a metal and n-type semiconductor. The Fermi level (E_{FS}) of an n-type semiconductor is close to its conduction band (E_C). When the metal and semiconductor are connected, electrons start moving from the semiconductor to the metal until the

Fermi levels are at equilibrium. This phenomenon creates a depletion region in the semiconductor, lowering the band edges in the bulk material relative to the energy at the junction as shown in **Figure 1.3b**.[16] The barrier height (Φ_B) is the result of energy disparity between the band edge of the semiconductor and the Fermi level of the metal (E_{FM}). Using an n-type semiconductor, the barrier height (Φ_B) is calculated as shown in **equation 1.1**, where Φ_M is the work function of the metal, and χ_S is the electron affinity of semiconductor.

$$\Phi_B = \Phi_M - \chi_S \tag{1.1}$$

In the case of a p-type semiconductor, the difference between the valence band edge of the semiconductor (E_V) and the Fermi energy in the metal represents the barrier height (Φ_B). This relationship is shown mathematically in **equation 1.2**. A barrier with rectifying characteristics is known as a Schottky barrier; to get over this barrier, the electrons must have enough energy. The function of a diode relies on the rectifying characteristics of the Schottky barriers. Any semiconductor, either n-type or p-type, can construct Schottky contacts. Lowering the barrier height (e.g., by annealing), or by creating narrower barriers (e.g., by doping), can create Ohmic M-S junctions whose resistance is unaffected by the applied voltage.

$$\Phi_B = E_V - \Phi_M \tag{1.2}$$

1.2.4 Electrical Properties of Nanomaterials

Both resistivity and conductivity are important characteristics of materials because they reveal electrical transport properties. Electrical conductivity indicates how readily electrons move through the material. Conductivity and resistivity are inversely related to each other: if conductivity is high, resistivity is low. Mathematically, they are related as shown in **equation 1.3**, where conductivity is measured in 1/Ω-m, and resistivity is measured in Ω m.

$$\text{Conductivity } (\sigma) = \frac{1}{\text{resistivity } (\rho)} \tag{1.3}$$

The interfaces established between two metals or between a metal and a semiconductor show different electrical characteristics based on the type of material. The relationship between current (I) flowing across the junction, and the voltage (V) applied is graphically represented in the form of curves, which are well-known as I-V curves (**Figure 1.4**).

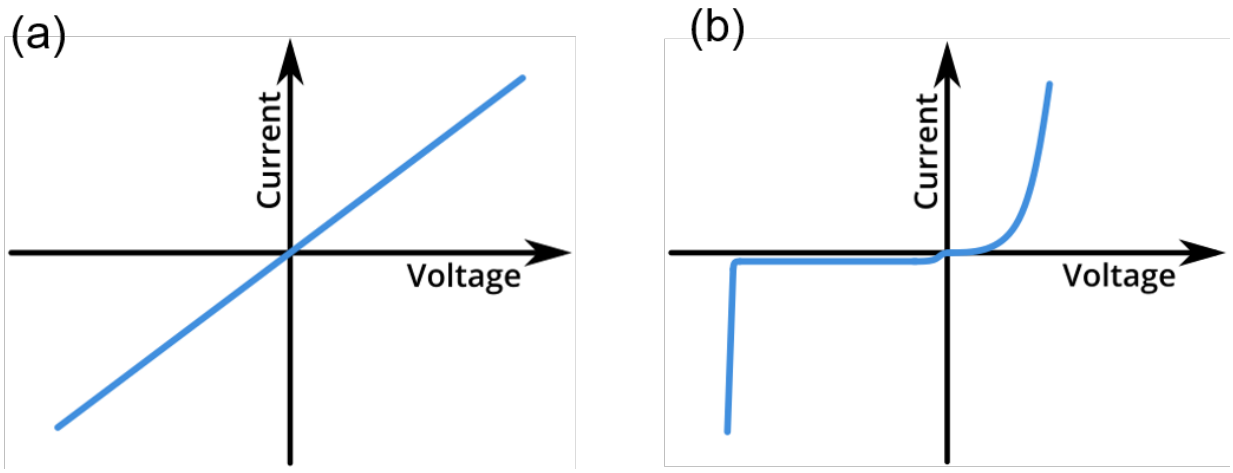

Figure 1.4 I-V curves for (a) an Ohmic contact, and (b) a Schottky contact.

Ohmic contacts follow Ohm's law, which states that voltage (V) applied to a device is directly proportional to the product of current (I) and resistance (R). This means that current passing through the device depends on the voltage applied, and a plotting of I vs V should give a line passing through the origin. In contrast, the interfaces with the Schottky barriers exponentially rise with current at positive voltages (forward bias), but the current does not flow at negative voltages until the break-down voltage is reached.

1.3 DNA NANOTECHNOLOGY

Deoxyribonucleic acid (DNA) is used in DNA nanotechnology as a material to design and generate nanoscale structures with arbitrary shape and size, apart from a genetic carrier. DNA-

based nanotechnology employs single-stranded, double-stranded, and well-programmed DNA architectures, such as 2-dimensional (2D) and 3-dimensional (3D) DNA origami, with high spatial resolution for technological use.[17, 18] These DNA structures, ranging in size from nanometers to millimeters, possess promising applications that benefit numerous research fields of drug delivery, bio-sensing, bio-medical engineering, nano-electronics and bio-imaging.[18]

Nanofabrication involves the production of nanoscale components, devices and functional materials, while preferably minimizing cost and material volume.[5] DNA's use in nanofabrication has inaugurated unprecedented opportunities and possibilities because of the precise and powerful self-assembly of DNA strands governed by Watson-Crick base paring interactions (Adenine-Thymine, Guanine-Cytosine).[5, 19] Diverse nanomaterials can be incorporated in DNA platforms to build versatile heterostructures with appealing applications in scientific explorations. In the early 1980s, Nadrian Seeman[20] put forward the concept of building nanostructures by exploiting oligomeric nucleic acid sequences that prefer selective binding with complementary sequences. He formed immobile junctions by preferential interaction of DNA strands and predicted DNA strands as potential bioengineering entities. Much later, in 2006, Paul Rothemund[21] helped to advance this concept toward reality by fabricating arbitrary shapes, including smiley faces, from single-stranded DNA assembled together by short "staple" strands. Since then, DNA-enabled nanofabrication has emerged as a fascinating bottom-up technology which can create programmed 1D, 2D and 3D DNA nanostructures ranging from nanometers to micrometers.[22, 23] The ability to generate arbitrary-shaped DNA nanostructures with high resolution (~5 nm) makes DNA nanofabrication unique among other bottom-up nanofabrication technologies.[24]

1.4 DNA AS A NANOFABRICATION MATERIAL

DNA behaves as a unique building block in biomolecule-based nanofabrication. DNA molecules are scalable and programmable because of their unique structural properties, and can be used as well-defined subunits which provide a foundation for building complex DNA structures.[25] Owing to nanoscale geometry, biocompatibility, and molecular recognition properties, DNA molecules are well-suited for nanofabrication. Simple 1D, 2D and high-level 3D architectures can be achieved from DNA scaffolds by appropriate manipulation of complementary base sequences and their binding environments.[26, 27] Such arbitrary DNA structures can further serve as templates to assemble other nanomaterials including metals and semiconductors into functional components, which possess a wide range of applications, for example in molecular biology, drug discovery and delivery, and polymer science.[28]

1.4.1 DNA Structure

In the biological world, DNA molecules in each organism exist in the form of two strands, i.e., a double helix with four different nucleotide units in each chain (**Figure 1.5**).[28] A nucleotide unit consists of a five-carbon sugar, one or more phosphate groups and a nitrogen-containing base. A chain of alternating phosphate-sugar-phosphate-sugar groups, called a DNA strand, is formed by covalent linking between the nucleotides.[29] The phosphate groups create a negative charge on the DNA backbone. In each polynucleotide chain, sugar and phosphate groups remain the same, but the bases can differ. The four bases are adenine (A), cytosine (C), guanine (G), and thymine (T). Hydrogen bonds and π-π stacking hold two polynucleotide chains together in a DNA molecule.[29] The directionality of a DNA strand is denoted by 3' (hydroxyl) and 5' (phosphate) terminals.

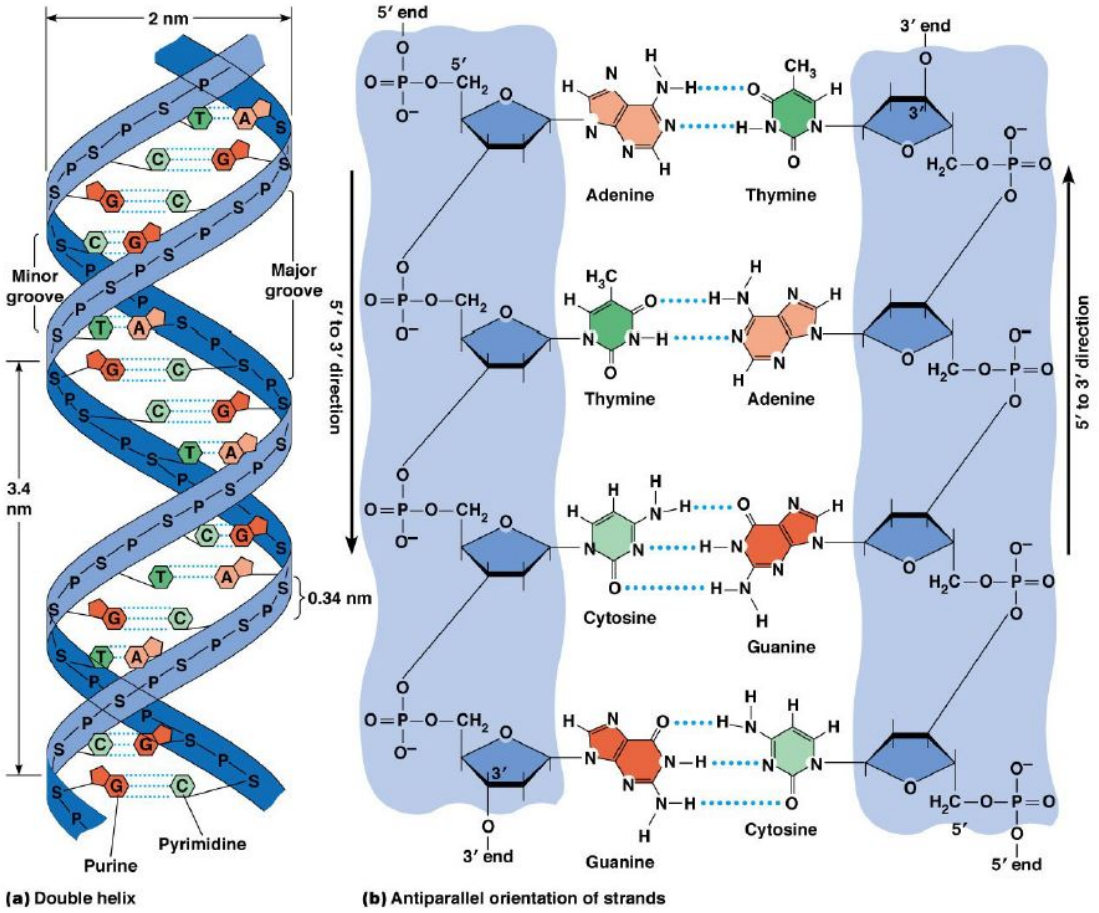

Figure 1.5 DNA structure. (a) Double helix; (b) antiparallel orientation of strands.[28] Reprinted with permission from MDPI. Copyright 2019

1.4.2 Self-Assembly of DNA

Self-assembly refers to the process of formation of ordered structures or patterns that takes place due to specific internal interactions between components themselves in a system, without the aid of external forces or factors.[30] The components in the system may be atoms, molecules, or macroscopic particles.

DNA self-assembly entails fabrication of DNA structures in the absence of external control. The self-assembling ability of DNA is related to the Watson-Crick base paring rules (**Figure 1.5b**).[28,31] Adenine pairs with thymine, with the aid of two hydrogen bonds, and guanine pairs with cytosine

using three hydrogen bonds. Therefore, DNA with more GC pairs exhibits higher stability toward denaturation or melting. The precise, accurate and well understood interactions between A-T and G-C base sequences are exploited to obtain self-assembled DNA nanostructures.

1.5 DNA ORIGAMI

In 2006, Rothemund reported 2D DNA origami made by folding a long single-stranded DNA.[21] This process involves the folding of single-stranded scaffold DNA into a desired shape with hundreds of short DNA staple strands (**Figure 1.6**). In 2009, Shih and coworkers introduced 3D DNA origami structures.[32] Researchers have created diverse static structures (tiles,[33] ribbons,[34] and tubes[35]) and dynamic structures such as switches[36] based on DNA origami. Despite several applications, DNA origami also has some limitations for nanofabrication such as the size of the traditionally used M13 genome, structural stability, and difficulties in selective metallization.

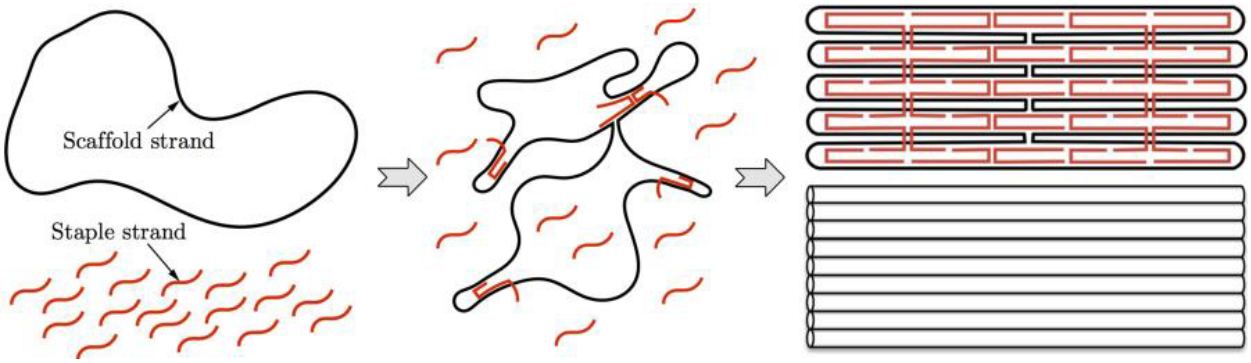

Figure 1.6 Schematic diagram of the folding of DNA origami into a desired structure.

1.5.1 Applications of DNA Origami

DNA origami offers nanoscale DNA objects with arbitrary 1D, 2D and 3D designs.[37] Such nanoscale structures may have scientific applications in both biological and non-biological fields. Some research fields which utilize DNA origami structures are nanomedicine, molecular computation, nanorobotics, nanoelectronics, light, energy, biomolecules and nanomaterials

science (**Figure 1.7**).[16, 37] For example, the nanomedicine field uses DNA origami structures as drug carriers or in therapeutics in association with other nanomaterials.[38] In electronics, researchers are attempting to build DNA-templated electronic nanodevices.[39] The study of biological molecules such as proteins and amino acids has been assisted by DNA origami structures as nano breadboards.[37] In addition, DNA nanostructures can be customized with functional groups to extensively enhance their applications.[40]

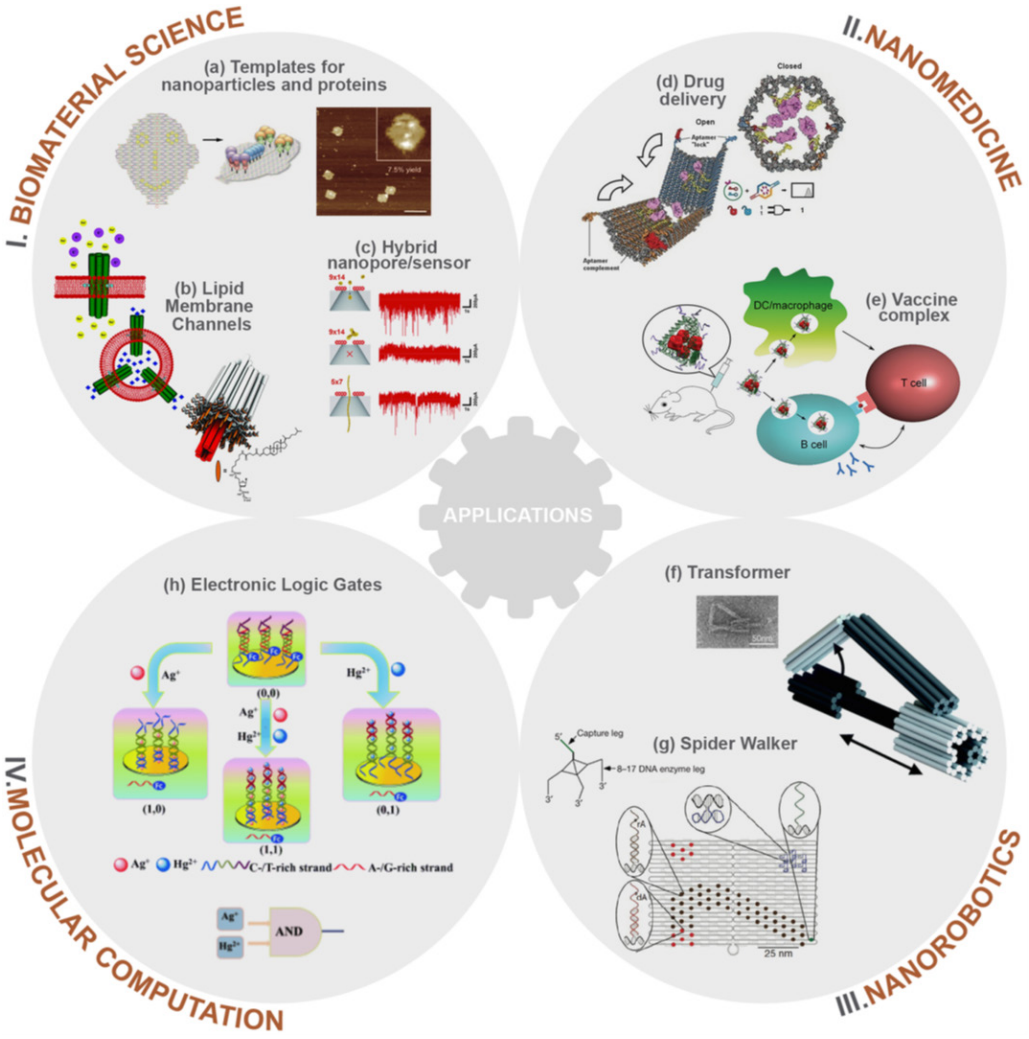

Figure 1.7 Applications of DNA origami structures.[40] Reprinted with permission from American Chemical Society. Copyright 2015

1.6 NANOMATERIAL ATTACHMENT TO DNA TEMPLATES

DNA templates can accommodate nanomaterials in various forms, such as ions, nanoparticles, or nanorods. As such, they can facilitate creating conductive structures through seeding and metallization approaches. In many cases, DNA templates dissolved in solution are deposited onto a substrate by exploiting electrostatic interactions between the negatively charged DNA backbone and a positively charged substrate (i.e., Si or mica after treatment with divalent cations). Seeding, the binding of nanomaterials to DNA templates, is performed by depositing seeding material through nonspecific or location-specific interactions with DNA. DNA templates can either be incubated with a seeding solution, or the seeding solution can be added to a substrate with pre-deposited DNA templates. Seeding is a critical process because it guides the fabrication of conductive structures in subsequent steps. Various tactics of seeding such as ionic, site-specific and nonspecific are in practice.

1.6.1 Ionic Seeding

In ionic seeding, metal ions interact electrostatically with the phosphate backbone of DNA, as shown in **Figure 1.8a**. Metallization of DNA was first demonstrated by incorporating silver ions into λ-DNA scaffolds by Braun et al.[41] Since then, different procedures have been utilized to incorporate metal ions onto DNA strands to construct metal nanostructures. For example, Kasyanenko et al.[42] bound bis(1,10-phenanthroline) silver(I) monohydrate (Ag-Phen) to DNA in solution where the phenanthroline ligands ensured uniform binding of silver on DNA structures. The Ag-Phen-DNA complexes were treated with sodium borohydride reducing agent to form Ag metal on the DNA fibrils. Vecchioni et al.[43] reported intercalation of Ag^+ into cytosine-mismatched DNA duplexes to create conductive C11-(Ag^+)11-C11 duplexes. With silver plating, the Ag^+ ion-coordinated DNA duplexes demonstrated a significant enhancement in single-molecule

conductivity. González-Olvera et al.[44] showed binding of metal cations such as Ag^{+}, Zn^{2+}, Fe^{2+}, and Cu^{2+} with deprotonated guanine or thymine groups on short single-stranded DNA. They synthesized silver, zinc, and copper nanoparticles by reducing their cationic aggregates in alkaline aqueous solution. This technique of DNA metallization can be used for the fabrication of DNA-based nanostructures.

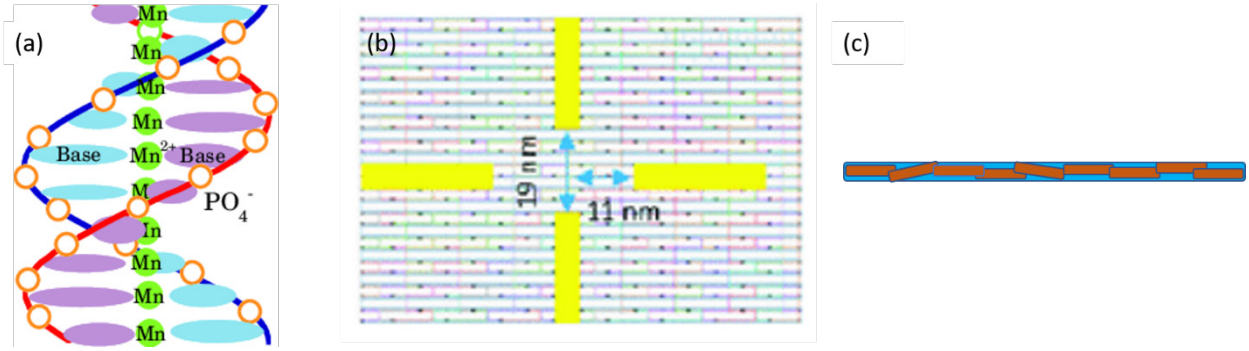

Figure 1.8 Seeding methods on DNA templates. (a) Ionic, (b) site-specific, and (c) non-specific.[45] Panel (a) is reprinted with permission from SPIE-IS&T. Copyright 2015

1.6.2 Site-specific Seeding

Site-specific metallization of DNA origami involves attachment of metal nanoparticles or nanorods via chemical interaction or sequence-specific binding on desired areas of the DNA template. In **Figure 1.8b**, nanorods (yellow colored) are selectively attached to a rectangular-shaped tile DNA template. Various materials have been bound to DNA templates including Au,[33, 34] Ag,[46, 47] Cu,[48] Ni,[49] Pd,[50] Te,[39] and carbon nanotubes[51] through site-specific or non-site-specific placement. Pilo-Pais et al.[46] reported site-specific placement of DNA-coated gold nanoparticles on DNA origami, but, they did not carry out plating to connect the gold particles and generate wires. Uprety et al.[48] utilized DNA-functionalized gold nanorods for site-specific metallization of DNA origami. They demonstrated the controlled placement of gold on selected sites of DNA origami and directional growth of the nanorods to create nanowires through electroless plating. The use of

other metals or semiconductors would increase the utility of the structures created, and the development of electroless plating of various metals and semiconductors to allow connections to other components would be further useful.

1.6.3 Nonspecific Seeding

Non-site-specific binding refers to the attachment of nanomaterials to entire substrates rather than to selective areas. **Figure 1.8c** shows non-preferential binding of nanorods to a ribbon-shaped DNA origami structure (blue background). Non-selective binding of nanoparticles or nanorods to surface DNA origami is achieved by electrostatic interactions between charged groups on the seeds and DNA. Formation of gold nanowires has been demonstrated by nonselective binding of Au nanorods to DNA origami structures followed by plating.[34, 52] Uprety et al.[34] reported fabrication of ~7 nm wide conductive gold nanowires on DNA origami structures that were ~410 nm long and 17 nm wide. The gold nanorods were coated with cetyltrimethylammonium bromide (CTAB) and deposited on the surface with DNA origami. The negative charge on the DNA attracted the positively charged CTAB so nanorods were placed onto the DNA origami without locational selectivity.

1.7 ELECTROLESS PLATING

Plating entails filling gaps and building connections between nanomaterials either by isotropic or anisotropic metal deposition. Continuous and conductive structures are made by eliminating gaps between seeded nanomaterials on the DNA templates. Electroless plating is more widely used over electroplating to form electrical contacts during nanowire metallization due to advantages, such as forming films of uniform thickness, producing nanometer-thickness layers, and depositing material on complicated templates. The controlled electroless plating process is a redox reaction induced by a chemical reducing agent that provides electrons to reduce metal

cations in solution to form metallic deposits. During this process, the metal itself acts as a catalyst to drive metal cation reduction and accumulate more metal on the catalytic metal surface, resulting in an autocatalytic reaction as shown in **equation 1.4**.

$$\text{Metal Ion}_{(aq)} + \text{Reducing Agent}_{(aq)} \rightarrow \text{Metal}_{(s)} + \text{Oxidized Product}_{(aq)} \quad (1.4)$$

1.8 DNA-BASED NANOELECTRONICS

Electronics utilize active components, such as transistors, diodes, sensors, integrated circuits, etc.,[53, 54] and nanoelectronics represent a fast-developing field that relies heavily on nanofabrication. A theme of nanoelectronics is how to increase the capabilities of devices while reducing their weight, size, and power consumption. However, the building of electronic devices comprises technological and fundamental challenges at dimensions below the 20-nm regime.[53]

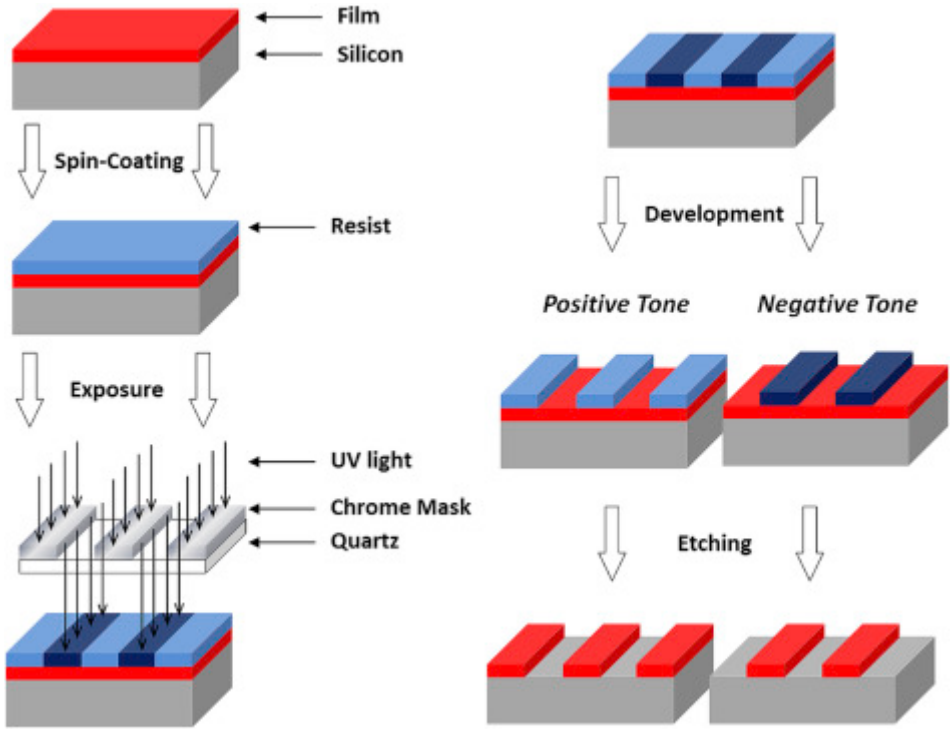

Figure 1.9 Steps of traditional top-down lithographic patterning.[55] Reprinted with permission from Elsevier. Copyright 2016

The current method for patterning electronic devices involves photolithography (**Figure 1.9**). Some advantages of this top-down technique are that it 1) is well-established, 2) has high precision, 3) has high resolution (< 20 nm), and 4) offers parallel patterning.[53, 54] On the other hand, high-resolution photolithography is complicated, expensive and requires extremely clean conditions.[53, 54] Hence, conventional lithographic methods, though the primary technique used in manufacturing micro and nanodevices, inherently possess some limitations.

Researchers are keen to develop bottom-up approaches to making nanoelectronics, which may be able to address challenges associated with top-down methods. DNA origami is one of the emerging bottom-up methods for designing and fabricating nanocomponents, as described in **section 1.5**. This approach allows for control over nanoscale shapes, for example, as substrates or masks, to create metallic nanostructures or wires.[56, 57] However, useful progress is still needed, particularly in the area of DNA-based nanoelectronic circuits, and placing metal and semiconductor materials on DNA nanostructures to generate desired circuits. Thus, practical and functional nanoelectronics are still in the conceptual phase because the understanding of 3D DNA assemblies and the addition of inorganic components to these assemblies are still in progress. In order to address these shortcomings, contemporary research specifically focuses on the high-yield creation of metal-semiconductor nanostructures on DNA via controlled seeding and plating, along with electrical characterization.

1.9 TECHNIQUES FOR NANOMATERIAL CHARACTERIZATION

To study the electrical properties of nanomaterials including metallized DNA structures, conductivity measurements are necessary. However, the measurements are limited by the size of nanomaterials and available facilities. For imaging and topographical study of nanoscale materials, atomic force microscopy (AFM), scanning electron microscopy (SEM) and transmission electron

microscopy (TEM) are valuable techniques. Unlike imaging and morphological inspection, electrical characterization demands conductive connections to nanostructures, with the patterns created by techniques such as photolithography, electron beam lithography, direct contacting or electron beam induced deposition. For qualitative verification of conductivity of nanomaterials, conductive AFM and scanning tunneling microscopy (STM) are also instrumental options.

1.9.1 AFM

AFM can image topography at high resolution and perform surface measurements on a wide range of micro or nanomaterials.[58] A cantilever, typically made from silicon or silicon nitride with a very sharp tip, scans over the sample surface. A laser beam is used to probe cantilever deflection; any bending by the cantilever will cause slight changes in the direction of the reflected laser, and a position-sensitive photodiode tracks these changes. AFM creates topographical images based on the changes in laser position on the detector. Depending on the information needed, AFM can operate in different modes, such as contact or tapping mode.[59]

1.9.2 SEM

SEM is a powerful and multifunctional method designed to characterize micro or nanomaterials.[60] SEM is primarily useful for imaging, studying elemental composition, and surface characterization of materials, where the interaction between electrons and the materials is the source of information. A focused electron beam hits the sample surface under a high vacuum; as the electrons interact with the sample, they produce secondary electrons, backscattered electrons, and characteristic X-rays. These signals are collected by one or more detectors to form images and elucidate other sample characteristics.

1.9.3 Two-point and Four-point Probe Techniques

It is essential to characterize the electrical properties of nanomaterials, particularly nanowires, to find out their ability to allow current flow. A resistance meter is used to measure highly resistive materials,[61] whereas two-terminal or four-terminal measurements are done for higher conductivity materials.[62] Richter et al.[63] reported the conductivity of palladium nanowires ~50 nm in diameter with a two-terminal measurement technique. Uprety et al.[34] described the measurement of electrical properties of gold nanowires (~400 nm long) on DNA origami. They measured a resistivity as low as 8.9×10^{-7} Ω·m using a two-terminal setup with electron beam lithography to make connections to the wires. Four-terminal measurement is a better technique to make precise electrical determinations[64, 65] because one pair of contact pads measures the current and the other pair applies the voltage, which eliminates the effect of contact resistance.

1.10 OVERVIEW OF THE DISSERTATION

DNA origami has broadened the horizons of nanotechnology; 2D and 3D DNA origami structures are now used in biomaterials, nanomedicine, molecular computation, and nanorobotics. A variety of metal nanoparticles or nanorods have been synthesized and attached to DNA substrates in a controlled manner to fabricate conductive and functional DNA-mediated nanodevices. However, semiconducting materials, a critical component of electronic devices, have not been integrated extensively into the fabrication. In this dissertation, bottom-up fabrication of DNA origami-created metal and metal-semiconductor nanostructures has been studied along with their electrical characterization. Particularly, site-specific metallization of DNA origami templates, and fabrication of multiple metal-semiconductor junctions on a single DNA origami template by electroless plating and annealing in the presence of a heat-resistant polymer, are the novel outcomes I achieved. This work is important because research on DNA-based nanoelectronics has

attracted attention due to the unique capability of DNA to serve as a versatile substrate for creating precise, continuous and conductive nanostructures. To expand current DNA nanofabrication and provide a fundamental framework for the creation of nanoelectronic devices, this dissertation advances metallization of DNA templates using metal and semiconductor nanorods and nanoparticles.

In **chapter 2**, I describe the location-specific metallization of DNA origami with high yields and then their electrical characterization. I created plus, cross, and C-shaped gold nanowires on tile DNA templates, placing the DNA-functionalized gold nanorods on desired sites. Electroless gold plating successfully joined Au nanorods through directional growth along their lengths. Finally, C-shaped nanowires were characterized by a four-point probe technique to calculate resistance values.

In **chapter 3**, I describe the fabrication of multiple metal-semiconductor junctions on single DNA origami templates along with their electrical characterization. I synthesized tellurium and gold nanorods and attached them to DNA origami. Electroless plating of gold was performed to establish connections between Au and Te nanorods, forming Au-Te-Au structures. The non-linear current-voltage curves obtained from the Au-Te-Au nanowires provide evidence that metal and semiconductor nanorods were connected electrically.

Chapter 4 presents the formation of metal/semiconductor nanowires by annealing polymer-coated nanorods on DNA origami templates. Instead of using conventional solution-based plating, I employed an annealing method to link metal and semiconductor nanorods into nanowires. Polymer-coated gold and tellurium nanorods pre-attached to DNA origami in a Au/Te/Au chain were annealed at 170 °C for 2 min to connect the Au and Te nanorods. Annealing

relocated some gold onto the tellurium nanorods to generate Au/Te/Au nanowires, which were found to be electrically connected through two-point measurement of current-voltage curves.

Chapter 5 summarizes the outcomes and presents conclusions for this work. It also covers promising future work associated with the fabrication of metal-semiconductor nanowires.

1.11 REFERENCES

1. Zhao, Y.; Dai, X.; Wang, F.; Zhang, X.; Fan, C.; Liu, X., Nanofabrication based on DNA nanotechnology. *Nano Today* **2019,** *26*, 123-148.

2. Michel, B.; Bernard, A.; Bietsch, A.; Delamarche, E.; Geissler, M.; Juncker, D.; Kind, H.; Renault, J.-P.; Rothuizen, H.; Schmid, H., Printing meets lithography: Soft approaches to high-resolution patterning. *IBM J. Res. Dev.* **2001,** *45* (5), 697-719.

3. Carlson, A.; Bowen, A. M.; Huang, Y.; Nuzzo, R. G.; Rogers, J. A., Transfer printing techniques for materials assembly and micro/nanodevice fabrication. *Adv. Mater.* **2012,** *24* (39), 5284-5318.

4. Peng, Z.; Liu, H., Bottom-up Nanofabrication Using DNA Nanostructures. *Chem. Mater.* **2016,** *28* (4), 1012-1021.

5. Li, H.; Carter, J. D.; LaBean, T. H., Nanofabrication by DNA self-assembly. *Mater. Today* **2009,** *12* (5), 24-32.

6. Dolez, P. I., Nanomaterials definitions, classifications, and applications. In *Nanoengineering*, Elsevier: 2015; pp 3-40.

7. Darweesh, H. H. M., Nanomaterials: Classification and Properties-Part I. Nanoscience: 2017.

8. Sudha, P. N.; Sangeetha, K.; Vijayalakshmi, K.; Barhoum, A., Nanomaterials history, classification, unique properties, production and market. In *Emerging Applications of Nanoparticles and Architecture Nanostructures*, Elsevier: 2018; pp 341-384.

9. Martinet, S., Nanomaterials for rechargeable lithium batteries. In *Nanomaterials for Sustainable Energy*, Springer: 2016; pp 471-512.

10. Ghassan, A. A.; Mijan, N.-A.; Taufiq-Yap, Y. H., Nanomaterials: an overview of nanorods synthesis and optimization. *Nanorods and Nanocomposites* **2020**, 11.

11. Sapoval, B.; Hermann, C., *Physics of semiconductors*. Springer Science & Business Media: 2003.

12. Adachi, S., *Handbook on physical properties of semiconductors*. Springer Science & Business Media: 2004; Vol. 2.

13. Mitchell, B. S., *An introduction to materials engineering and science for chemical and materials engineers*. John Wiley & Sons: 2004.

14. Milnes, A. G., *Heterojunctions and metal semiconductor junctions*. Elsevier: 2012.

15. Sharma, B., *Metal-semiconductor Schottky barrier junctions and their applications*. Springer Science & Business Media: 2013.

16. Chakrapani, V., Semiconductor junctions, solid-solid junctions. *Encyclopedia of Applied Electrochemistry* **2014**, 1882-1893.

17. Nummelin, S.; Kommeri, J.; Kostiainen, M. A.; Linko, V., Evolution of Structural DNA Nanotechnology. *Adv. Mater.* **2018,** *30* (24), 1703721.

18. Sun, L.; Yu, L.; Shen, W., DNA nanotechnology and its applications in biomedical research. *J. Biomed. Nanotech.* **2014,** *10* (9), 2350-2370.

19. Seeman, N. C., An overview of structural DNA nanotechnology. *Mol. Biotechnol.* **2007,** *37* (3), 246-257.

20. Seeman, N. C., Nucleic acid junctions and lattices. *J. Theor. Biol.* **1982,** *99* (2), 237-247.

21. Rothemund, P. W., Folding DNA to create nanoscale shapes and patterns. *Nature* **2006,** *440* (7082), 297-302.

22. Chidchob, P.; Sleiman, H. F., Recent advances in DNA nanotechnology. *Curr Opin Chem Biol* **2018,** *46*, 63-70.

23. Chen, Y. J.; Groves, B.; Muscat, R. A.; Seelig, G., DNA nanotechnology from the test tube to the cell. *Nat. Nanotechnol.* **2015,** *10* (9), 748-60.

24. Strauss, M. T.; Schueder, F.; Haas, D.; Nickels, P. C.; Jungmann, R., Quantifying absolute addressability in DNA origami with molecular resolution. *Nat. Commun.* **2018,** *9* (1), 1600.

25. Turberfield, A. J. P. w., DNA as an engineering material. **2003,** *16* (3), 43.

26. Seeman, N. C., DNA in a material world. *Nature* **2003,** *421* (6921), 427-431.

27. Wang, P.; Meyer, T. A.; Pan, V.; Dutta, P. K.; Ke, Y., The Beauty and Utility of DNA Origami. *Chem* **2017,** *2* (3), 359-382.

28. Roy, T.; Szuttor, K.; Smiatek, J.; Holm, C.; Hardt, S., Conformation and dynamics of long-chain end-tethered polymers in microchannels. *Polymers* **2019,** *11* (3), 488.

29. Travers, A.; Muskhelishvili, G. J. T. F. j., DNA structure and function. **2015,** *282* (12), 2279-2295.

30. Whitesides, G. M.; Grzybowski, B. J. S., Self-assembly at all scales. **2002,** *295* (5564), 2418-2421.

31. Zhang, D. Y.; Hariadi, R. F.; Choi, H. M.; Winfree, E. J. N. c., Integrating DNA strand-displacement circuitry with DNA tile self-assembly. **2013,** *4* (1), 1-10.

32. Douglas, S. M.; Marblestone, A. H.; Teerapittayanon, S.; Vazquez, A.; Church, G. M.; Shih, W. M., Rapid prototyping of 3D DNA-origami shapes with caDNAno. *Nucleic Acids Res.* **2009,** *37* (15), 5001-5006.

33. Uprety, B.; Jensen, J.; Aryal, B. R.; Davis, R. C.; Woolley, A. T.; Harb, J. N., Directional growth of DNA-functionalized nanorods to enable continuous, site-specific metallization of DNA origami templates. *Langmuir* **2017,** *33* (39), 10143-10152.

34. Uprety, B.; Westover, T.; Stoddard, M.; Brinkerhoff, K.; Jensen, J.; Davis, R. C.; Woolley, A. T.; Harb, J. N., Anisotropic electroless deposition on DNA origami templates to form small diameter conductive nanowires. *Langmuir* **2017,** *33* (3), 726-735.

35. Mohammed, A. M.; Schulman, R., Directing self-assembly of DNA nanotubes using programmable seeds. *Nano lett.* **2013,** *13* (9), 4006-4013.

36. Wang, F.; Liu, X.; Willner, I., DNA switches: from principles to applications. *Angew. Chem. Int. Ed.* **2015,** *54* (4), 1098-1129.

37. Chandrasekaran, A. R.; Anderson, N.; Kizer, M.; Halvorsen, K.; Wang, X., Beyond the fold: Emerging biological applications of DNA origami. *Chem Bio Chem* **2016,** *17* (12), 1081-1089.

38. Udomprasert, A.; Kangsamaksin, T., DNA origami applications in cancer therapy. *Cancer Sci.* **2017,** *108* (8), 1535-1543.

39. Aryal, B. R.; Ranasinghe, D. R.; Westover, T. R.; Calvopiña, D. G.; Davis, R. C.; Harb, J. N.; Woolley, A. T., DNA origami mediated electrically connected metal—Semiconductor junctions. *Nano Res.* **2020,** *13* (5), 1419-1426.

40. Jabbari, H.; Aminpour, M.; Montemagno, C., Computational approaches to nucleic acid origami. *ACS Comb. Sci.* **2015,** *17* (10), 535-547.

41. Braun, E., Eichen; Sivan, U.; Ben-Yoseph, G. *Nature* **1998,** *391*, 775-778.

42. Kasyanenko, N.; Qiushi, Z.; Bakulev, V.; Osolodkov, M.; Sokolov, P.; Demidov, V., DNA binding with acetate bis (1, 10-phenanthroline) silver (I) monohydrate in a solution and metallization of formed structures. *Polymers* **2017,** *9* (6), 211.

43. Vecchioni, S.; Capece, M. C.; Toomey, E.; Nguyen, L.; Ray, A.; Greenberg, A.; Fujishima, K.; Urbina, J.; Paulino-Lima, I. G.; Pinheiro, V., Construction and characterization of metal ion-containing DNA nanowires for synthetic biology and nanotechnology. *Sci. Rep.* **2019,** *9* (1), 6942.

44. González-Olvera, J. C.; Mercader-Trejo, F.; Ramos-López, E.; Rodríguez-López, A.; Álvarez-López, A.; Flores-Juárez, C. R.; Herrera-Basurto, R., Crystallization of metallic nanoparticles on short DNA oligonucleotides in alkaline aqueous solution. *J. Nanopart. Res.* **2020,** *22* (3), 63.

45. Mizoguchi, K. In *Physical properties of natural DNA and metal ion inserted M-DNA*, Nanobiosystems: Processing, Characterization, and Applications, International Society for Optics and Photonics: 2008; p 70400Q.

46. Pilo-Pais, M.; Goldberg, S.; Samano, E.; LaBean, T.; Finkelstein, G., Connecting the nanodots: programmable nanofabrication of fused metal shapes on DNA templates. *Nano lett.* **2011,** *11* (8), 3489-3492.

47. Shen, B.; Linko, V.; Tapio, K.; Kostiainen, M. A.; Toppari, J. J., Custom-shaped metal nanostructures based on DNA origami silhouettes. *Nanoscale* **2015,** *7* (26), 11267-11272.

48. Uprety, B.; Gates, E. P.; Geng, Y.; Woolley, A. T.; Harb, J. N., Site-specific metallization of multiple metals on a single DNA origami template. *Langmuir* **2014,** *30* (4), 1134-1141.

49. Arora, A. A.; de Silva, C., Beyond the smiley face: applications of structural DNA nanotechnology. *Nano Rev. Exp.* **2018,** *9* (1), 1430976.

50. Geng, Y.; Liu, J.; Pound, E.; Gyawali, S.; Harb, J. N.; Woolley, A. T., Rapid metallization of lambda DNA and DNA origami using a Pd seeding method. *J. Mater. Chem.* **2011,** *21* (32), 12126-12131.

51. Eskelinen, A. P.; Kuzyk, A.; Kaltiaisenaho, T. K.; Timmermans, M. Y.; Nasibulin, A. G.; Kauppinen, E. I.; Törmä, P., Assembly of single-walled carbon nanotubes on DNA-origami templates through streptavidin–biotin interaction. *Small* **2011,** *7* (6), 746-750.

52. Westover, T. R.; Aryal, B. R.; Ranasinghe, D. R.; Uprety, B.; Harb, J. N.; Woolley, A. T.; Davis, R. C., Impact of Polymer-Constrained Annealing on the Properties of DNA Origami-Templated Gold Nanowires. *Langmuir* **2020,** *36* (24), 6661-6667.

53. Lu, W.; Lieber, C. M., Nanoelectronics from the bottom up. *Nanoscience And Technology: A Collection of Reviews from Nature Journals* **2010**, 137-146.

54. Zhang, X.; Sun, C.; Fang, N., Manufacturing at nanoscale: Top-down, bottom-up and system engineering. *J. Nanopart. Res.* **2004,** *6* (1), 125-130.

55. Lawson, R. A.; Robinson, A. P., Overview of materials and processes for lithography. In *Frontiers of Nanoscience*, Elsevier: 2016; Vol. 11, pp 1-90.

56. Liu, J.; Geng, Y.; Pound, E.; Gyawali, S.; Ashton, J. R.; Hickey, J.; Woolley, A. T.; Harb, J. N., Metallization of branched DNA origami for nanoelectronic circuit fabrication. *Acs Nano* **2011,** *5* (3), 2240-2247.

57. Diagne, C. T.; Brun, C.; Gasparutto, D.; Baillin, X.; Tiron, R., DNA origami mask for sub-ten-nanometer lithography. *ACS Nano* **2016,** *10* (7), 6458-6463.

58. Liu, S.; Wang, Y., Application of AFM in microbiology: a review. *Scanning* **2010,** *32* (2), 61-73.

59. Khan, M.; Wang, Q.; Fitzpatrick, M. E., Atomic force microscopy (AFM) for materials characterization. In *Materials Characterization Using Nondestructive Evaluation (NDE) Methods*, Elsevier: 2016; pp 1-16.

60. Zhou, W.; Wang, Z. L., *Scanning microscopy for nanotechnology: techniques and applications*. Springer science & business media: 2007.

61. Grände, P. O.; Borgström, P., An electronic differential pressure flowmeter and a resistance meter for continuous measurement of vascular resistance. *Acta Physiol. Scand.* **1978,** *102* (2), 224-230.

62. Valdes, L. B., Resistivity measurements on germanium for transistors. *Proceedings of the IRE* **1954,** *42* (2), 420-427.

63. Richter, J.; Mertig, M.; Pompe, W.; Mönch, I.; Schackert, H. K., Construction of highly conductive nanowires on a DNA template. *Appl. Phys. Lett.* **2001,** *78* (4), 536-538.

64. Schuetze, A. P.; Lewis, W.; Brown, C.; Geerts, W. J., A laboratory on the four-point probe technique. *Am. J. Phys.* **2004,** *72* (2), 149-153.

65. Aryal, B. R.; Westover, T. R.; Ranasinghe, D. R.; Calvopiña, D. G.; Uprety, B.; Harb, J. N.; Davis, R. C.; Woolley, A. T., Four-point probe electrical measurements on templated gold nanowires formed on single DNA origami tiles. *Langmuir* **2018,** *34* (49), 15069-15077.

CHAPTER 2: FOUR POINT PROBE ELECTRICAL MEASUREMENTS ON TEMPLATED GOLD NANOWIRES FORMED ON A SINGLE DNA ORIGAMI TILES ‡

2.1 ABSTRACT

Bottom-up nanofabrication is increasingly making use of self-assembled DNA to fabricate nanowires and potential integrated circuits, although yields of such electronic nanostructures are inadequate, as is the ability to reliably make electrical measurements on them. In this chapter, I report improved yields and unprecedented conductivity measurements for Au nanowires created on DNA origami tile substrates. I created several different self-assembled Au nanowire arrangements on DNA origami tiles that are approximately 70 nm x 90 nm, through anisotropic growth of Au nanorods attached to specific sites. Modifications to the tile design increased yields of the final desired nanostructures as much as six fold. In addition, I measured the conductivity of Au nanowires created on these DNA tiles (~130 nm long, 10 nm diameter and 40 nm spacing between measurement points) with a four-point measurement technique that utilized electron beam induced metal deposition to form probe electrodes. These nanowires formed on single DNA origami tiles were electrically conductive, having resistivities as low as 4.24×10^{-5} Ω m. This work demonstrates the creation and measurement of inorganic nanowires on single DNA origami tiles as a promising path toward future bottom-up fabrication of nanoelectronics.

2.2 INTRODUCTION

Nanofabrication is well-known for generating functional structures at the nanometer scale, with particular emphasis on electronic devices and integrated circuits.[1] Current commercial

---

‡ This chapter is reprinted with permission from Aryal, B. R.; Westover, T. R.; Ranasinghe, D. R.; Calvopiña, D. G.; Uprety, B.; Harb, J. N.; Davis, R. C.; Woolley, A. T. *Langmuir* **2018**, *34* (49), 15069-15077.

nanofabrication makes use of traditional, well-established, top-down techniques. In addition, other emerging lithographic techniques, such as soft,[2] nanoimprint[3] and block copolymer,[4] are becoming increasingly important. Typical top-down approaches require increasingly complex patterning processes and tools,[1, 5] therefore, alternative techniques, including bottom-up methods, are in demand to provide improvements in quality, speed, and/or cost.[6, 7]

DNA-based methods are promising bottom-up alternatives that may be particularly well suited for complex 3D nanofabrication.[8-12] DNA molecules are robust, versatile and highly effective materials for creating precise, high-quality nanostructures in a variety of shapes[6, 13, 14] owing to self-assembly enabled by complementary base pairing. Exploiting these simple base-pair rules, Rothemund[15] created DNA origami by designing and folding a longer single-stranded DNA with the help of oligonucleotide staple strands to produce complex 2D and, eventually, 3D designs.[16, 17] Since then, researchers have fabricated a wide range of DNA structures including tiles,[15] ribbons and tubes,[18, 19] and various dynamic systems such as switches,[20] walkers[21] and circuits.[22] In addition, Ke et al.[23] demonstrated scaffold-free techniques that utilize "DNA bricks" to fabricate multiple shapes. Hence, the unique properties of DNA enable nanofabrication of components, devices and systems at relatively low cost, with low energy consumption and without the need for complex patterning tools.[7, 24-26]

Over the past few years, there has been interest in assembling inorganic nanostructures through the use of biological molecules. DNA is a popular substrate to which metals or semiconductors can be attached, providing a fundamental framework for the creation of functional nanodevices.[27, 28] These materials attach to DNA via chemical/electrostatic interaction or base pairing to specific sites.[24] Various materials have been bound to DNA templates including Au,[19, 24-26, 29-31] Ag,[32, 33] Cu,[29, 33-35] Ni,[36] Pd,[37, 38] Te,[39] and carbon nanotubes[40, 41] through site-specific or

non-site-specific placement. Site-specific attachment permits molecularly directed placement of select components at particular locations on predesigned DNA templates. Such controlled localization of materials on DNA substrates facilitates fabrication of wires and, ultimately, more complex circuits.

Spherical nanoparticles have generally been used as the seeding materials for metallization on DNA templates. Such particles grow isotropically during plating, enlarging the diameter and ultimately resulting in nanowires that consist of a large number of individually interconnected particle grains. In work done previously, Uprety et al.[19] reported the fabrication of continuous wires on DNA origami using Au nanorod seeds, and compared the results to wires similarly formed on DNA from plated nanoparticles. It was demonstrated that seeded Au nanorods contributed to anisotropic growth in the length direction with minimum increase in nanowire width/diameter. Two-point conductance measurements were performed on nanowires formed on DNA origami templates ~430 nm long. In a more recent study, different arrangements of metal nanostructures were formed by site-specific deposition of Au nanorods on DNA tiles and subsequent electroless plating; however, yields for fabricated designs were lower than desired.[24] In addition, although the nanowires appeared to be continuous, their lengths were too small to allow conductance measurement using electron beam patterned electrodes as it was done previously for longer nanowires.[19]

This chapter addresses several deficiencies in previous work by describing methods used to improve yields and to perform four-point probe electrical measurements on Au nanowires fabricated on individual DNA origami tile templates. These DNA tiles (~70 nm x 90 nm) were formed with standard origami methods using an M13mp18 scaffold, where staple strands were extended to provide sticky end attachment points for DNA-coated Au nanorods. I report improved

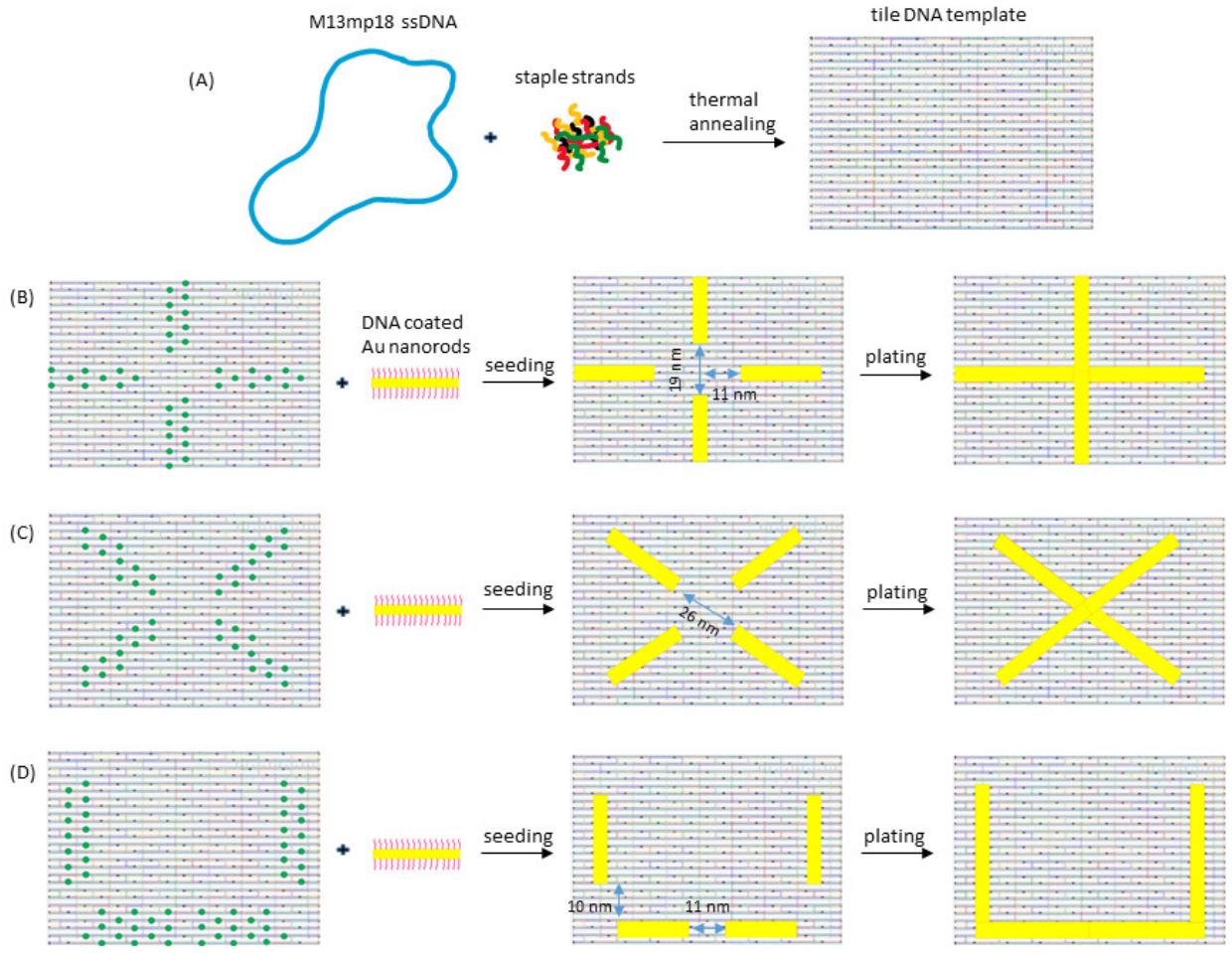

Figure 2.1 Schematic diagram of (A) folding single-stranded DNA into tile DNA origami where green dots represent protruding sticky end sequence sites on the staple strands. Site-specific placement of DNA-coated Au nanorods on tile DNA templates to create (B) plus, (C) cross and (D) C shapes through seeding and plating.

formation yield results for three different shapes, a "plus," a "cross" and a "C-shaped" structure formed on DNA tile surfaces by seeding with Au nanorods followed by electroless deposition as illustrated schematically in **Figure 2.1**. These structures are too small for conductance measurements to be made using contact electrodes formed by electron beam lithography patterning and liftoff as previously done.[19, 25, 26, 28, 29] Thus I instead demonstrate electrical measurements that utilize electron beam induced deposition (EBID) of conductive metal contacts, which enable

inorganic structures smaller than a single templating DNA origami tile to be characterized electrically. The EBID approach further enables the use of a four-point probe measurement technique to eliminate the influence of contact resistances to which the previous two-point method was susceptible. These key advances offer a clear path forward for the creation and electrical characterization of increasingly complex electronic structures on individual DNA origami tiles.

2.3 EXPERIMENTAL SECTION

2.3.1 Chemicals and Materials

All chemicals utilized were similar to those reported by Uprety et al.[24] M13mp18 single-stranded DNA was purchased from New England Biolabs (Ipswich, MA). Staple strands for DNA origami folding were obtained from Eurofins MWG Operon (Huntsville, AL). The dry staple strands were diluted in water to prepare solutions of desired concentrations. For coating DNA on Au nanorods, single-stranded DNA having a thiol group attached to the 5' end was purchased from Eurofins MWG Operon with PAGE purification and diluted to 1 mM in water. Tris(hydroxymethyl) aminomethane (Tris base) was purchased from Fisher Scientific (Fair Lawn, NJ). Ethylenediaminetetraacetic acid (EDTA) was purchased from Life Technologies (Carlsbad, CA). Acetic acid, hydrochloric acid (HCl), magnesium chloride ($MgCl_2$), and magnesium acetate ($MgAc_2.4H_2O$) were obtained from EMD Chemicals (Gibbstown, NJ). For preparing 10× TAE-Mg^{2+} (pH 8.3) buffer, 400 mM Tris base, 200 mM acetic acid, 10 mM EDTA, and 125 mM $MgAc_2 \cdot 4H_2O$ were used. Cetyl trimethylammonium bromide (CTAB) (H5882, 98%), ascorbic acid and chloroauric acid ($HAuCl_4$) were purchased from Sigma-Aldrich (St. Louis, MO). Silver nitrate was obtained from Mallinckrodt Chemicals (Phillipsburg, NJ). Bis(*p*-sulfonatophenyl) phenylphosphine dihydrate dipotassium salt (BSPP) was purchased from Strem Chemicals (Newburyport, MA). Sodium borohydride ($NaBH_4$) was from Acros (Newark, NJ). Tris(2-

carboxyethyl)phosphine (TCEP) was purchased from Alfa Aesar (Ward Hill, MA). Water (18.3 MΩ cm) for aqueous solution preparation as well as rinsing was processed with a Barnstead EASYpure UV/UF purification system (Dubuque, IA).

2.3.2 Gold Nanorod Synthesis and DNA-coated Gold Nanorod Preparation

Au nanorod synthesis followed a reported method used previously in the lab,[42] except the gold reduction time was increased to 4.5 hr to synthesize nanorods of appropriate length (25-30 nm). Coating Au nanorods with DNA also followed a published method,[43] except I used 0.1 M instead of 1 M NaCl during DNA reaction with the Au nanorods.

2.3.3 DNA Origami Design

The tile DNA origami template utilized 6812 of the 7249 bases in the M13mp18 scaffold as reported previously.[24] I designed plus, cross and C shapes where Au nanorods were captured on tile surfaces. The staple strands for capturing Au nanorod seeds had an additional length of 10 adenine nucleotides on the 3′ end. **Figure 2.1** schematically illustrates tile DNA assembly and linking of Au nanorods to tile DNA templates. Further information about specific staple strand sequences is included in the Appendix A.

2.3.4 DNA Origami Folding

The tile DNA origami structures were constructed by folding M13mp18 DNA with staple strands in a TECHNE TC-3000 thermal cycler. A mixture of M13mp18 scaffold (2 nM) and staple strands (40 nM of each staple strand) in 10× TAE-Mg^{2+} buffer was initially heated to 95°C for 3 min and then cooled to 4°C over 1.5 hr.[24]

2.3.5 Deposition of Tile DNA Origami onto Si Wafers

The deposition method of tile DNA origami onto Si wafers is similar to what had been previously reported in the literature.[19, 29] Oxidized Si wafers (1 cm x 1 cm) were plasma cleaned

in a Harrick Plasma Asher (PDC-32G) for 30 s at 18 W. Then, 3 µL of DNA origami (1 nM) in 10× TAE-Mg^{2+} buffer was added to the central region of a cleaned surface and left to adsorb for 25 min at 20°C in a humid chamber. The wafers were then rinsed by gently adding water drops for 9-10 s. The surfaces were then dried with flowing filtered air and imaged using a MultiMode Atomic Force Microscope (MMAFM-2, Bruker, Santa Barbara, CA).

2.3.6 Seeding and Plating Nanorods on DNA Origami

Seeding was done as described by Uprety et al.,[24] except I rinsed the surface with water instead of magnesium acetate solution. In brief, an Au nanorod seeding solution was pipetted onto a Si wafer surface that had DNA tiles previously deposited, and was left for 1 hr in a humid chamber, then rinsed and dried under flowing air. Plating also followed a published approach I adapted,[19] except the rinsing was done with water only. In short, Au plating solution was applied on the seeded DNA tiles for 30 min at room temperature, and after plating the samples were rinsed and dried as was done in the seeding step.

2.3.7 Atomic Force Microscopy (AFM) Imaging

DNA on Si wafers was imaged by AFM using 'Peak Force' tapping mode using ScanAsyst automatic image optimization technology with Bruker silicon tips on nitride cantilevers (ScanAsyst-Air and ScanAsyst-Air HD).

2.3.8 Scanning Electron Microscopy (SEM) Imaging

DNA samples seeded and plated with Au nanorods were imaged by SEM in ultra-high-resolution mode on a FEI Helios Nanolab 600, in high-vacuum mode on a Philips XL30 ESEM FEG, or on a ThermoScientific Verios UC G4 SEM.

2.3.9 Electrical Contact Patterning

Gold contact pads were formed using a lift-off process as follows. A 1 µm thick polymer layer with 100 µm patterned square holes was formed on 1x1 in^2 silicon chips by depositing AZ3312 (Merck kGaA) photoresist, exposing in a Karl Suss MA150 contact aligner, and developing in AZ300MIF (Merck kGaA). Following the lithography step, 7 nm of chromium (as an adhesion layer) and 50 nm of gold were sequentially evaporated onto the silicon substrate using a custom thermal evaporator. The photoresist was lifted off by immersing the substrate in 1-methyl-2 pyrrolidinone (Sigma-Aldrich) in an ultrasonic bath for 5 min. The substrates were rinsed in flowing distilled water for 5 s and dried with nitrogen.

Metal contact traces were made from the metallized DNA origami to the 100 µm gold pads using EBID of platinum in a FEI Helios Nanolab 600. EBID is a direct write process typically done in a dual beam scanning electron microscope.[44] The electron beam is scanned in the desired pattern in the presence of an organometallic gas released through a gas injection needle close to the surface. The electron beam decomposes the gas, depositing metal on the surface under the beam. The resulting deposit is not pure metal but a metal carbon mix that results in high resistance metal traces. Geier et al.[45] found that EBID written platinum lines can be purified after writing yielding much more conductive traces.

Platinum traces were written at 10 kV and 86 pA. The particular writing parameters were tuned to yield conductive traces while minimizing conductive overspray. Fine platinum traces (~25 nm wide) were written to make direct contact to the metalized origami structure using the line dose setting with target height of 200 nm. Larger traces were written to connect the fine platinum traces

to the 100 μm gold pads using the area dose setting with a target 250 nm width and 250 nm height. Due to the low conductance of the as-deposited platinum, which had a significant carbon impurity, I used a subsequent purification step,[45] by exposing the EBID features to an electron beam for 8 min/μm^2 in a Philips XL30 ESEM FEG using low vacuum mode at 0.5 Torr.

2.3.10 Electrical measurements

A micromanipulator probe station was used to contact the 100 μm gold pads for two-point and four-point resistance measurements. A DL Instruments 1211 current preamplifier was used to detect current, and data were collected using a National Instruments DAQ and a custom LabVIEW program. Applied voltages were between 0 and 1 volt.

2.3.11 Yield Calculations and Determination

From AFM images of DNA samples on silicon wafers, the tiles were classified as 'well-formed', 'small defects' or 'deformed' based on their appearance in the AFM data. The yield percentage for each category of tile DNA was determined by counting the number of each tile classification out of the total tiles for all three tile types. SEM images of seeded and plated tile DNA samples were used to compute the yield values for seeded and plated structures. Seeded structures for all three designs were categorized as 'well-seeded', 'misaligned', 'missing 1 rod' and 'missing >1 rod'. The yields were calculated from the number of structures of a given category out of the total tiles observed. Overall yields for all three structures were determined from the yields calculated for different batches of samples.

2.4 RESULTS AND DISCUSSION

Figure 2.2 shows AFM images of assembled tile DNA deposited onto Si wafers. In the large area image (**Figure 2.2A**), almost half of the tiles were 'well-formed'; some tiles had small defects and others were more deformed. The zoomed in image (**Figure 2.2B**) clearly displays well-

formed tile DNA origami. These results show that I had good overall assembly and surface placement yields for the tiles. Additional AFM images are in **Figure 2.3**; a more quantitative yield assessment is given later in this paper.

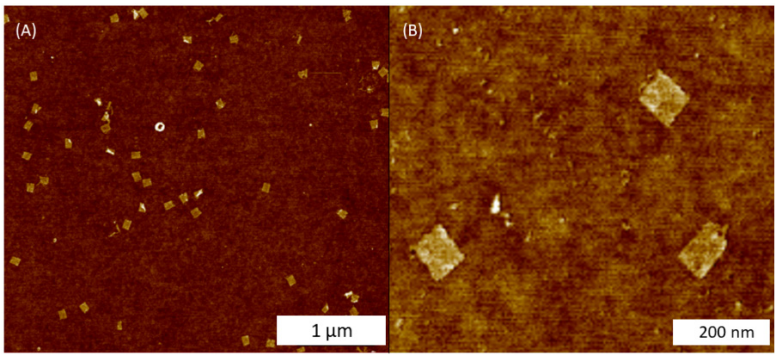

Figure 2.2 AFM images of self-assembled tile DNA templates. (A) Large area and (B) zoomed in images. The height scale is 5 nm.

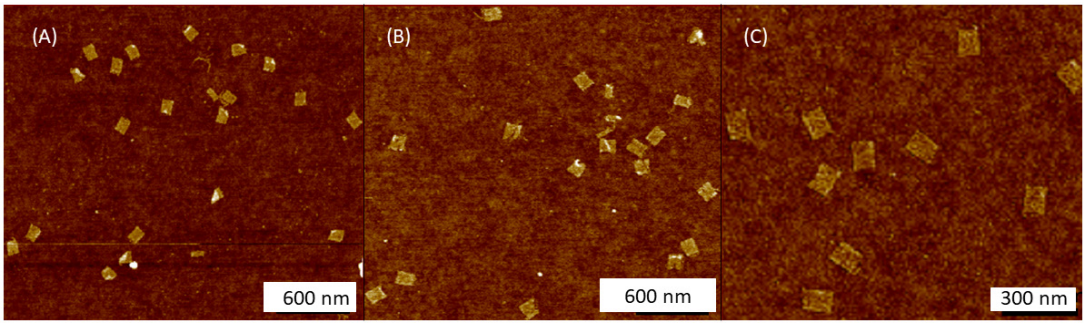

Figure 2.3 AFM images of the tile DNA templates utilized to create (A) plus, (B) cross and (C) C shapes. The height scale is 5 nm.

SEM images of Au nanorod seeded tiles were obtained for the plus, cross, and C designs, as shown in **Figure 2.4**. The darker rectangular features in the background are the DNA tiles, whereas the Au nanorods appear as brighter features in **Figure 2.4**. Inspection of the plus design (**Figure 2.4A**) demonstrated that many DNA tiles had the correct arrangement of four Au nanorods. Additionally, some tiles had four Au nanorods, but they were not properly positioned to create plus structures; similarly, some tiles had just three Au nanorods (missing one) and still others

were missing more than one Au nanorod. Additional SEM images and AFM data are in **Figure 2.5**. **Figure 2.4B** shows a zoomed in view of the plus design, in which the gaps between nanorods are more clearly visible than in the Au nanorod seeded large area image.

Figure 2.4(C-D) corresponds to Au nanorod seeded cross-shaped structures. Many of the DNA tiles (rectangular darker areas) had perfectly aligned Au nanorods that yielded cross structures. Similar to the plus structures, some tiles had four Au nanorods, but with incorrect orientation, others were missing one rod, and still others were missing more than one rod. Additional SEM images and AFM data on cross structures are provided in **Figure 2.6**. **Figure 2.4D** gives a close view of cross structures with visible spaces in between the diagonally placed nanorods on the tiles.

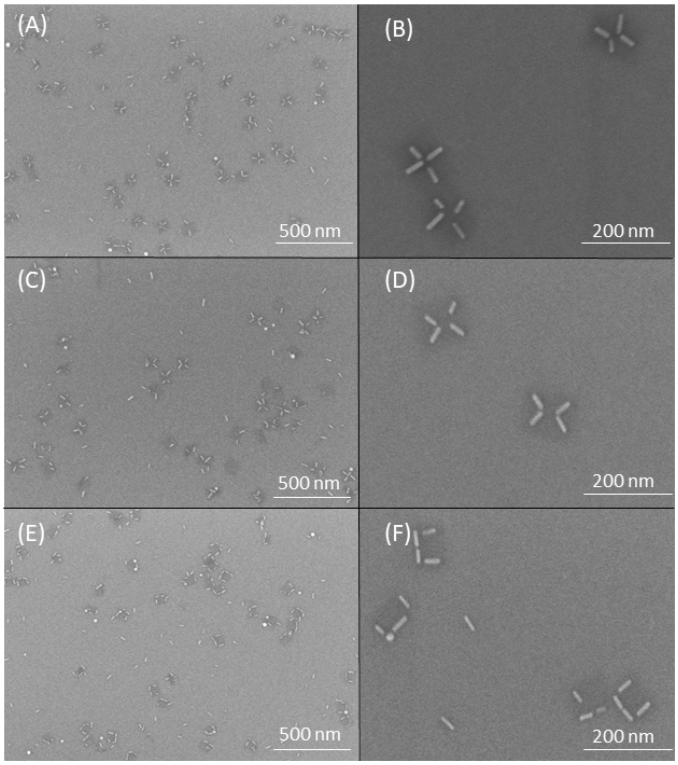

Figure 2.4 SEM images of tile DNA origami after seeding with Au nanorods. (A-B) Plus arrangement. (C-D) Cross arrangement. (E-F) C arrangement.

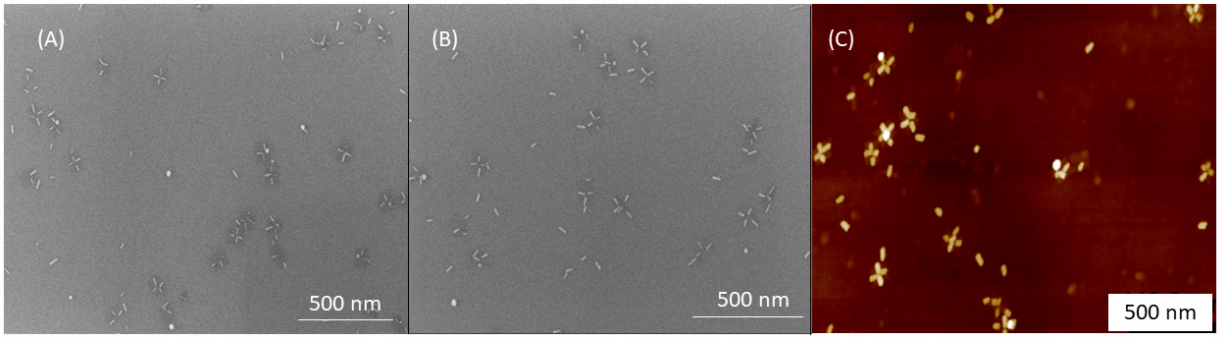

Figure 2.5 (A-B) SEM images and (C) AFM images of plus structures on tile DNA templates after seeding with Au nanorods. The height scale in (C) is 25 nm.

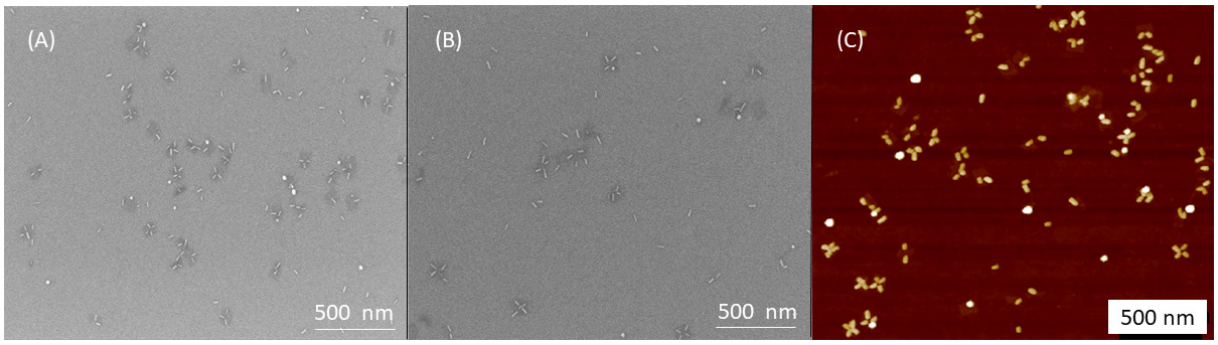

Figure 2.6 (A-B) SEM images and (C) AFM image of tile DNA templates seeded with Au nanorods to create cross structures. The height scale in (C) is 25 nm.

Figure 2.4(E-F) shows the C-shape on tiles after Au nanorod seeding. Many well-formed C shapes were found in the large area image while some of the tiles had misaligned Au nanorods, a few had just three (missing one), and some tiles were missing more than one nanorod. More SEM images and AFM data of C shapes are included in **Figure 2.7**. The zoomed-in image (**Figure 2.4F**) shows some DNA tiles with four Au nanorods attached to give a C shape. Additional structures with missing nanorods or a nanoparticle instead of one of the nanorods are also visible. I hypothesize that the seeded structures for the three designs are closely dependent on how the tiles landed on the Si wafers during deposition. Thus, well-formed tiles facilitated well-seeded

structures whereas incomplete plus, cross, and C structures on tiles likely resulted from tiles having small defects or incomplete assembly. As seen in **Figure 2.4**, nearly all DNA tiles had Au nanorods on them, even though the sticky end sequences all protrude from just one face of the DNA origami. I believe that either the protruding sticky ends cause nearly all the DNA tiles to deposit with the protruding sequences facing up, or the sticky ends are long enough to pass through to the top side even if the tiles deposit with the protruding sequences facing down.

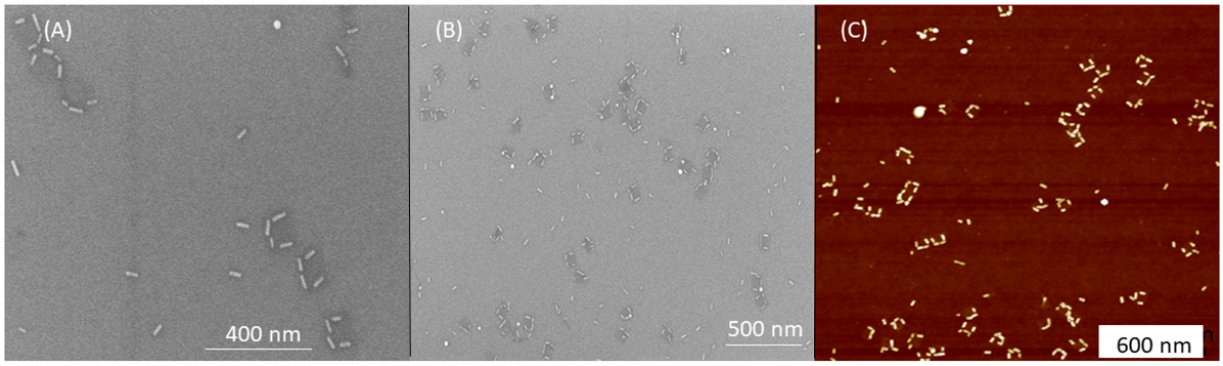

Figure 2.7 (A-B) SEM images and (C) AFM image of C shapes on tile DNA templates after seeding with Au nanorods. The height scale in (C) is 20 nm.

Yield calculations were performed for DNA tiles as well as all on the three structures after seeding, and **Figure 2.8** presents the consolidated results. **Figure 2.8A** demonstrates that almost 50% of the tiles were well formed, with 24% having small defects and 27% being deformed. Lack of planar landing on the surface due to inherent tension/twist in these DNA origami tiles[46] might have caused folding at corners of tiles leading to small defects. Some deformed structures could be caused by improper folding of M13mp18 DNA with staple strands. Tile DNA assembly did not utilize the full length of the M13mp18 DNA, so the remaining unutilized scaffold bases resulted in a short tail on one edge of the tile that could connect tiles end-to-end.[15] In order to separate those tiles from each other, the DNA origami was mixed well before deposition, which might have

deformed some tiles. To overcome this problem, the use of the full length of the scaffold DNA for assembly would help to form independent tiles without the more thorough mixing step that could deform the structures.

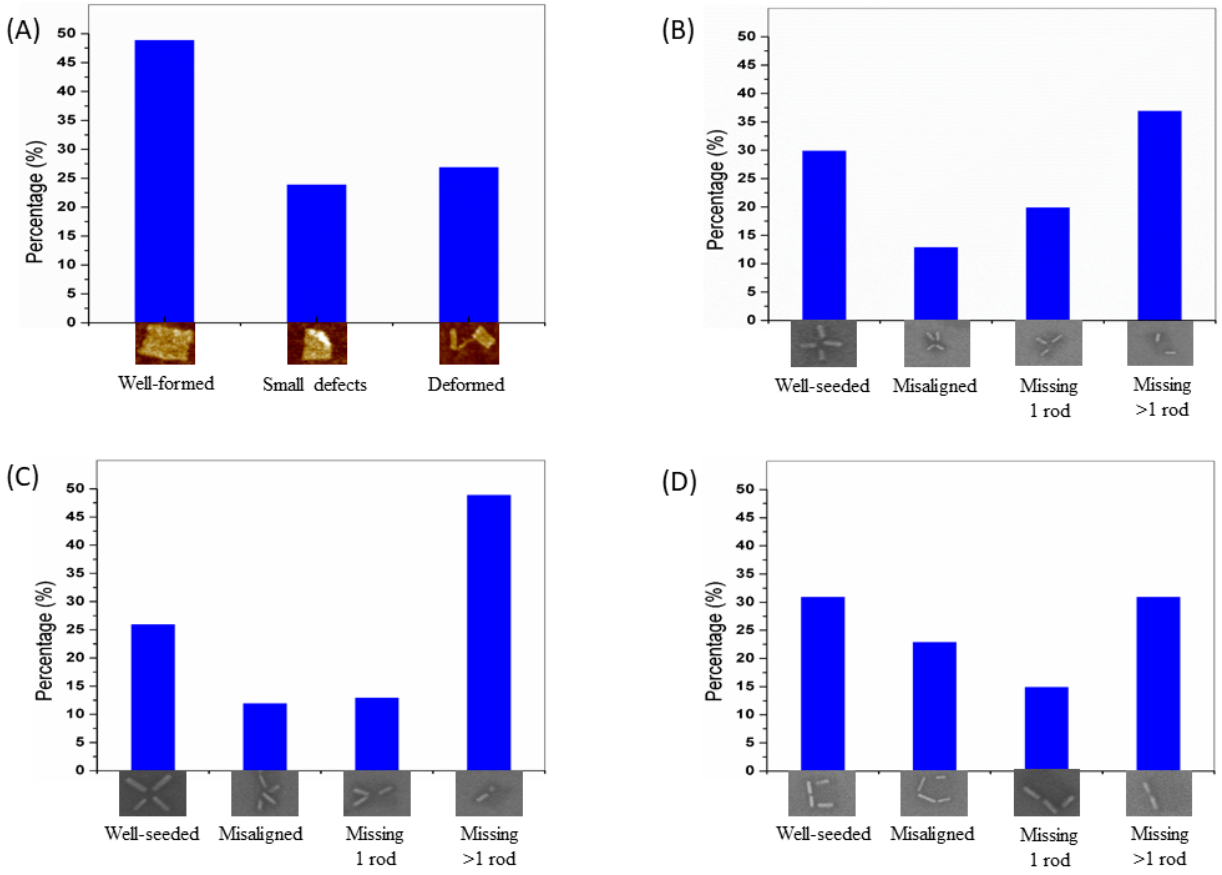

Figure 2.8 Yield percentages for unseeded and seeded tiles. (A) Tile DNA origami after deposition onto a Si wafer (n = 364). Yield results for (B) plus (n = 283), (C) cross (n = 318) and (D) C arrangements (n = 345) after seeding with Au nanorods.

I also determined the yield of seeded structures from the SEM images. **Figure 2.8B** shows the yield of seeded plus structures which were classified as 'well-seeded' (i.e., all four nanorod seeds were placed with the correct alignment), 'misaligned', 'missing 1 rod' or 'missing >1 rod'. The yield percentage for the well-seeded tiles was ~30%; however, >35% of the tiles were missing more than one Au nanorod. The yield of well-formed tiles on surfaces limits yields in subsequent

seeding steps, as well-seeded structures can only be generated on well-formed tiles. Tiles that have small defects are more likely to result in tiles with misaligned nanorods or with a missing nanorods. Similarly, structures missing more than one nanorod may result from deformed or poorly assembled tiles. **Figure 2.8C** gives the yield for different arrangements of Au nanorods in a cross structure. I found that 26% of the tiles had a well-seeded cross design with a similar percentage of tiles having a misaligned or a missing Au nanorod. For this design, nearly half of the tiles were missing more than one Au nanorod. **Figure 2.8D** shows the yield for C shapes on seeded tiles. Quantitative analysis of seeding results showed well-seeded C shapes for 31% of tiles, with over 20% of tiles having four Au nanorods, but with one misaligned. About 15% were missing one Au nanorod and over 30% were missing more than one nanorod. Overall, well-seeded yields for the three structures were similar (~30%). In contrast, overall yields for Au nanorod-seeded structures in the previous studies were <10%.[24] Since only 50% of tiles were well-formed and could thus result in well-seeded structures, the yield of correctly seeded structures from well-formed tiles could be considered as >60%, a major improvement over prior work with Au nanorod seeding.[24] These favorable yields for correctly seeded structures open up possibilities for studying plating and making electrical measurements.

My new tile designs for these three structures have better yields than those published earlier,[24] because of changes to the DNA origami design for the seeding step. The most important change was that I increased the number of attachment points for each Au nanorod on the tiles. Each Au nanorod attachment site on tiles had 2 or 3 rows of sticky end DNA sequences protruding (see **Figure 2.1**). In previous designs, 1 or 2 rows of sticky end DNA were provided for capturing DNA-functionalized Au nanorods. I compared the yields between one vs. two rows of attachment sites for the cross structure. For a single row of attachment points, the yield for well-seeded

structures was <5% (see **Figure 2.9**); importantly, two rows of attachment points improved yields to ~30% (**Figure 2.8**) as noted above.

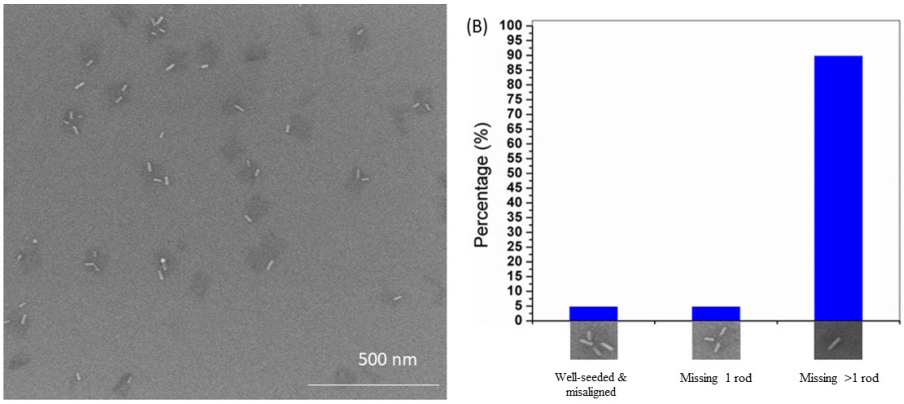

Figure 2.9 (A) SEM image of Au nanorod seeded cross structures on DNA tiles that have a single attachment sequence row for each Au nanorod. (B) Seedingyield of the cross structures in (A).

The seeded structures for plus, cross and C shapes were plated to connect the Au nanorods. **Figure 2.10A** shows a large area SEM image of plated plus structures in which the Au nanorods appear to be connected in most structures. **Figure 2.10B** contains zoomed-in plated plus structures without visible gaps in between nanorods. Comparing the seeded plus structures in **Figure 2.4(A-B)** with similar shapes after electroless deposition in **Figure 2.10(A-B)**, the gaps between Au nanorods are mostly filled in. Uprety et al.[24] previously observed that during plating, the Au nanorods grew anisotropically, with elongation about four times greater than widening. This anisotropic growth allowed the plated nanorods to fill the gaps and provide continuous structures. Similar to the plus structures, plated cross and C shapes (**Figures 2.10(C-D)** and **2.10(E-F)**, respectively) were also analyzed. The gaps between nanorods are largely filled in, as observed in the zoomed images with nanowires that appear connected, in contrast to the seeded structures in **Figure 2.4(C-F)**. For all three types of structures after plating, an increase occurred in width and length of plated nanorods. The widths of plated nanorods were measured (n = 25) from the three

types of structures, and the average was 11.3 ± 1.2 nm. Likewise, the end-to-end lengths of the C-shaped plated structures were measured on well-plated C shapes (n = 20), and the average (± standard deviation) was 127 ± 14 nm. The overall yield for plated plus, cross and C structures in zoomed SEM images that gave clear views was calculated (n = 76). Well-plated structures with no visible gaps in the SEM data comprised 39% of the total, whereas 61% of the structures had small gaps visible in the SEM images. C-shapes had the fewest observable gaps in the SEM data compared to plus and cross shapes; this trend is consistent with the smaller designed gap size in the C-shape DNA origami (see **Figure 2.1**). These overall yields for plated structures were improved compared to previous studies;[24] the improved yield is especially promising for electrical characterization, due to greater availability of well-plated structures on wafer surfaces.

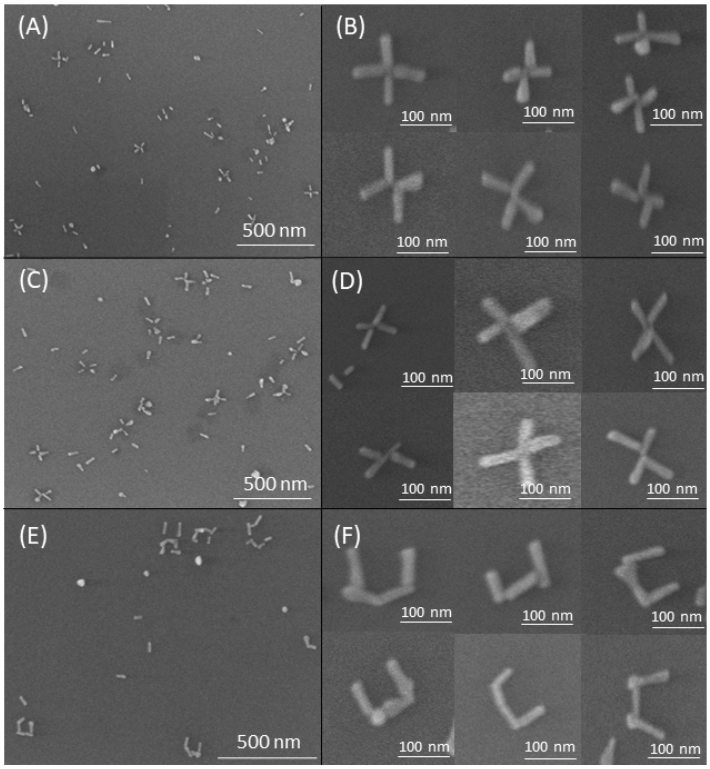

Figure 2.10 SEM images of plated structures. (A-B) plus shapes, (C-D) cross shapes, and (E-F) C shapes.

Upon completion of electroless plating on tiles, electrical characterization was performed to determine the continuity and conductance of the wires. EBID platinum traces were written to make contact to metallized DNA origami structures. Platinum traces with widths <25 nm were created, allowing four contacts to a single C-shape nanowire on a DNA origami tile (**Figure 2.11**). Indeed, this is the first work to perform four-point electrical characterization on nanowires on individual DNA origami tiles that are smaller than 100 nm x 100 nm.

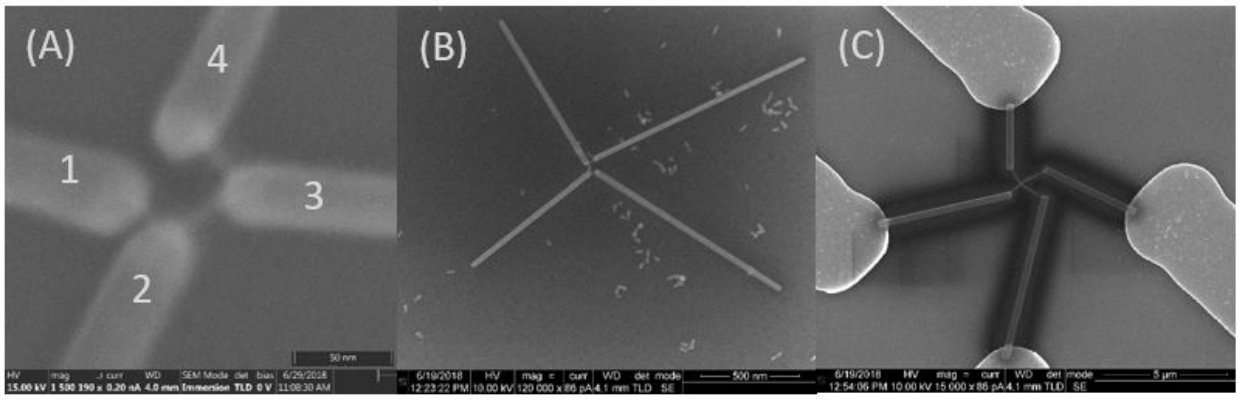

Figure 2.11 SEM images of EBID connections. (A) C-shaped Au nanowire with four distinct platinum contacts; two point measurements were performed using leads 1 and 4. When performing four point measurements leads 2 and 3 measured voltage. (B) Larger view of Pt contacts to nanowire. (C) Completed Pt pattern connecting the nanowire to Au pads.

EBID writing of conductive platinum wires has shortcomings that need to be taken into account in the characterization process. A key issue is that the as-written platinum is highly resistive. Thus, an EBID line can have a resistance >10 MΩ, making four-point measurement interpretation challenging as the lead resistance is comparable to the input resistance of the measurement device. This high resistance is due to the large amount of carbon that is co-deposited with the platinum.[45] The EBID metal purification technique of Geier et al.[45] reduces this problem to a major extent. I found post-purification EBID platinum lines to have resistances of ~100 kΩ,

multiple orders of magnitude less than the input resistance of the measurement hardware I used. However, this contact lead resistance still requires four point measurements.

To measure the resistance of metallized C-shape Au nanowires on DNA origami tiles, the input voltage was scanned from 0 to 1 V. **Figure 2.12A** shows a typical two point I-V curve, measured between leads 1 and 4 in **Figure 2.11A**. **Figure 2.12B** was obtained by measuring the voltage drop between the inner electrodes (leads 2 and 3 in **Figure 2.11A**) for each data point. Electrical resistances for five different C-shape nanowires on two separate Si wafers were characterized by both two- and four-point measurement as shown in **Table 2.1**. The two-point resistance was calculated by taking the slope of the IV curve while four point took the slope of the voltage drop vs current graph. To verify that leads two and three did not impact resistance measurements standalone two point measurements were conducted and gave similar values with and without leads two and three. The resistivities of the nanowires measured ranged from 0.124 to 4.24 x 10^{-5} Ω m. The 5 nanowires studied had widths of 10-20 nm, which are among the narrowest DNA templated Au nanowires characterized to date. These nanowires are more resistive than those made by Uprety et al.[19] who measured resistivities between 6.7 x 10^{-5} and 8.9 x 10^{-7} Ω m for Au nanowires with widths between 13-29 nm. Ongaro et al.[47] reported a resistivity of 10^{-4} Ω m for Au nanowires with a mean width of 40 nm, while Pearson et al.[17] reported 6.2 x 10^{-6} Ω m for 33 nm wide wires. Other values have been reported with lower resistivities but with larger widths.[48]

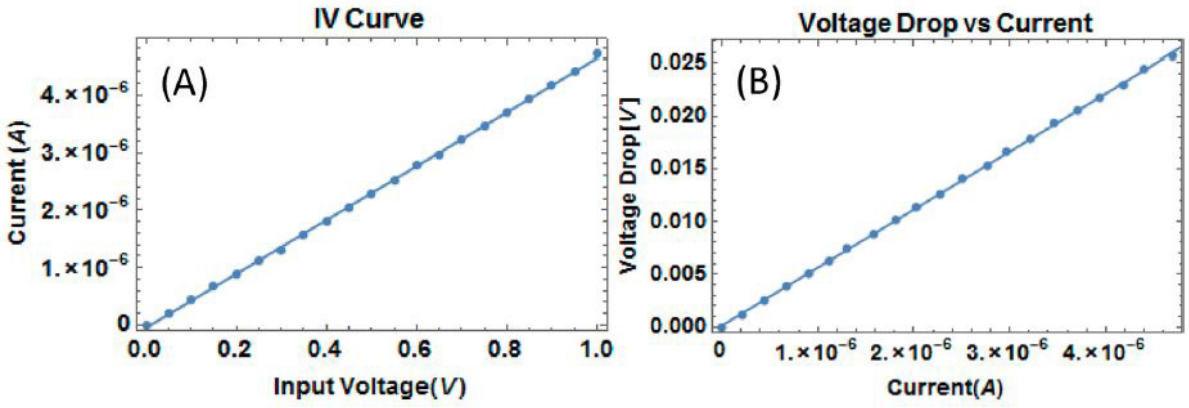

Figure 2.12 Four-point electrical characterization of a single nanowire on a DNA origami tile. (A) I-V curve from a C-shape nanowire with input voltages spanning 0 to 1 V. (B) Measured voltage drop between inner electrodes on the C shape.

Table 2.1 Two and four-point resistances as well as calculated resistivities for 5 different C-shape Au nanowires.

sample no.	two-point (MΩ)	four-point (MΩ)	resistivity (Ω m)
1	3.31	0.934	9.79×10^{-3}
2	1.01	0.0849	9.03×10^{-4}
3	273	11.7	0.124
4	76.4	2.61	0.0283
5	0.221	0.00558	4.24×10^{-5}

Possible reasons for the higher resistivity values reported here (compared to other publications) include the smaller nanowire diameters in this study, and differences in the processing of the nanowires after electroless plating. Electron beam lithography patterning has a resist prebake step that Uprety et al.[19] found caused a change in the morphology of the nanowires. This morphological change appeared to smooth edges, reducing surface roughness and potentially resulting in fewer gaps or lower conduction barriers between grains, which would increase conductivity. Importantly, EBID allows electrical measurements on as-formed nanowires. Furthermore, since EBID is a direct write technique, it allows facile connection to randomly

oriented structures, and the <25 nm width traces enable multiple connections to ~100 nm scale devices.

2.5 CONCLUSION

In this chapter, I have examined the fabrication yield and electrical properties of different Au nanowire structures created on DNA origami tiles by site-specific attachment of Au nanorods to molecularly programmed sites. A careful assessment of the structures formed showed that yields of plated nanowires were limited to a degree by the seeding process. Consequently, additional attachment sites were added to the DNA tiles to provide more effective linking of DNA-functionalized Au nanorods to the desired sites. As a result, the measured yields improved by a factor of six over recently published studies. The improved yields combined with anisotropic plating on the Au nanorods enabled successful fabrication of the desired nanowire structures. In addition, I demonstrated, for the first time, the ability to perform a four-point resistance measurement on an individual metal nanostructure formed on a single 70 nm x 90 nm DNA origami tile. The measurement was made possible through the use of electron beam induced deposition to form conductive connecting leads to the Au nanowire. Electrical measurements on thin C-shaped Au nanowires 130 nm long and 10 nm in diameter with 40 nm spacing between measurement points were carried out, and nanowires were found to have resistivities as low as 4.24×10^{-5} Ω m.

These advances offer great promise for future nanoelectronics studies on biological templates. Subsequent work on the reproducibility and scalability of bottom-up nanofabrication of conductive inorganic nanostructures should be feasible with this new toolset. Additionally, it may be possible to study the effects of sample preparation processes on nanowire electrical properties. Finally, this platform provides opportunities for electrical characterization of more complex self-

assembled nanostructures involving junctions between different materials, an important endeavor for future studies.

2.6 REFERENCES

1. Biswas, A.; Bayer, I. S.; Biris, A. S.; Wang, T.; Dervishi, E.; Faupel, F., Advances in top–down and bottom–up surface nanofabrication: Techniques, applications & future prospects. *Adv. Colloid Interface Sci.* **2012,** *170* (1-2), 2-27.

2. Qin, D.; Xia, Y.; Whitesides, G. M., Soft lithography for micro- and nanoscale patterning. *Nat. Protoc.* **2010,** *5* (3), 491-502.

3. Austin, M. D.; Ge, H.; Wu, W.; Li, M.; Yu, Z.; Wasserman, D.; Lyon, S. A.; Chou, S. Y., Fabrication of 5nm linewidth and 14nm pitch features by nanoimprint lithography. *Appl. Phys. Lett.* **2004,** *84* (26), 5299-5301.

4. Cheng, J. Y.; Ross, C.; Chan, V. H.; Thomas, E. L.; Lammertink, R. G.; Vancso, G. J., Formation of a cobalt magnetic dot array via block copolymer lithography. *Adv. Mater.* **2001,** *13* (15), 1174-1178.

5. Mijatovic, D.; Eijkel, J. C.; van den Berg, A., Technologies for nanofluidic systems: top-down vs. bottom-up—a review. *Lab on a Chip* **2005,** *5* (5), 492-500.

6. Ozin, G. A.; Hou, K.; Lotsch, B. V.; Cademartiri, L.; Puzzo, D. P.; Scotognella, F.; Ghadimi, A.; Thomson, J., Nanofabrication by self-assembly. *Mater. Today* **2009,** *12* (5), 12-23.

7. Li, H.; Carter, J. D.; LaBean, T. H., Nanofabrication by DNA self-assembly. *Mater. Today* **2009,** *12* (5), 24-32.

8. Nummelin, S.; Kommeri, J.; Kostiainen, M. A.; Linko, V., Evolution of structural DNA nanotechnology. *Adv. Mater.* **2018**, 1703721.

9. Douglas, S. M.; Dietz, H.; Liedl, T.; Hogberg, B.; Graf, F.; Shih, W. M., Self-assembly of DNA into nanoscale three-dimensional shapes. *Nature* **2009,** *459* (7245), 414-418.

10. Xu, A.; Harb, J. N.; Kostiainen, M. A.; Hughes, W. L.; Woolley, A. T.; Liu, H.; Gopinath, A., DNA Origami: The Bridge from Bottom to Top. *MRS Bull.* **2017,** *42*, 943-950.

11. Kuzyk, A.; Jungmann, R.; Acuna, G. P.; Liu, N., DNA Origami Route for Nanophotonics. *ACS Photonics* **2018,** *5* (4), 1151-1163.

12. Tørring, T.; Voigt, N. V.; Nangreave, J.; Yan, H.; Gothelf, K. V., DNA origami: a quantum leap for self-assembly of complex structures. *Chem. Soc. Rev.* **2011,** *40* (12), 5636-5646.

13. Jones, M. R.; Seeman, N. C.; Mirkin, C. A., Programmable materials and the nature of the DNA bond. *Science* **2015,** *347* (6224), 1260901.

14. LaBean, T. H.; Li, H., Constructing novel materials with DNA. *Nano Today* **2007,** *2* (2), 26-35.

15. Rothemund, P. W., Folding DNA to create nanoscale shapes and patterns. *Nature* **2006,** *440* (7082), 297-302.

16. Douglas, S. M.; Dietz, H.; Liedl, T.; Hogberg, B.; Graf, F.; Shih, W. M., Self-assembly of DNA into nanoscale three-dimensional shapes. *Nature* **2009,** *459* (7245), 414-418.

17. Wang, P.; Meyer, T. A.; Pan, V.; Dutta, P. K.; Ke, Y., The Beauty and Utility of DNA Origami. *Chem* **2017,** *2* (3), 359-382.

18. Mohammed, A. M.; Schulman, R., Directing self-assembly of DNA nanotubes using programmable seeds. *Nano Lett* **2013,** *13* (9), 4006-13.

19. Uprety, B.; Westover, T.; Stoddard, M.; Brinkerhoff, K.; Jensen, J.; Davis, R. C.; Woolley, A. T.; Harb, J. N., Anisotropic Electroless Deposition on DNA Origami Templates To Form Small Diameter Conductive Nanowires. *Langmuir* **2017,** *33* (3), 726-735.

20. Wang, F.; Liu, X.; Willner, I., DNA switches: from principles to applications. *Angew. Chem. Int. Ed.* **2015,** *54* (4), 1098-1129.

21. Sherman, W. B.; Seeman, N. C., A precisely controlled DNA biped walking device. *Nano lett.* **2004,** *4* (7), 1203-1207.

22. Seelig, G.; Soloveichik, D.; Zhang, D. Y.; Winfree, E., Enzyme-free nucleic acid logic circuits. *Science* **2006,** *314* (5805), 1585-1588.

23. Ke, Y.; Ong, L. L.; Shih, W. M.; Yin, P., Three-dimensional structures self-assembled from DNA bricks. *Science* **2012,** *338* (6111), 1177-1183.

24. Uprety, B.; Jensen, J.; Aryal, B. R.; Davis, R. C.; Woolley, A. T.; Harb, J. N., Directional Growth of DNA-Functionalized Nanorods to Enable Continuous, Site-Specific Metallization of DNA Origami Templates. *Langmuir* **2017,** *33* (39), 10143-10152.

25. Geng, Y.; Pearson, A. C.; Gates, E. P.; Uprety, B.; Davis, R. C.; Harb, J. N.; Woolley, A. T., Electrically conductive gold- and copper-metallized DNA origami nanostructures. *Langmuir* **2013,** *29* (10), 3482-90.

26. Pearson, A. C.; Liu, J.; Pound, E.; Uprety, B.; Woolley, A. T.; Davis, R. C.; Harb, J. N., DNA origami metallized site specifically to form electrically conductive nanowires. *J Phys Chem B* **2012,** *116* (35), 10551-60.

27. Chen, Z.; Liu, C.; Cao, F.; Ren, J.; Qu, X., DNA metallization: principles, methods, structures, and applications. *Chem Soc Rev* **2018**.

28. Liu, J.; Geng, Y.; Pound, E.; Gyawali, S.; Ashton, J. R.; Hickey, J.; Woolley, A. T.; Harb, J. N., Metallization of branched DNA origami for nanoelectronic circuit fabrication. *Acs Nano* **2011,** *5* (3), 2240-2247.

29. Uprety, B.; Gates, E. P.; Geng, Y.; Woolley, A. T.; Harb, J. N., Site-specific metallization of multiple metals on a single DNA origami template. *Langmuir* **2014,** *30* (4), 1134-41.

30. Helmi, S.; Ziegler, C.; Kauert, D. J.; Seidel, R., Shape-controlled synthesis of gold nanostructures using DNA origami molds. *Nano Lett.* **2014,** *14* (11), 6693-6698.

31. Bayrak, T.; Helmi, S.; Ye, J.; Kauert, D.; Kelling, J.; Schonherr, T.; Weichelt, R.; Erbe, A.; Seidel, R., DNA-Mold Templated Assembly of Conductive Gold Nanowires. *Nano Lett.* **2018,** *18* (3), 2116-2123.

32. Pilo-Pais, M.; Goldberg, S.; Samano, E.; Labean, T. H.; Finkelstein, G., Connecting the nanodots: programmable nanofabrication of fused metal shapes on DNA templates. *Nano Lett* **2011,** *11* (8), 3489-92.

33. Shen, B.; Linko, V.; Tapio, K.; Kostiainen, M. A.; Toppari, J. J., Custom-shaped metal nanostructures based on DNA origami silhouettes. *Nanoscale* **2015,** *7* (26), 11267-72.

34. Watson, S. M.; Wright, N. G.; Horrocks, B. R.; Houlton, A., Preparation, characterization and scanned conductance microscopy studies of DNA-templated one-dimensional copper nanostructures. *Langmuir* **2010,** *26* (3), 2068-75.

35. Monson, C. F.; Woolley, A. T., DNA-templated construction of copper nanowires. *Nano letters* **2003,** *3* (3), 359-363.

36. Arora, A. A.; de Silva, C., Beyond the smiley face: applications of structural DNA nanotechnology. *Nano Rev. Exp.* **2018,** *9* (1), 1430976.

37. Geng, Y.; Liu, J.; Pound, E.; Gyawali, S.; Harb, J. N.; Woolley, A. T., Rapid metallization of lambda DNA and DNA origami using a Pd seeding method. *J. Mater. Chem.* **2011,** *21* (32), 12126.

38. Richter, J.; Seidel, R.; Kirsch, R.; Mertig, M.; Pompe, W.; Plaschke, J.; Schackert, H. K., Nanoscale palladium metallization of DNA. *Adv. Mater.* **2000,** *12* (7), 507-510.

39. Liu, J.; Uprety, B.; Gyawali, S.; Woolley, A. T.; Myung, N. V.; Harb, J. N., Fabrication of DNA-templated Te and Bi2Te3 nanowires by galvanic displacement. *Langmuir* **2013,** *29* (35), 11176-84.

40. Eskelinen, A. P.; Kuzyk, A.; Kaltiaisenaho, T. K.; Timmermans, M. Y.; Nasibulin, A. G.; Kauppinen, E. I.; Torma, P., Assembly of single-walled carbon nanotubes on DNA-origami templates through streptavidin-biotin interaction. *Small* **2011,** *7* (6), 746-50.

41. Xin, H.; Woolley, A. T., DNA-Templated Nanotube Localization. *J Am Chem Soc* **2003,** *125*, 8710-8711.

42. Ali, M. R.; Snyder, B.; El-Sayed, M. A., Synthesis and optical properties of small Au nanorods using a seedless growth technique. *Langmuir* **2012,** *28* (25), 9807-15.

43. Liu, K.; Zheng, Y.; Lu, X.; Thai, T.; Lee, N. A.; Bach, U.; Gooding, J. J., Biocompatible gold nanorods: one-step surface functionalization, highly colloidal stability, and low cytotoxicity. *Langmuir* **2015,** *31* (17), 4973-80.

44. van Dorp, W. F.; Hagen, C. W., A critical literature review of focused electron beam induced deposition. *J. Appl. Phys.* **2008,** *104* (8), 081301.

45. Geier, B.; Gspan, C.; Winkler, R.; Schmied, R.; Fowlkes, J. D.; Fitzek, H.; Rauch, S.; Rattenberger, J.; Rack, P. D.; Plank, H., Rapid and Highly Compact Purification for Focused Electron Beam Induced Deposits: A Low Temperature Approach Using Electron Stimulated H2O Reactions. *J. Phys Chem. C* **2014,** *118* (25), 14009-14016.

46. Woo, S.; Rothemund, P. W., Self-assembly of two-dimensional DNA origami lattices using cation-controlled surface diffusion. *Nature Commun.* **2014,** *5*, 4889.

47. Ongaro, A.; Griffin, F.; Beecher, P.; Nagle, L.; Iacopino, D.; Quinn, A.; Redmond, G.; Fitzmaurice, D., DNA-Templated Assembly of Conducting Gold Nanowires between Gold Electrodes on a Silicon Oxide Substrate. *Chem. Mater.* **2005,** *17* (8), 1959-1964.

48. Satti, A.; Aherne, D.; Fitzmaurice, D., Analysis of Scattering of Conduction Electrons in Highly Conducting Bamboolike DNA-Templated Gold Nanowires. *Chem. Mater.* **2007,** *19* (7), 1543-1545.

CHAPTER 3: DNA ORIGAMI MEDIATED ELECTRICALLY CONNECTED METAL-SEMICONDUCTOR JUNCTIONS[††]

3.1 ABSTRACT

DNA-based nanofabrication of inorganic nanostructures has potential application in electronics, catalysis, and plasmonics. Previous DNA metallization has generated conductive DNA-assembled nanostructures; however, the use of semiconductors and the development of well-connected nanoscale metal-semiconductor junctions on DNA nanostructures are still at an early stage. Herein, I report the first fabrication of multiple electrically connected metal-semiconductor junctions on individual DNA origami by location-specific binding of gold and tellurium nanorods. Nanorod attachment to DNA origami was via DNA hybridization for Au and by electrostatic interaction for Te. Electroless gold plating was used to create nanoscale metal-semiconductor interfaces by filling the gaps between Au and Te nanorods. Two-point electrical characterization indicated that the Au-Te-Au junctions were electrically connected, with current-voltage properties consistent with a Schottky junction. DNA-based nanofabrication of metal-semiconductor junctions opens up potential opportunities in nanoelectronics, demonstrating the power of this bottom-up approach.

3.2 INTRODUCTION

The study of metal-semiconductor junctions remains an active area of research [1, 2]; depending on properties, Schottky or Ohmic junctions are formed, influencing electrical characteristics [3-5]. Conventional semiconductor fabrication requires costly technology and a

[††] This chapter is reprinted with permission from Aryal, B. R.; Ranasinghe, D. R.; Westover, T. R.; Calvopiña, D. G.; Davis, R. C.; Harb, J. N.; Woolley, A. T. *Nano Res.* **2020**, *13* (5), 1419-1426.

cleanroom environment. Thus, the appeal is increasing for alternative approaches, such as molecularly directed placement of materials on self-assembled DNA nanostructures, wherein various geometries are possible with potential to create 3D designs.

DNA-based nanofabrication is a versatile bottom-up approach that utilizes the base-pairing properties of DNA to scalably produce nanoscale patterns on substrates [6-8]. In particular, DNA origami [9] is a powerful nanofabrication technology; it has been nearly a decade since DNA origami templates were first demonstrated as robust and convenient substrates for binding inorganic nanoparticles and electrochemically creating continuous metal structures [10]. Since then, DNA origami metallization has generated various patterns of nanowires in diverse structures with applications in catalysis, sensing, and biomedical engineering [11]. A wide range of materials such as Au [10, 12-14], Ag [15, 16], Cu [14] and carbon nanotubes [17, 18] have been deposited on DNA origami to generate conductive nanostructures or nanowires. For the formation of nanowires, nanoparticles are attached to designated locations on DNA substrates, and then connected through plating.

Multiple researchers have fabricated different-shaped Au nanowires on DNA origami, followed by their electrical characterization. Uprety et al. [12] created ~400 nm long, ~10 nm wide gold nanowires on DNA origami by connecting Au nanorods; they then measured the electrical conductivity. Bayrak et al. [19] utilized assembled DNA to act as a mold to fabricate conductive gold nanowires; electrical characterization was performed between 4.2 K and room temperature. Aryal et al. [20] fabricated gold nanowires on 70 nm x 90 nm DNA origami tiles by site-specific attachment of Au nanorods, followed by plating. They also performed four-point electrical measurements on C-shaped gold nanowires (~130 nm long with a width of ~10 nm) and reported resistivities as low as 4.24 x 10^{-5} Ωm. Ye et al. [6] described a method to fabricate gold nanostructures by using a

modular DNA platform; however, they did not show electrical characterization. These papers demonstrate the potential for using DNA to assemble conductive nanomaterials.

A key next step in developing nanoelectronic devices is the creation of metal-semiconductor junctions self-assembled on DNA. Indeed, Weichelt et al. [21] recently formed metal-semiconductor heterostructures by hybridizing DNA-functionalized CdS nanorods to self-assembled DNA molds preloaded with Au nanoparticles and electrochemically plating the Au nanoparticles to connect to the CdS nanorods; however, electrical characterization was not performed.

Tellurium is a p-type semiconductor with narrow bandgap energy (0.35 eV) and unique properties; it is photoconductive, thermoelectric, photoelectric, piezoelectric, and has non-linear optical properties [22, 23]. Tellurium has been used in solar panel manufacturing, as it forms compounds that demonstrate increased electrical conductivity when combined with elements such as Cd [24]. Several approaches have been utilized for Te nanostructure synthesis, such as hydrothermal reduction [22, 25], microwave-assisted methods [26], vacuum vapor deposition [27], sublimation-condensation [28], and refluxing [29]. Here, I performed a simple chemical synthesis of Te nanorods using a procedure adapted from published work [23].

In this chapter, I present the fabrication and characterization of gold-tellurium-gold nanowire junctions on individual DNA origami as outlined schematically in **Figure 3.1**. DNA-functionalized Au nanorods were bound to designed locations on DNA origami, followed by the placement of individual cetyltrimethylammonium bromide (CTAB)-coated Te nanorods into the gaps between Au nanorods. Electroless plating selectively lengthened the Au nanorods to Te nanorod edges to form Au-Te-Au junctions. I performed two-point electrical characterization of multiple Au-Te-Au structures to check electrical continuity. The I-V curves for Au-Te-Au

structures show electrical conductivity with Schottky junction characteristics. The formation of well-connected metal-semiconductor junctions on DNA origami templates is an important advance toward creating DNA-assembled nanodevices.

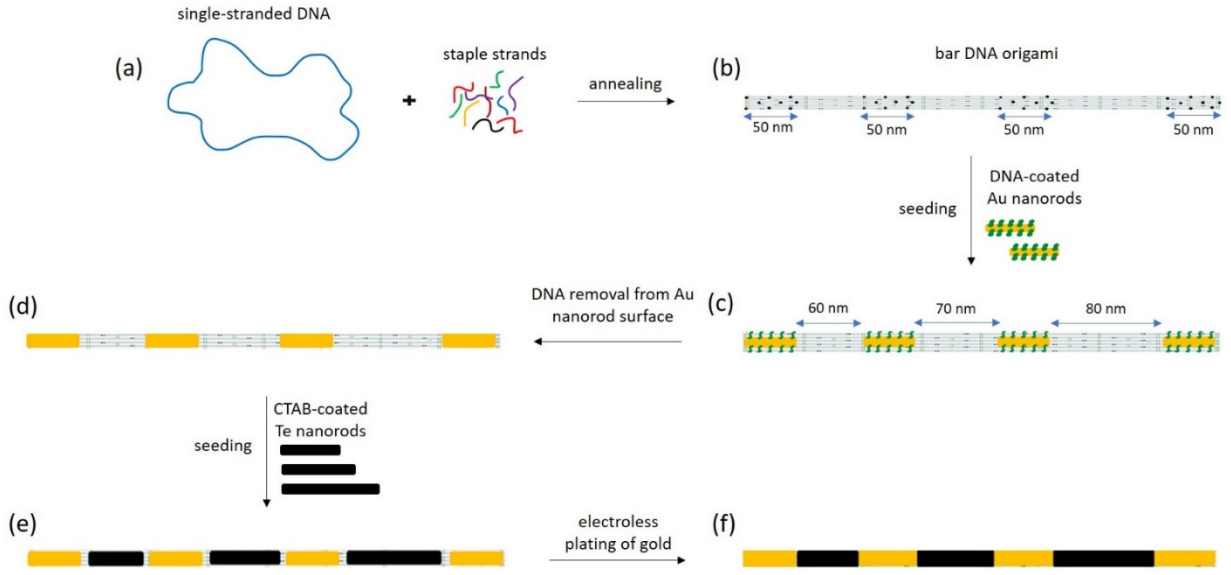

Figure 3.1 Schematic diagram of the creation of Au-Te-Au junctions. (a) Folding single-stranded M13mp18 DNA with staple strands to form (b) bar DNA origami; black dots represent protruding sticky-ends that facilitate DNA-functionalized Au nanorod hybridization. (c) Site-specific hybridization of Au nanorods on DNA origami with nonidentical gaps. (d) Au nanorods after treatment with plating solution to remove DNA from their surfaces. (e) Placement of CTAB-coated Te nanorods into the gaps. (f) Multiple Au-Te-Au junctions after electroless plating of gold.

3.3 EXPERIMENTAL SECTION

3.3.1 Chemicals and Materials

M13mp18 single-stranded DNA was purchased from New England Biolabs (Ipswich, MA). For DNA origami formation, synthetic staple strands (22-46 bases), with or without 10 additional protruding adenines, were obtained from Eurofins MWG Operon (Huntsville, AL). Single-stranded poly T DNA with a thiol group attached to the 5' end (8-mer, gel purified) was obtained from Eurofins MWG Operon. In order to attach DNA oligonucleotides to Au nanorods,

the dry poly T DNA was dissolved and diluted to 1 mM in water. Ethylenediaminetetraacetic acid (EDTA) was purchased from Life Technologies (Carlsbad, CA). Tris(hydroxymethyl)aminomethane (Tris base), ascorbic acid and sodium chloride were obtained from Fisher Scientific (Fair Lawn, NJ). Acetic acid, hydrochloric acid, magnesium chloride, and magnesium acetate ($MgAc_2.4H_2O$) were obtained from EMD Chemicals (Gibbstown, NJ). TAE-Mg^{2+} buffer (10X, pH 8.3) was prepared using 400 mM Tris base, 200 mM acetic acid, 10 mM EDTA, and 125 mM $MgAc_2.4H_2O$. CTAB (H5882, 98%), $HAuCl_4$, 1-methyl-2-pyrrolidinone (NMP), Te powder (99.8%) and Tween 20 were obtained from Sigma-Aldrich (St. Louis, MO). Silver nitrate was purchased from Mallinckrodt Chemicals (Philipsburg, NJ). $NaBH_4$ was obtained from EMD Millipore (Burlington, MA). Tris(2-carboxyethyl)phosphine (TCEP) was acquired from Alfa Aesar (Ward Hill, MA). Bis(p-sulfonatophenyl)phenylphosphine dihydrate dipotassium salt (BSPP) was purchased from Strem Chemicals (Newburyport, MA). GoldEnhance EM solution was obtained from Nanoprobes (Yaphank, NY). For solution preparation and sample rinsing, water (18.3 MΩ) was processed with a Barnstead EASYpure UV/UF purification system (Dubuque, IA).

3.3.2 Gold Nanorod Synthesis and DNA-Gold Nanorod Conjugation

Gold nanorods were synthesized following a published method [30], except I decreased the $NaBH_4$ concentration from 9.6 μM to 2.5 μM in the reaction mixture to create ~50 nm long nanorods. For coating DNA on Au nanorods, I followed reported methods [20, 31]. However, concentrations of Tween 20, BSPP and DNA were increased to 0.1%, 6.8 mM and 0.1 mM, respectively, in 300 μL total mixture solution. The molar ratio of thiol DNA to Au nanorods was ~250:1.

3.3.3 Tellurium Nanorod Synthesis and Characterization

Tellurium nanorods were synthesized using Te powder, CTAB, and $NaBH_4$. First, 2.5 g CTAB was dissolved in 40 mL water at 60 °C with slight stirring from a magnetic bar. Then, 1 mg Te powder was added to the CTAB solution, followed by the addition of 20 mg $NaBH_4$, after which the solution was stirred vigorously for 5 sec and then kept undisturbed at 60 °C for 100 min. The CTAB-coated tellurium nanorods were collected by centrifugation of the growth solution and were characterized by scanning electron microscopy (SEM) after deposition on thermally oxidized Si wafer sections with DNA origami attached (see Section 2.4). For Te nanorod synthesis, CTAB provides a cationic surfactant, which both directs Te nanorod growth and stabilizes the nanorods after synthesis by forming a double layer on the Te nanorod surfaces, resulting in a net positive surface charge on the nanorods. Energy dispersive X-ray (EDX) spectroscopy was used to confirm the chemical composition of the nanorods.

3.3.4 DNA Origami Design, Folding and Deposition onto Oxidized Silicon Wafers

Bar DNA origami was made from M13mp18 single-stranded DNA, adapted from my previous work [20]. For the attachment of DNA-functionalized Au nanorods, staple strands with 10 additional adenine bases were extended from the DNA origami as sticky-end sequences, whereas no protruding DNA was designed in the CTAB-coated Te nanorod binding region (Fig. 1). The three Te nanorod binding regions were designed with nonidentical sizes to study the fundamentals of seeding and allow for localization of different sizes of nanorods, since their size distribution was not monodisperse. For folding of bar DNA origami, a 100 µL solution containing M13mp18 single-stranded DNA (2 nM) and staple strands (40 nM) was heated initially to 95 °C and cooled to 4 °C in a TC-3000 thermal cycler (Techne, Burlington, NJ) for 1.5 hr. All staple strand sequences are given in Appendix A. Oxidized Si wafer squares (1x1 cm^2) were cleaned in a plasma

asher (Harrick, PDC-32G, Ithaca, NY) for 1 min at 18 W. Then, bar DNA origami (4 µL, 1 nM) in 10x TAE-Mg^{2+} buffer was deposited onto the plasma-cleaned, oxidized Si wafer sections in a humid chamber for 20 min at room temperature. Finally, the wafer pieces with bar DNA origami attached were rinsed with distilled water for 5 sec and dried with flowing air for 1-2 sec.

3.3.5 Localizing Gold and Tellurium Nanorods on DNA Origami

Au and Te nanorod attachment were each performed sequentially in separate steps. Au nanorod binding was started by depositing as-prepared DNA-functionalized Au nanorods in solution (20 µL) onto a Si substrate with DNA origami previously deposited, and incubating in a humidified chamber for 1 hr. The samples were then rinsed slowly with distilled water and dried under gentle flow of dry air. I treated the Au-seeded DNA with 40 µL of GoldEnhance EM plating solution for 25 sec to remove thiol-modified DNA from Au nanorods [32]. The samples were subsequently rinsed with distilled water and dried with air. Finally, Te nanorod placement was completed by placing 20 µL of as-prepared Te nanorod solution on the gold nanorod seeded DNA samples immediately after synthesis of CTAB-coated Te nanorods and storing in a humid chamber for 1 hr. Rinsing and drying steps were the same as those used for Au nanorod binding.

3.3.6 Electroless Plating to Form Electrically Connected Structures

Plating followed a published method [12], except HCl was not used in the gold plating solution, to increase plating rate since low pH slows gold deposition [30]. In brief, plating was performed by placing 50 µL of gold plating solution onto the surface of a Si substrate where DNA had previously been deposited and seeded with Au and Te nanorods. Plating was performed for 1 min in a water bath at 25 °C to maintain temperature and prevent CTAB precipitation. Following plating, the samples were rinsed with water and then dried in a flowing air stream for 1-2 sec.

3.3.7 Atomic Force Microscopy (AFM) Imaging

A MultiMode atomic force microscope (Bruker, Santa Barbara, CA) with ScanAsyst automatic image optimization and Peak Force tapping mode was used to image bar DNA origami that had been deposited on the surface. Bruker silicon tips on nitride cantilevers (ScanAsyst-Air and ScanAsyst-Air-HD) were used for imaging.

3.3.8 SEM Imaging

Seeded and plated DNA samples were imaged by SEM in ultrahigh-resolution mode on a FEI Helios Nanolab 600 or on a Thermo Verios UC G4 SEM. The small yellow '+' sign in some SEM images indicates the center of the initially captured image.

3.3.9 Electrical Contacts

Electrical contacts were patterned onto the surface according to a published procedure [20]. In brief, photolithography was done on 1x1 cm^2 silicon chips using hexamethyldisilazane adhesion promotor and AZ3312 photoresist (Merck kGaA). After a 1 min bake, the samples were exposed in a Karl Suss MA150 contact aligner for 5 sec and developed in AZ300MIF (Merck kGaA). This process formed 100 µm patterned holes in a 1 µm thick photoresist layer. Next, 7 nm of chromium was deposited in a thermal evaporator as an adhesion layer, followed by deposition of 50 nm of gold to form the desired contact pads. The sample substrate was then immersed in NMP in an ultrasonic bath for 10 min to lift off the remaining photoresist. After liftoff, samples were rinsed with distilled water for 5 sec and dried with nitrogen. To connect to the metallized DNA structures, ~25 nm wide x 200 nm tall platinum traces were written using a line dose setting of 5 kV and 0.17 nA for electron-beam induced deposition (EBID) of platinum in the Helios Nanolab SEM. Larger Pt lines, 100 nm wide and 250 nm high, were written using an area dose setting at 5 kV and 0.34 nA to link the small platinum traces to the gold pads. Deposited platinum was purified [20, 33] by

exposure to an electron beam under low vacuum in an Apreo SEM (Thermo) for 10 min/μm^2 at 0.5 torr.

3.3.10 Electrical Measurement

A micromanipulator probe station was utilized to connect to the gold pads for current vs. voltage (I-V) studies; current was measured using a DL Instruments 1211 current preamplifier. A National Instruments DAQ and custom LabVIEW program were used to collect data for applied voltages from either 0 V to +10 V or from –10 V to + 10 V.

3.4 RESULTS AND DISCUSSION

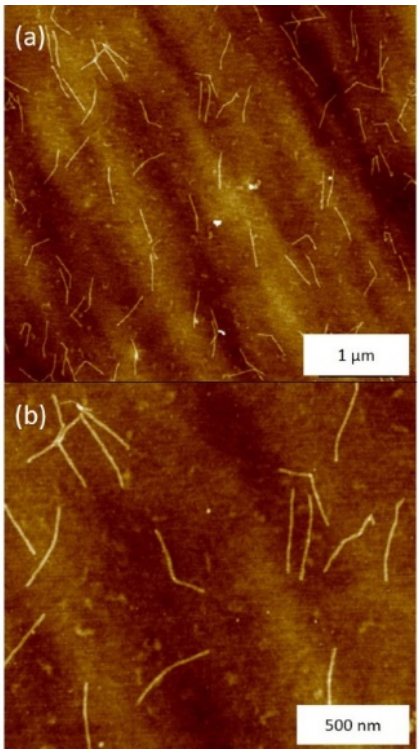

Figure 3.2 AFM images of bar DNA origami. (a) Large area and (b) zoomed in image. Height scale is 5 nm.

I used DNA origami as a template to enable the formation of multiple Au-Te-Au junctions in a single connected "wire." Successful assembly of the template was confirmed by AFM

following deposition of the DNA onto a Si substrate (**Figure 3.2**). The DNA origami template was designed to be ~400 nm long with a ~17 nm width. Individual bar DNA origami are clearly seen in the zoomed-in image, **Figure 3.2b**. While most of the templates are properly formed, some have twisted or bent shapes, possibly due to inherent strain or improper landing [9, 20].

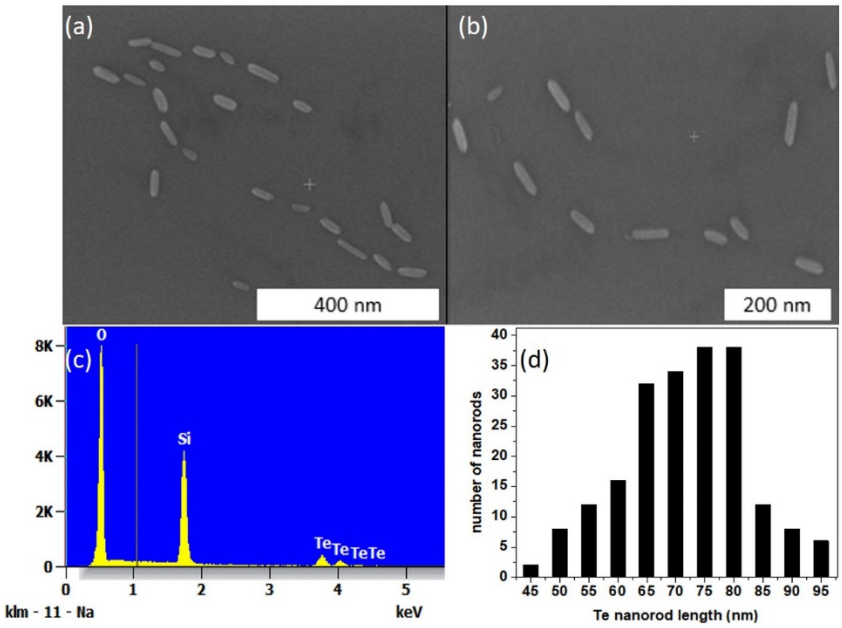

Figure 3.3 Tellurium nanorod characterization. (a-b) SEM images of tellurium nanorods deposited on bar DNA origami on thermally oxidized Si. (c) EDX analysis of tellurium nanorods on thermally oxidized Si. (d) Length distribution histogram of Te nanorods (n = 204).

To create Au-Te-Au junctions, I developed a procedure for synthesis of Te nanorods <100 nm long. I used CTAB in the synthesis because nanorods coated with CTAB interact electrostatically with DNA. **Figure 3.3(a-b)** shows individual tellurium nanorods attached to bar DNA origami on an oxidized Si surface. The EDX spectrum in **Figure 3.3c** shows the relative abundance of elements; oxygen and silicon signals came from the oxidized Si substrate, and the tellurium peaks indicate the presence of tellurium from the nanorods. The vertical line between the oxygen and silicon peaks indicates the position where sodium signal would appear if present. The

absence of a sodium peak indicates that the nanorods are not an intermediate product such as NaHTe or Na_2Te, which have been described in the literature [23, 34]. **Figure 3.3d** provides length distribution data for the Te nanorods, revealing that the majority of nanorods had lengths between 60 nm to 85 nm, but nanorods outside of this range were also present. The average length (± standard deviation) of Te nanorods was 72 ± 15 nm, with a width of 21 ± 3 nm.

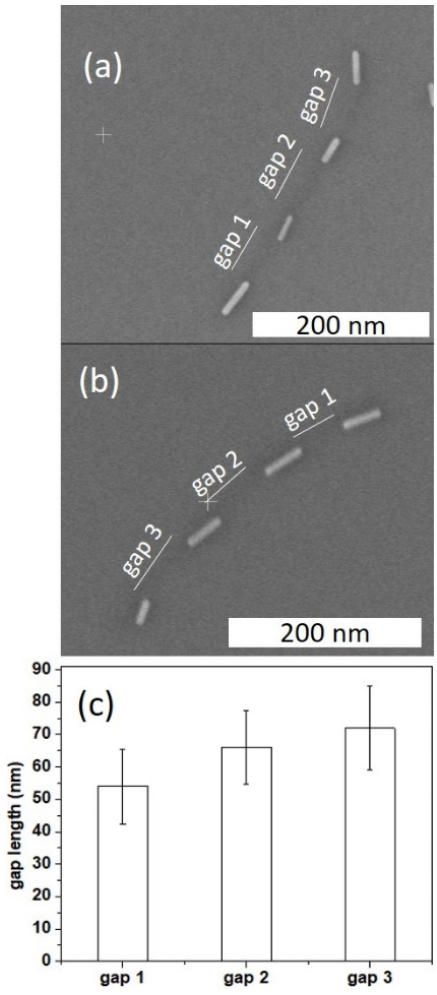

Figure 3.4 Site-specific binding of Au nanorods to bar DNA origami. (a-b) SEM images where bright features are gold nanorods and the darker features are the DNA; the 3 gaps between Au nanorods are indicated. (c) Gap distribution analysis histogram (n = 43 for each gap type); bars are mean and error bars are standard deviation.

Position-selective placement of nanorods is essential to the formation of Au-Te junctions on DNA templates. The next step after template assembly was site-specific attachment of Au nanorods to the DNA origami as shown schematically in **Figure 3.1c**. The results in **Figure 3.4** demonstrate attachment of DNA-functionalized Au nanorods through complementary sequence hybridization to protruding sequences in the bar DNA origami, resulting in nonidentical gaps consistent with the design in **Figure 3.1**. Additional SEM images of Au-seeded origami are given in **Figure 3.5**. The underlying DNA template is evident as darker segments between the Au nanorods. The average length of the Au nanorods (n= 64) was 44 ± 9 nm. The three gaps in Au nanorod-seeded bar DNA origami are referred to as gap 1, gap 2, and gap 3, representing anticipated 60, 70, and 80 nm gap lengths, respectively (see **Figure 3.1**). As expected, three gaps of increasing size appeared in **Figure 3.4(a-b)**. The three gap lengths were analyzed from 43 Au nanorod seeded bar DNA strands, and the histogram of the data given in **Figure 3.4c** revealed that most Au-seeded structures had distinct gap sizes increasing in length from gap 1 to gap 3. The average gap lengths and standard deviations for gap 1, gap 2, and gap 3 were 54±12 nm, 66±11 nm, and 72±13 nm, respectively. In some seeded structures, the length of the Au nanorods affected the measured gap sizes. For example, a shorter than average Au nanorod could lead to a longer than average gap on either side; similarly, longer than average Au nanorods could result in shorter than average gaps on either side. A tighter distribution of Au nanorod lengths from an improved synthesis could reduce the gap size variability. These results show the ability to successfully deposit Au nanorods in controlled locations on DNA origami templates.

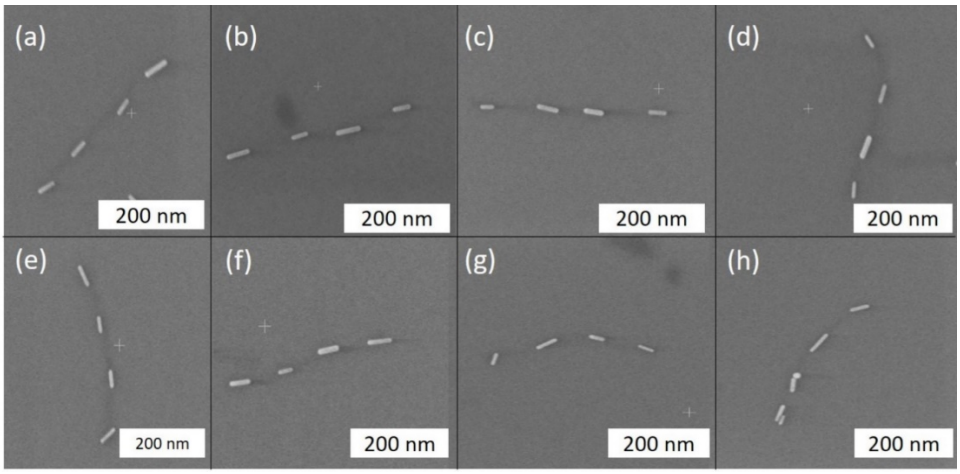

Figure 3.5 Additional SEM images of site-specific binding of Au nanorods to bar DNA origami.

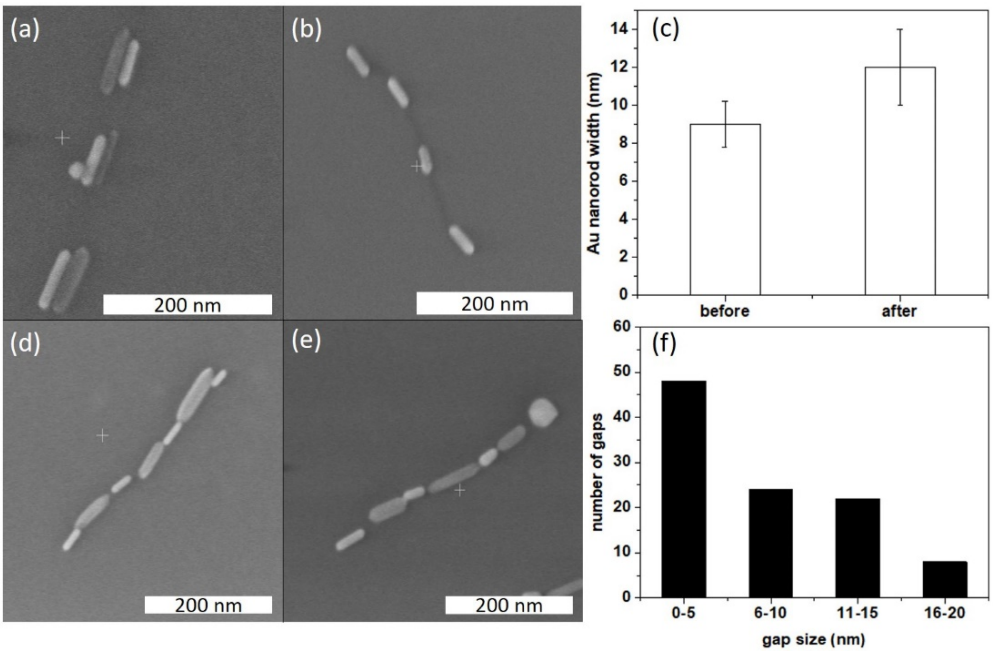

Figure 3.6 Tellurium nanorod attachment in gaps between Au nanorods. (a) SEM image of CTAB-coated Te nanorods (dim features) sticking to as-seeded DNA-coated Au nanorods (bright features) on bar DNA origami. (b) Au nanorods after brief treatment with Gold Enhance EM plating solution. (c) Au nanorod widths before and after the brief Au plating step; the bars give the average and error bars show the standard deviation. (d-e) SEM images of Te nanorods seeded into the gaps between Au nanorods after the brief plating step. (f) Gap size distribution histogram (n = 102); gap size is the width of the space between Au and Te nanorods in seeded structures.

Having established a procedure for site-specific binding of Au nanorods on DNA origami, I next sought to deposit Te nanorods into the gaps to create metal-semiconductor interfaces. I initially tried deposition of CTAB-coated Te nanorods directly after seeding DNA origami with DNA-coated Au nanorods. When CTAB-coated Te nanorods in 10x TAE-Mg^{2+} buffer were deposited on bar DNA origami samples freshly seeded with Au nanorods, the Te nanorods typically attached directly to the Au nanorods rather than in the gaps, as seen in **Figure 3.6a** and **Figure 3.7**. This issue was most likely due to interaction between negatively charged protruding DNA on the gold nanorods and positively charged CTAB surrounding the tellurium nanorods. Thus, I sought to remove the DNA coating from the DNA-localized Au nanorods, so the negatively charged DNA origami in the gap regions would more strongly attract the positively charged CTAB-coated Te nanorods. To remove the thiolated DNA from Au nanorods without affecting the DNA origami, I utilized a commercially available gold plating solution that had been used previously to remove thiolated DNA from Au [35]. Although the exact mechanism is unknown, the chemical change associated with gold ion reduction onto the nanorods likely disrupts thiol DNA S-Au bonding. After this brief plating step, the Au nanorods had a distinct morphological change with an increase in diameter and decrease in aspect ratio (see **Figure 3.6b**) and **Figure 3.8**). I analyzed the diameter of Au nanorods before and after gold plating solution treatment, as shown in **Figure 3.6c**. The average width (± standard deviation) of Au nanorods before plating was 9 ± 2 nm, whereas after treatment, the average width increased to 12 ± 2 nm.

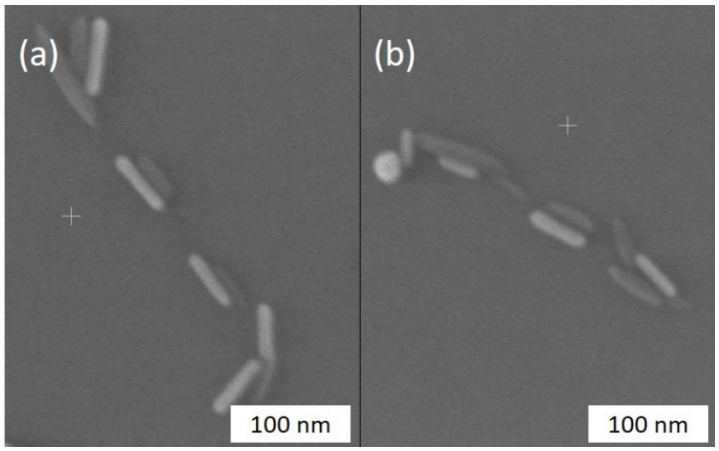

Figure 3.7 Additional SEM images of CTAB-coated Te nanorods sticking to DNA-coated Au nanorods.

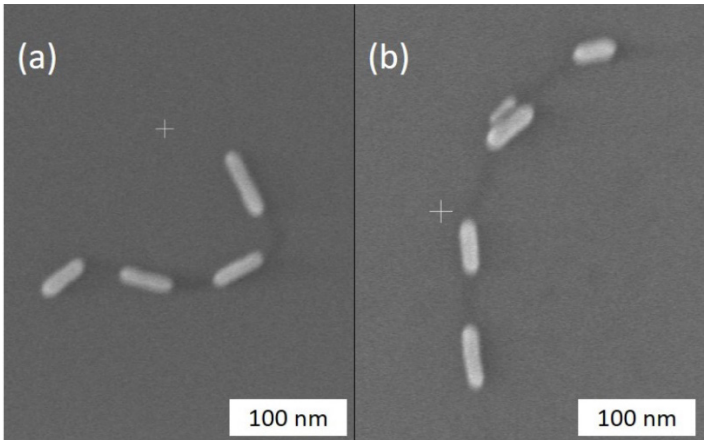

Figure 3.8 Additional SEM images of Au nanorods on bar DNA origami after the brief plating step that removes DNA from their surfaces.

This brief plating step solved the problem of Te nanorod attachment to Au nanorods. **Figure 3.6(d-e)** presents SEM images of Au and Te nanorods attached to bar DNA origami after the brief Au plating process; additional SEM images are given in **Figure 3.9**. The CTAB-coated Te nanorods are localized into the gaps via electrostatic interaction between CTAB and the DNA origami. Most of the Te nanorod seeded structures follows the expected pattern (i.e., longer Te nanorods in the wider gaps and shorter Te nanorods in shorter gaps). In some structures, individual

short Te nanorods were found in wider gaps, but two or more short Te nanorods were rarely seen in the wider gaps. The distance between Au and Te nanorods in seeded structures or 'gap size' ranged from negligible (apparently in contact) to some more noticeable spaces. I analyzed this gap size, and found it to vary from 0-20 nm (**Figure 3.6f**). Approximately 50% of the gaps between Au and Te nanorods were between 0-5 nm, with most of the rest between 6-15 nm, and the remaining <10% from 16-20 nm. Overall, Te nanorods were placed site-specifically into the designed gaps between the Au nanorods. The selective placement of Au and Te nanorods onto DNA origami is critical because it affects proximity, orientation and connection.

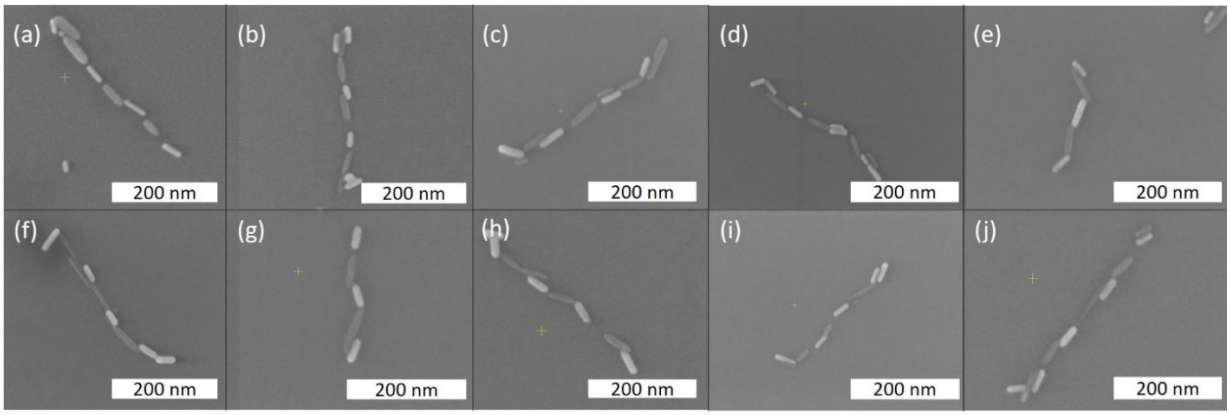

Figure 3.9 Additional SEM images of Au and Te nanorods seeded on bar DNA origami.

These seeded DNA origami structures have sufficiently small gaps to allow electroless plating to connect the junctions electrically. I thus utilized these bar DNA origami seeded with Au and Te nanorods to fabricate metal-semiconductor junctions. To fill the gaps between nanorods, I carried out electroless gold plating as described in **Section 3.3.6**. In initial experiments, I found that the gold plating solution plated not only on Au, but also on Te nanorods. To better understand this matter, I took Te nanorod-seeded bar DNA origami and evaluated gold plating following a method demonstrated by Lin et al [36]. **Figure 3.10** illustrates the effects of gold plating time on Te

nanorods. For short plating times (~1 min), gold accumulation occurred on the Te nanorod ends. The CTAB double layer likely prevented gold ions from reaching the nanorod sides; however, on the ends, fewer and less tightly packed CTAB molecules allowed gold ions to reach the Te substrate and be plated. Interestingly, gold accumulated on only one end of Te nanorods, likely assisted by Ostwald ripening [36]. Plating for 7 min generated enough Au to encapsulate the Te nanorods or form a gold-tellurium alloy (**Figure 3.10c**).

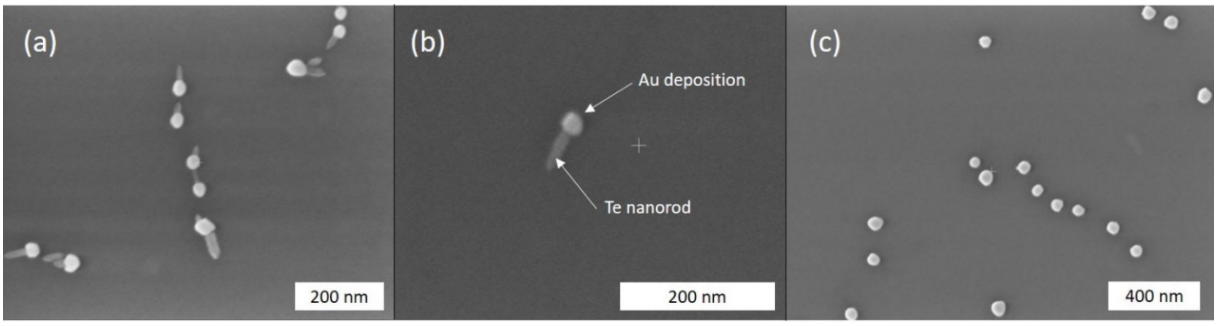

Figure 3.10 Effect of electroless Au plating on Te nanorods. SEM images of (a) Au deposition on only one end of Te nanorods after 1 min plating. (b) Close view of Au accumulated on a Te nanorod end. (c) Au particles encapsulating Te nanorods or forming an alloy of Au and Te after 7 min plating time.

With this understanding of how Au plating times affected Te nanorods, I sought to use electroless Au plating to electrically connect Au and Te on DNA origami. **Figure 3.11** shows SEM images of multiple Au-Te-Au junctions that were formed through electroless gold plating of Au/Te seeded DNA origami. Additional SEM images of Au-Te-Au interfaces are included in **Figure 3.12**. Two simultaneous processes occurred in electroless gold plating: plating on Au nanorods and Au deposition on Te nanorod ends; the SEM data in **Figure 3.11** and **Figure 3.12** show little if any Au deposition onto the sides of the Te nanorods. Those two processes filled the gaps between Au and Te nanorods to create Au-Te-Au junctions. After Au plating, the gaps between Au and Te nanorods were no longer discernible, indicating likely electrical connectivity. In some plated

structures in **Figure 3.11**, the gold particles appeared non-uniform; improved Au seeding conditions could create more uniform structures. I observed via SEM that >50% of bar DNA origami (n = 48) had at least one apparently connected Au-Te-Au structure after electroless gold plating. With this approach, it is possible to simultaneously form millions of such junctions on a surface. Future work will be needed to examine ways to exploit such junctions, and must include methods for placement, orientation and connection to form nanodevices. Furthermore, adjustments to seeding and plating conditions could allow formation of junctions with semiconductors other than Te.

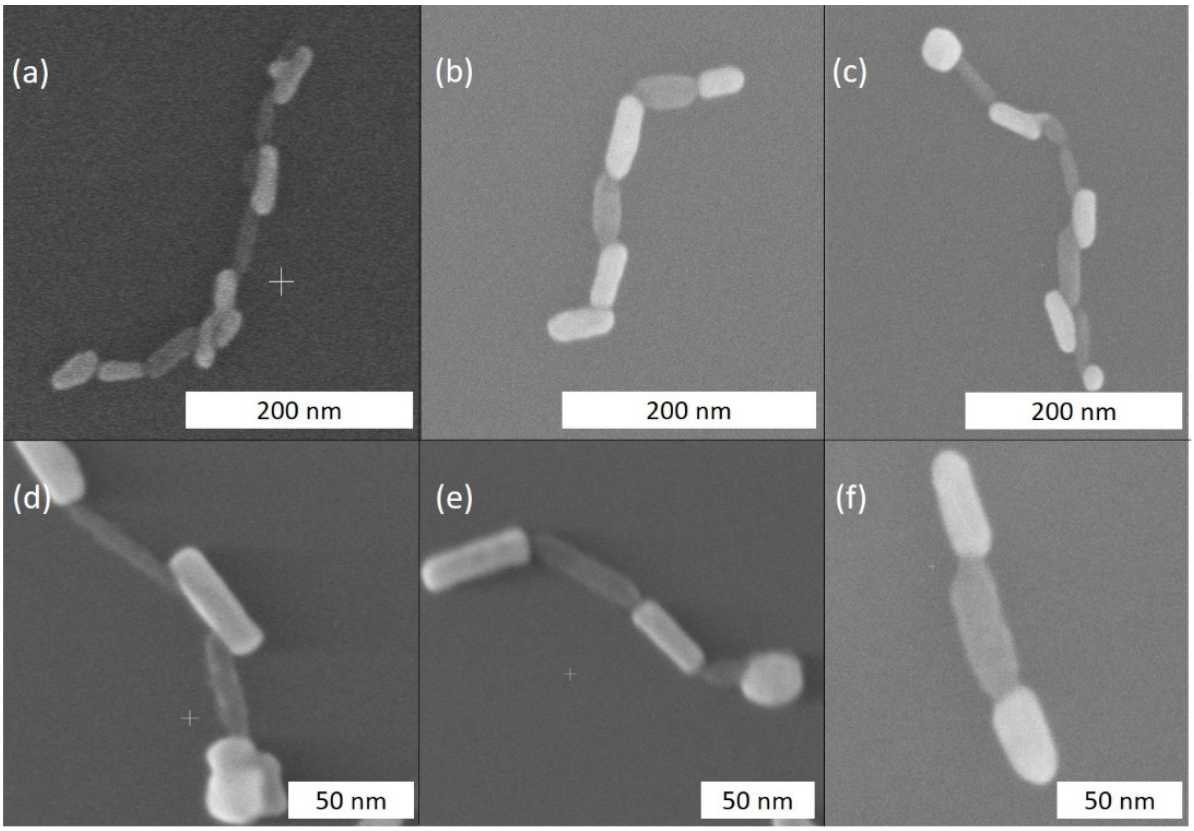

Figure 3.11 SEM images of connected Au-Te-Au junctions after electroless plating of gold.

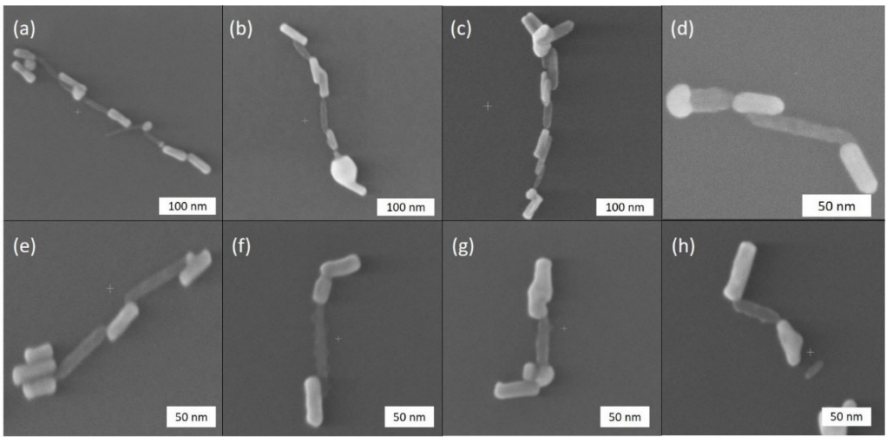

Figure 3.12 Additional SEM images of connected Au-Te-Au junctions after electroless plating of gold.

With apparently connected Au-Te-Au junctions created, I prepared to perform two-point probe electrical characterization. The majority of the Au-Te-Au nanostructures electrically characterized were linear, although some were bent or twisted, following the shape of the deposited DNA origami (**Figure 3.2**). I used EBID to write electrical contacts that were purified under electron beam irradiation to improve conductance and decrease associated carbon impurities [20]. **Figure 3.13** shows SEM images of connections to a single Au-Te-Au structure. **Figure 3.13a** shows a large area view of a two-point connection created between gold pads and the Au-Te-Au structure, linked by EBID contacts. **Figure 3.13b** displays a zoomed view of the yellow box in **Figure 3.13a**, in which two larger and smaller EBID traces each connected to one end of an Au nanorod. A zoomed image in **Figure 3.13c** shows an Au-Te-Au nanowire structure with two small EBID Pt contacts. The single, dim feature in the middle of the nanorod structure is Te, while the two brighter features between the Te and EBID contacts are Au nanorods.

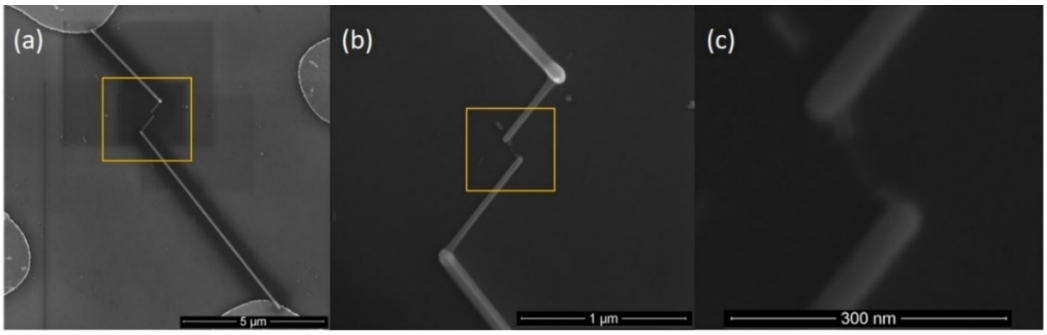

Figure 3.13 SEM images of EBID connections. (a) Large-area view of EBID connections between gold pads and an Au-Te-Au structure. (b) Two larger (outer) and smaller (inner) platinum contacts connecting an Au-Te-Au structure in the middle. (c) Au-Te-Au structure connected to two platinum contacts.

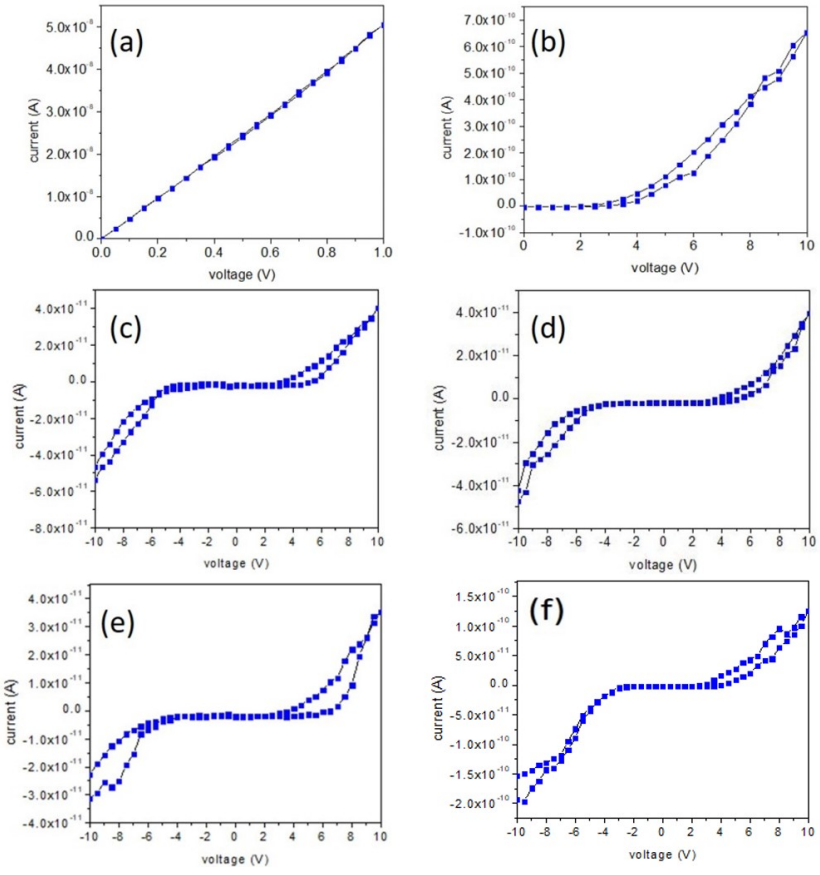

Figure 3.14 Two-point I-V electrical characterization of nanostructures. I-V curves of (a) single Au nanorod without connecting to Te nanorods, (b) an Au-Te-Au structure measured from 0 V to +10 V, and (c-f) four different Au-Te-Au junctions measured from –10 V to +10 V.

Having Au-Te-Au nanostructures now connected to larger contact pads allowed me to measure their electrical properties. I also generated an I-V curve for a single Au nanorod, as seen in **Figure 3.14a**. This linear I-V curve is indicative of an ohmic response, as I have seen previously for DNA-templated Au nanowires [20]. In contrast, the I-V data in **Figure 3.14(b-f)**, generated from five different Au-Te-Au structures, resulted in non-Ohmic I-V curves indicative of a Schottky junction. More than 60% of the Au-Te-Au structures that appeared connected in SEM (n = 13) were found to be electrically conductive. Additional I-V curves for Au-Te-Au nanostructures are included in **Figures 3.15** and **3.16**. The lower traces in the I-V plots correspond to increasing voltage, and the higher traces are for decreasing voltage, which likely have greater current due to heating during the voltage ramp, increasing electron mobility. In contrast, no current was recorded when I ramped the voltage from 0-10 V in a blank experiment wherein I formed Pt EBID contacts with a similar gap size on an oxidized Si surface without Au-Te-Au structures. The Au-Te-Au junctions were symmetric, and the I-V measurements in **Figures 3.14**, **3.15** and **3.16** were carried out by scanning either from 0 to +10 V or from –10 V to +10 V. Due to the symmetry in the Au-Te-Au junctions I expected I-V curves to be symmetric about zero, to within the reproducibility of the measurement. The I-V curve measurements from –10 V to +10 V on four different Au-Te-Au junctions were consistent with this expectation of symmetry about zero, as shown in **Figure 3.14(c-f)**. I did not observe differences in I-V curves for bent or twisted Au-Te-Au structures compared to straight ones. I also collected an I-V curve on a self-assembled Au-Te-Au-Te-Au structure; as seen in **Figure 3.16d** the I-V curve shape was similar to that for Au-Te-Au junctions. The non-linear nature of the I-V curves complicates determination of the resistivity of the Au-Te-Au nanowires; however, at +7 V and room temperature the resistivity was in the range of 10-100

Ω m. These electrical measurements, combined with the SEM data, offer clear evidence that I have self-assembled metal-semiconductor junctions on DNA origami.

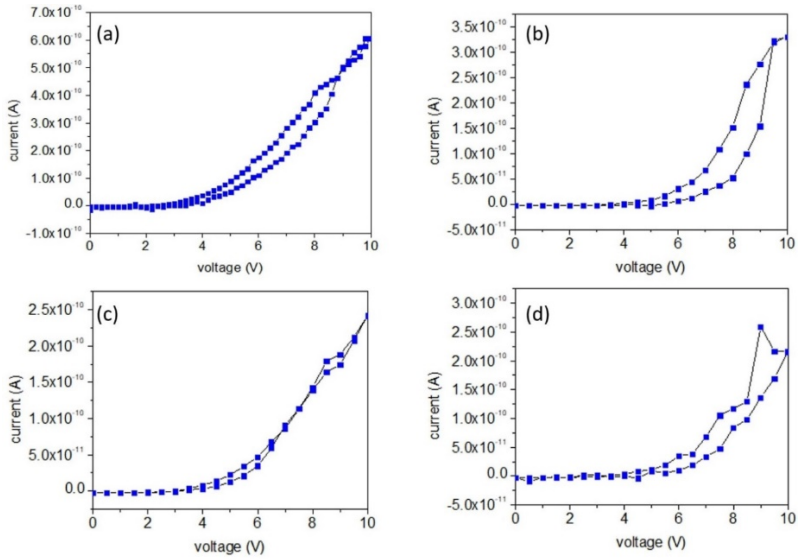

Figure 3.15 Additional I-V curves of Au-Te-Au junctions from different Au-Te-Au structures.

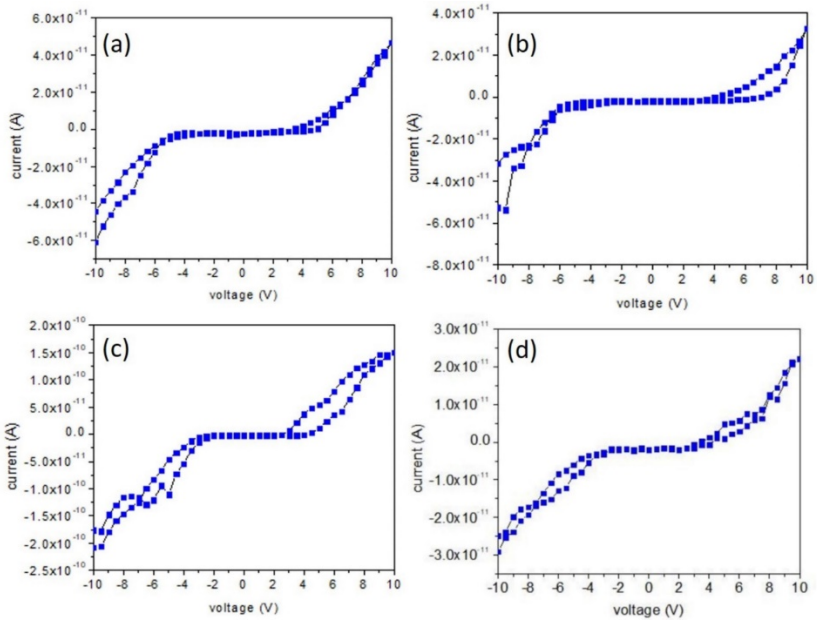

Figure 3.16 Additional I-V curves from –10 to +10 V of (a-c) three different Au-Te-Au junctions and (d) an Au-Te-Au-Te-Au structure.

This demonstration of the self-assembly of nanoscale DNA-based Au-Te-Au junctions shows how DNA origami has potential to facilitate the production of nanoscale metal-semiconductor heterostructures for possible incorporation into electrical nanodevices. Moreover, the ability to electrically connect to these nanoscale metal-semiconductor junctions and measure I-V properties enables researchers to characterize, understand and model their behavior. The studies reported herein thus offer a promising route to the self-assembly, formation, evaluation and optimization of nanoscale electronics.

3.5 CONCLUSION

I have demonstrated the self-assembly of multiple, well-connected Au-Te-Au junctions through location-specific binding of Au and Te nanorods on individual DNA origami templates, accompanied by selective electroless gold deposition. To achieve this objective, I synthesized sub-100 nm Te nanorods with ~20 nm diameters and placed them in gaps between selectively seeded gold nanorods on DNA origami. After site-specific seeding of Au and Te nanorods, electroless gold deposition under appropriate conditions filled the gaps between Au and Te nanorods. I used electron beam induced deposition to connect microfabricated gold pads to these Au-Te-Au junctions and carried out two-point I-V measurements on multiple Au-Te-Au structures, which yielded results consistent with Schottky junction properties. Other possibilities such as doping from the DNA origami or breakdown voltage, although less likely, could also result in similar I-V characteristics. This is the first demonstration of the creation and electrical characterization of multiple self-assembled nanoscale metal-semiconductor junctions on individual DNA nanostructures.

Building on these results, it would be valuable in future studies to create semiconductor-semiconductor junctions, and also perform gated I-V measurements, which would enable more

complete device property characterization. In addition, although my approach for connecting individual nanowires to contact pads works for present numbers of devices, a scalable approach, perhaps involving self-assembly, would facilitate straightforward connection to larger numbers of structures. Importantly, my work offers a strong foundation for future self-assembly and characterization of DNA-based nanoelectronics.

3.6 REFERENCES

1. Liu, Y.; Guo, J.; Zhu, E.; Liao, L.; Lee, S. J.; Ding, M.; Shakir, I.; Gambin, V.; Huang, Y.; Duan, X., Approaching the Schottky-Mott limit in van der Waals metal-semiconductor junctions. *Nature* **2018,** *557* (7707), 696-700.

2. Liu, Y.; Stradins, P.; Wei, S.-H., Van der Waals metal-semiconductor junction: Weak Fermi level pinning enables effective tuning of Schottky barrier. *Sci. Adv.* **2016,** *2* (4), e1600069.

3. Al-Ta'ii, H. M.; Periasamy, V.; Amin, Y. M., Electronic Properties of DNA-Based Schottky Barrier Diodes in Response to Alpha Particles. *Sensors (Basel)* **2015,** *15* (5), 11836-53.

4. Dutta, S. K.; Mehetor, S. K.; Pradhan, N., Metal Semiconductor Heterostructures for Photocatalytic Conversion of Light Energy. *J. Phys. Chem. Lett.* **2015,** *6* (6), 936-944.

5. Al-Ta'ii, H. M. J.; Periasamy, V.; Amin, Y. M., Detection of alpha particles using DNA/Al Schottky junctions. *J. Appl. Phys.* **2015,** *118* (11).

6. Ye, J.; Helmi, S.; Teske, J.; Seidel, R., Fabrication of Metal Nanostructures with Programmable Length and Patterns Using a Modular DNA Platform. *Nano Lett* **2019,** *19* (4), 2707-2714.

7. Hui, L.; Zhang, Q.; Deng, W.; Liu, H., DNA-Based Nanofabrication: Pathway to Applications in Surface Engineering. *Small* **2019,** *15* (26), e1805428.

8. Halley, P. D.; Patton, R. A.; Chowdhury, A.; Byrd, J. C.; Castro, C. E., Low-cost, simple, and scalable self-assembly of DNA origami nanostructures. *Nano Res.* **2019,** *12* (5), 1207-1215.

9. Rothemund, P. W. K., Folding DNA to create nanoscale shapes and patterns. *Nature* **2006,** *440* (7082), 297-302.

10. Liu, J.; Geng, Y.; Pound, E.; Gyawali, S.; Ashton, J. R.; Hickey, J.; Woolley, A. T.; Harb, J. N., Metallization of Branched DNA Origami for Nanoelectronic Circuit Fabrication. *ACS Nano* **2011,** *5* (3), 2240-2247.

11. Chen, Z.; Liu, C.; Cao, F.; Ren, J.; Qu, X., DNA metallization: principles, methods, structures, and applications. *Chem. Soc. Rev.* **2018,** *47* (11), 4017-4072.

12. Uprety, B.; Westover, T.; Stoddard, M.; Brinkerhoff, K.; Jensen, J.; Davis, R. C.; Woolley, A. T.; Harb, J. N., Anisotropic Electroless Deposition on DNA Origami Templates To Form Small Diameter Conductive Nanowires. *Langmuir* **2017,** *33* (3), 726-735.

13. Uprety, B.; Jensen, J.; Aryal, B. R.; Davis, R. C.; Woolley, A. T.; Harb, J. N., Directional Growth of DNA-Functionalized Nanorods to Enable Continuous, Site-Specific Metallization of DNA Origami Templates. *Langmuir* **2017,** *33* (39), 10143-10152.

14. Geng, Y.; Pearson, A. C.; Gates, E. P.; Uprety, B.; Davis, R. C.; Harb, J. N.; Woolley, A. T., Electrically Conductive Gold- and Copper-Metallized DNA Origami Nanostructures. *Langmuir* **2013,** *29* (10), 3482-3490.

15. Hossen, M. M.; Bendickson, L.; Palo, P. E.; Yao, Z.; Nilsen-Hamilton, M.; Hillier, A. C., Creating metamaterial building blocks with directed photochemical metallization of silver onto DNA origami templates. *Nanotechnology* **2018,** *29* (35), 355603.

16. Shen, B.; Linko, V.; Tapio, K.; Kostiainen, M. A.; Toppari, J. J., Custom-shaped metal nanostructures based on DNA origami silhouettes. *Nanoscale* **2015,** *7* (26), 11267-11272.

17. Maune, H. T.; Han, S.-p.; Barish, R. D.; Bockrath, M.; Iii, W. A. G.; Rothemund, P. W. K.; Winfree, E., Self-assembly of carbon nanotubes into two-dimensional geometries using DNA origami templates. *Nature Nanotech.* **2010,** *5* (1), 61-66.

18. Mangalum, A.; Rahman, M.; Norton, M. L., Site-Specific Immobilization of Single-Walled Carbon Nanotubes onto Single and One-Dimensional DNA Origami. *J. Am. Chem. Soc.* **2013,** *135* (7), 2451-2454.

19. Bayrak, T.; Helmi, S.; Ye, J.; Kauert, D.; Kelling, J.; Schönherr, T.; Weichelt, R.; Erbe, A.; Seidel, R., DNA-Mold Templated Assembly of Conductive Gold Nanowires. *Nano Lett.* **2018,** *18* (3), 2116-2123.

20. Aryal, B. R.; Westover, T. R.; Ranasinghe, D. R.; Calvopina, D. G.; Uprety, B.; Harb, J. N.; Davis, R. C.; Woolley, A. T., Four-Point Probe Electrical Measurements on Templated Gold Nanowires Formed on Single DNA Origami Tiles. *Langmuir* **2018,** *34* (49), 15069-15077.

21. Weichelt, R.; Ye, J.; Banin, U.; Eychmüller, A.; Seidel, R., DNA-Mediated Self-Assembly and Metallization of Semiconductor Nanorods for the Fabrication of Nanoelectronic Interfaces. *Chem. Eu. J.* **2019,** *25* (38), 9012-9016.

22. Zhu, H.; Zhang, H.; Liang, J.; Rao, G.; Li, J.; Liu, G.; Du, Z.; Fan, H.; Luo, J., Controlled Synthesis of Tellurium Nanostructures from Nanotubes to Nanorods and Nanowires and Their Template Applications. *J. Phys. Chem. C* **2011,** *115* (14), 6375-6380.

23. Gautam, U. K.; Rao, C. N. R., Controlled synthesis of crystalline tellurium nanorods, nanowires, nanobelts and related structures by a self-seeding solution process. *J. Mater. Chem.* **2004,** *14* (16).

24. Goldfarb, R. J., *Tellurium: The Bright Future of Solar Energy*. US Department of the Interior, US Geological Survey: 2014.

25. He, Z.; Yang, Y.; Liu, J. W.; Yu, S. H., Emerging tellurium nanostructures: controllable synthesis and their applications. *Chem Soc Rev* **2017,** *46* (10), 2732-2753.

26. Zhu, Y.-J.; Wang, W.-W.; Qi, R.-J.; Hu, X.-L., Microwave-Assisted Synthesis of Single-Crystalline Tellurium Nanorods and Nanowires in Ionic Liquids. *Angew. Chem. Int. Ed.* **2004,** *43* (11), 1410-1414.

27. Wang, Q.; Li, G.-D.; Liu, Y.-L.; Xu, S.; Wang, K.-J.; Chen, J.-S., Fabrication and Growth Mechanism of Selenium and Tellurium Nanobelts through a Vacuum Vapor Deposition Route. *J. Phys. Chem. C* **2007,** *111* (35), 12926-12932.

28. Riley, B. J.; Johnson, B. R.; Schaef, H. T.; Sundaram, S. K., Sublimation–Condensation of Multiscale Tellurium Structures. *J. Phys. Chem. C* **2013,** *117* (19), 10128-10134.

29. Yang, H.; Finefrock, S. W.; Albarracin Caballero, J. D.; Wu, Y., Environmentally Benign Synthesis of Ultrathin Metal Telluride Nanowires. *J. Am. Chem. Soc.* **2014,** *136* (29), 10242-10245.

30. Ali, M. R.; Snyder, B.; El-Sayed, M. A., Synthesis and optical properties of small Au nanorods using a seedless growth technique. *Langmuir* **2012,** *28* (25), 9807-15.

31. Liu, K.; Zheng, Y.; Lu, X.; Thai, T.; Lee, N. A.; Bach, U.; Gooding, J. J., Biocompatible gold nanorods: one-step surface functionalization, highly colloidal stability, and low cytotoxicity. *Langmuir* **2015,** *31* (17), 4973-80.

32. Herdt, A. R.; Drawz, S. M.; Kang, Y.; Taton, T. A., DNA dissociation and degradation at gold nanoparticle surfaces. *Colloids Surf., B* **2006,** *51* (2), 130-139.

33. Geier, B.; Gspan, C.; Winkler, R.; Schmied, R.; Fowlkes, J. D.; Fitzek, H.; Rauch, S.; Rattenberger, J.; Rack, P. D.; Plank, H., Rapid and Highly Compact Purification for Focused

Electron Beam Induced Deposits: A Low Temperature Approach Using Electron Stimulated H2O Reactions. *J. Phys. Chem. C* **2014,** *118* (25), 14009-14016.

34. Ananthakumar, S.; Ramkumar, J.; Moorthy Babu, S., Facile synthesis and transformation of Te nanorods to CdTe nanoparticles. *Mater. Sci. Semicond. Process.* **2014,** *27*, 12-18.

35. Uprety, B.; Gates, E. P.; Geng, Y.; Woolley, A. T.; Harb, J. N., Site-specific metallization of multiple metals on a single DNA origami template. *Langmuir* **2014,** *30* (4), 1134-41.

36. Lin, Z.-H.; Lin, Y.-W.; Lee, K.-H.; Chang, H.-T., Selective growth of gold nanoparticles onto tellurium nanowiresvia a green chemical route. *J. Mater. Chem.* **2008,** *18* (22), 2569-2572.

CHAPTER 4: ANNEALING OF POLYMER-ENCASED NANORODS ON DNA ORIGAMI TO FORM METAL-SEMICONDUCTOR NANOWIRES AND THEIR ELECTRICAL CHARACTERIZATION[†††]

4.1 ABSTRACT

DNA origami-assembled metal-semiconductor junctions have been formed in a step toward bottom-up fabrication of functional electronic nanodevices. Previously, techniques such as electroless plating, electrochemical deposition, or photochemical reduction have been used to connect metal and semiconductor nanomaterials into desired patterns on DNA templates. To improve over prior work and provide a more general framework for the creation of electronic nanodevices as an alternative nanofabrication step, I have developed a method to connect gold (Au) and tellurium (Te) nanorods on a single DNA origami template without electroplating by annealing after coating with a heat-resistant polymer. Bar DNA origami templates (17 nm × 410 nm) were seeded site-specifically with Au and Te nanorods in an alternating fashion. These templates were then coated with polymer and annealed at different temperatures. At 170 °C, the Au and Te nanorods were best connected, and I hypothesize that the junctions were established primarily due to the atomic mobility of gold. Electrical characterization of these Au/Te/Au assemblies revealed some nonlinear current-voltage curves, as well as linear plots that are explained. This annealing method and the metal-semiconductor heterostructures that are formed simply through controlled seeding and annealing on DNA origami templates have potential to yield complex electrical nanodevices in the future.

[†††] This chapter is reprinted with permission from Aryal, B. R.; Ranasinghe, D. R.; Pang, C.; Ehlert. A. E. F.; Westover, T. R.; Harb, J. N.; Davis, R. C.; Woolley, A. T. *ACS Nano* **2021** (to be submitted for publication).

4.2 INTRODUCTION

As an important nanofabrication material, deoxyribonucleic acid (DNA) has demonstrated its unique programmability, specificity, and robustness by generating complex nanoscale structures via bottom-up approaches.[1-3] The popular DNA origami technique[4] exploits self-assembly properties and folds DNA strands into prescribed geometrical designs. DNA origami, in association with inorganic or organic components, can form unique structures that have potential applications in multiple fields such as nanomedicine,[5, 6] nanorobotics,[7, 8] bio-imaging and sensing,[9, 10] and nanoelctronics.[11, 12]

DNA origami architectures have served as platforms for assembling various nanoparticles or nanorods such as gold (Au),[13-15] copper (Cu),[16] silver (Ag),[17] and carbon nanotubes (CNTs)[18] to form conductive nanostructures. Furthermore, the use of materials such as cadmium sulfide (CdS),[19] tellurium (Te),[20] and organic semiconductors[21] have broadened opportunities to build DNA-templated semiconductor nanodevices, although the practice is at an early stage. The initial phase of DNA-templated nanoelectronics is growing with the fabrication of functional electronic nanomaterials such as metal nanowires,[22-24] metal-semiconductor nanostructures,[19, 20] and transistors.[25] Amid the preliminary advancements in DNA-enabled nanoelectronics, unique methodologies are emerging to link metals and semiconductors in the fabrication of metal-semiconductor junctions.

Electroless deposition is a well-known plating technique in which metal ions in solution are reduced and isotropically or anisotropically deposited onto metal substrates. For example, Ag structures were formed by first binding and then reducing Ag^+ ions onto DNA strands; subsequently, the reduced Ag was grown into desired patterns using electroless Ag plating solution.[26-29] Jia et al.[30] created alphabet letters of Cu and Ag by first binding metal ions onto DNA

strands, and then performing electroless deposition of these metals on the desired sites on DNA templates through chemical reduction. Moreover, DNA origami-formed Au nanowires of various lengths from the nanometer to micrometer scale have been made by connecting Au nanoparticles[31-36] or nanorods[13, 23, 37, 38] through electroless deposition of Au in solution.

Additional methods for linking nanomaterials into nanowires or heterostructures include electrochemical, photochemical reduction, or heating. Mohamed et al.[39] carried out electrochemical reduction to form DNA-supported rhodium nanowires. Photochemical reduction was performed by Hossen et al.[17] to create a Ag structure on DNA origami. Westover et al.[40] formed Au nanowires by annealing Au nanorods attached to DNA origami via polymer-constrained process. Liu et al.[41] utilized an infrared femtosecond pulsed laser to connect Au nanorods pre-attached to DNA origami. However, in all these examples, the wires were made of a single conducting material and no semiconducting materials were used.

Recently, I described the formation of DNA origami-templated metal-semiconductor nanostructures,[20] where the fabrication of multiple Au-Te-Au junctions on a single DNA origami template was shown. The Au-Te interfaces were electrically characterized and demonstrated non-linear current-voltage (I-V) curves. Weichelt et al.[19] used CdS and Au nanoparticles to create metal-semiconductor interfaces on DNA origami, but electrical characterization was not performed. In both examples, solution-phase electroless plating of gold established connections between the metal and semiconductor. Importantly, decreasing the use of solution-based plating processes in favor of more standard semiconductor approaches in the fabrication of DNA origami-assembled metal-semiconductor heterostructures could be advantageous.

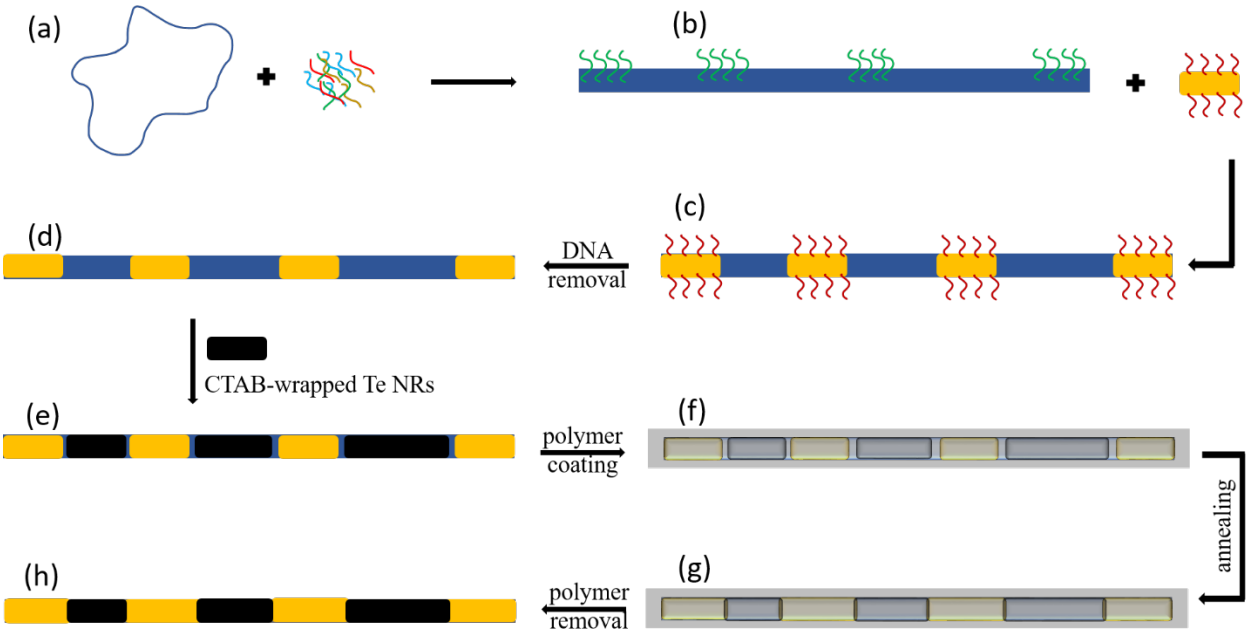

Figure 4.1 Schematic diagram of the formation of DNA origami templated Au/Te/Au nanowires by annealing polybenzimidazole (PBI)-coated Au and Te nanorods. (a) M13mp18 DNA is folded with staple DNA to create (b) bar DNA templates; green lines represent unhybridized single-stranded DNA that serve as binding sites for DNA-coated Au nanorods (yellow features with red lines). (c) Location-specific binding of Au nanorods to DNA templates leaving gaps for Te nanorods. (d) The DNA is removed from Au nanorod surfaces using gold plating solution. (e) Deposition of CTAB-wrapped Te nanorods to localize them in the gaps. (f) PBI coating on Au and Te nanorods attached to DNA templates prepares the sample for annealing. (g) Au-Te connections form after annealing the polymer-constrained Au and Te nanorods at 170 °C for 2 min. (h) Successful synthesis of an Au/Te/Au nanowire after removing the PBI coating.

In this chapter, I report the synthesis of DNA origami-templated Au/Te/Au heterostructures with multiple junctions by annealing Au and Te nanorods deposited onto bar-shaped DNA origami, after site-specific seeding and then polymer coating, as illustrated in **Figure 4.1**. First, DNA origami were hybridized with poly-T DNA-functionalized Au nanorods; subsequently, cetyltrimethylammonium bromide (CTAB)-wrapped Te nanorods were placed into gaps between the Au nanorods to generate Au/Te/Au chain structures.[20] A heat-resistive polymer was spin coated onto the Au/Te/Au structures, which were then annealed to connect into Au/Te/Au junctions. The

resulting structures were characterized by two-point probe electrical measurement of I-V curves, collected under forward and reverse bias, demonstrated that annealing successfully connected Au and Te nanorods. My synthesis of metal- semiconductor heterojunctions by annealing polymer-constrained nanorods is a novel technique, with potential advantages over solution-based plating, which could advance future nanoelectronics.

4.3 EXPERIMENTAL SECTION

4.3.1 Chemicals and Materials

All chemicals and materials employed for fabricating DNA origami-templated Au/Te/Au nanowires were identical to those used by Aryal et al.[20] Polybenzimidazole (PBI) was purchased from PBI Performance Products Inc. (Charlotte, NC) as a ready-to-use product. Silicon nitride transmission electron microscopy (TEM) grids (SN100-A50Q33, 50 nm thick film, 9 windows) were purchased from SiMPore Inc. (West Henrietta, NY).

4.3.2 Nanorod Synthesis

Published methods that I previously used were followed to synthesize,[20, 42] and functionalize[20, 37, 43] Au nanorods with DNA. Te nanorods were synthesized following my published procedure.[20, 44]

4.3.3 DNA Assembly

The design of DNA origami templates and their assembly is similar to my published work.[20] In brief, the DNA origami design possesses staple strands with 10 additional adenine bases as sticky sites for the attachment of poly-T-functionalized Au nanorods. In contrast, no protruding DNA was designed in the binding regions for the CTAB-coated Te nanorods (**Figure 4.1**). These nanorod binding regions, three for Te nanorods and four for Au nanorods, were designed to increase the total numbers of Au/Te/Au structures formed on a single DNA origami template. The

folding of bar DNA origami and their deposition onto oxidized Si surfaces were accomplished as reported in my published work.[20] In summary, M13mp18 single-stranded DNA with staple strands was folded into a bar-shaped DNA origami by heating the assembly solution to 95 °C and cooling to 4 °C in a thermal cycler for 1.5 hr. Staple DNA sequences were same as before.[20] Before DNA deposition, an oxidized Si wafer (1×1 cm^2) was cleaned in a plasma asher for 1 min at 18 W. The plasma-cleaned, oxidized silicon wafer pieces were utilized to deposit DNA origami in a humidified chamber for 20 min at room temperature. Finally, wafer pieces with deposited DNA templates were rinsed carefully with distilled water for 5 s and dried with gently flowing air for 1-2 s.

4.3.4 Nanorod Attachment to Self-Assembled DNA

The procedures for Au and Te nanorod attachment were identical to my reported method.[20] In summary, DNA-coated Au nanorod solution was deposited onto a Si wafer substrate with pre-deposited DNA origami and incubated in a humidified chamber for 1 hr. The substrate was then rinsed carefully with distilled water and dried with a gentle flow of dry air. To remove thiol-modified DNA from Au nanorods, the Au nanorod-seeded DNA was treated with GoldEnhance EM plating solution (Nanoprobes, Yaphank, NY) for 25 s. The surface was subsequently rinsed with distilled water and dried under flowing air. Finally, Te nanorods were placed in the gaps by applying Te nanorod solution in a humidified chamber for 1 hr. Rinsing and drying steps were identical to those used for Au nanorod attachment.

4.3.5 PBI Coating, Annealing, and Removal

DNA origami templates seeded with Au and Te nanorods were coated with PBI at 5000 rpm by spin coating at room temperature for 1 min using a Laurell WS-400B-6NPP/Lite Spin Coater (North Wales, PA), as in the published work.[40] Polymer-encased Au/Te/Au nanostructures

on thermally oxidized silicon surfaces were annealed for 2 min on a hotplate at a range of temperatures (recorded with a surface thermometer placed on the hotplate) from 150 °C to 230 °C. After annealing, the wafer pieces were immersed in 1-methyl-2-pyrrolidinone (NMP) for 5 min to remove the PBI coating.

4.3.6 Atomic Force Microscopy (AFM) Imaging

DNA origami templates deposited on oxidized Si were imaged using a MultiMode atomic force microscope (Bruker, Santa Barbara, CA) with ScanAsyst automatic image optimization and Peak Force tapping mode. Bruker silicon tips on nitride cantilevers (ScanAsyst-Air and ScanAsyst-Air-HD) were used for imaging.

4.3.7 Scanning Electron Microscopy (SEM) Imaging

Seeded DNA samples and ones annealed after seeding were imaged by SEM in ultrahigh-resolution mode on a FEI Helios Nanolab 600 (Hillsboro, Oregon) or on a Thermo Verios UC G4 instrument (Waltham, MA).

4.3.8 TEM Sample Preparation

TEM grids with 9 windows consisting of 50-nm-thick silicon nitride films were used for sample preparation. The silicon nitride surface was rinsed with magnesium acetate solution, plasma cleaned, and then DNA origami were deposited in a humidified chamber for 20 min at room temperature. DNA-coated Au nanorods and CTAB-coated Te nanorods were bound to pre-deposited DNA origami templates on the nitride surface of TEM grids, replicating the general procedure in **section 4.3.4**. PBI coating, annealing, and removal to make annealed Au/Te nanowires were repeated as described in **section 4.3.5**. A FEI Tecnai F20 transmission electron microscope (Hillsboro, Oregon) was utilized to image Au/Te interfaces from seeded structures and after annealing with a PBI coating.

4.3.9 Electrical Characterization

Electrical contacts were created by electron beam induced deposition (EBID), purification and electrical measurements, similarly to prior published methods.[20, 37] A series of steps including photolithography, thermal evaporation and liftoff were followed to create Au contact pads on the oxidized silicon wafer. Then, EBID of platinum was performed to connect between DNA-templated structures and the patterned pads.

I-V curves were collected from Au/Te/Au structures before and after annealing using a micromanipulator probe station. Current was measured using a DL Instruments 1211 current preamplifier, a National Instruments DAQ and a custom LabVIEW program as outlined in previous work.[20]

4.4 RESULTS AND DISCUSSION

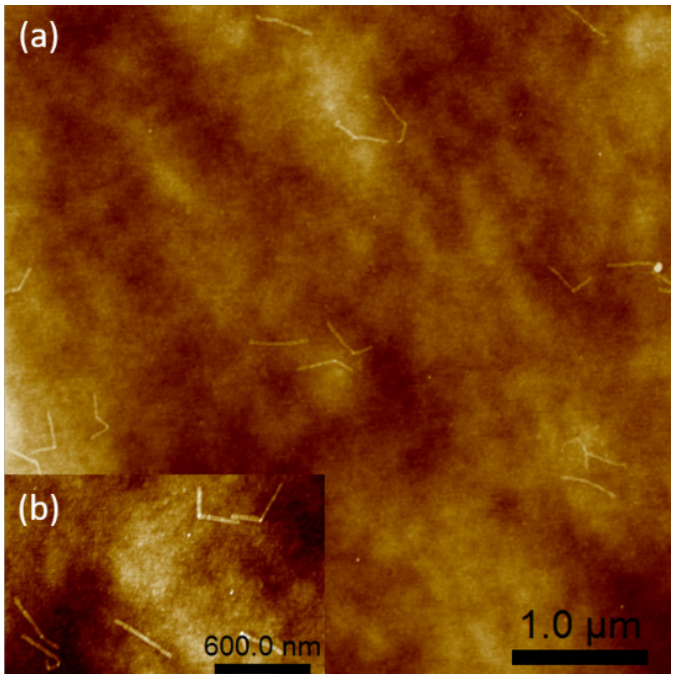

Figure 4.2 AFM images of bar DNA origami. (a) A large-area scan and (b) zoomed-in image, both with a height scale of 5 nm.

The bar DNA origami measuring 17 nm × 410 nm was folded using M13mp18 single-stranded DNA with a set of 227 staple strands to enable the synthesis of Au/Te/Au nanostructures, as reported previously.[20, 23] **Figure 4.2** confirms the formation of bar DNA origami that were imaged by AFM after deposition onto thermally oxidized silicon wafers. The large area image, **Figure 4.2a**, shows several bar DNA origami on a Si substrate, whereas the zoomed-in scan, **Figure 4.2b**, clearly shows distinct bar DNA templates.

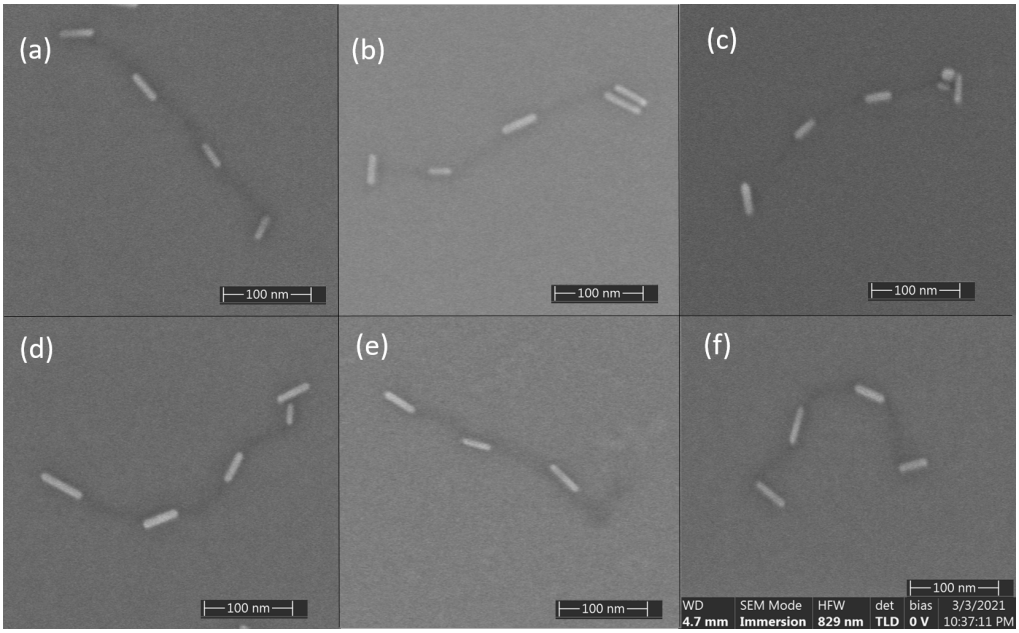

Figure 4.3 SEM images of Au nanorods attached site-specifically to bar DNA origami. The brighter features are Au nanorods, whereas the darker features between Au nanorods are the DNA origami. The three gaps in between the Au nanorods are sites for Te nanorod placement.

Site-specific binding of Au nanorods initiates the fabrication of DNA origami-templated Au/Te/Au structures. **Figure 4.3** shows SEM images of Au nanorods successfully attached to DNA origami on surfaces. Typically, four DNA-functionalized Au nanorods were attached at four separate locations on a single bar DNA template via hybridization, facilitated by the complementary sticky strands in the regions for binding Au nanorods. The DNA origami layout

leaves three non-identical gaps (60, 70 and 80 nm) in between the designed spaces for the four 50 nm Au nanorods, similar to my published design.[20] The average sizes (± standard deviation) of the three gaps in Au nanorod-seeded bar DNA origami (n=38) were measured to be 58 ± 10, 69 ± 8, and 75 ±11 nm for seeding with 37±7 nm long Au nanorods (n=128). In **Figure 4.3**, the darker lines on the surface between Au nanorods are DNA origami regions without the short protruding DNA. Additional SEM images of bar DNA origami with site-specifically attached Au nanorods are provided in **Figure 4.4**.

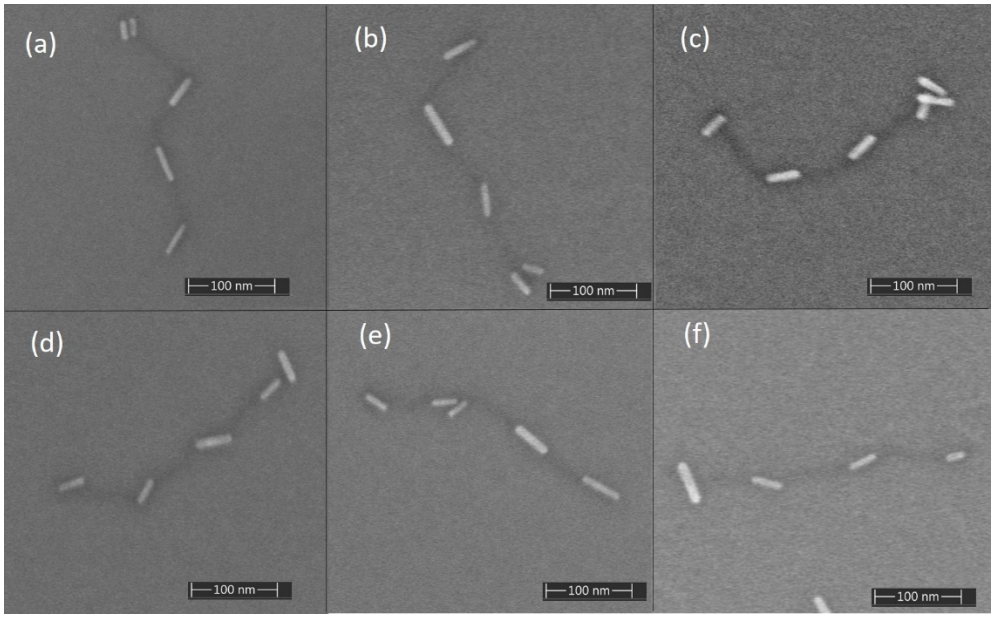

Figure 4.4 Additional SEM images of Au nanorods site-specifically attached to bar DNA origami.

Localization of Te nanorods into the gaps in Au nanorod-seeded DNA origami was essential to construct Au/Te/Au linear designs, as shown in **Figure 4.5**. To minimize the strong electrostatic interaction between DNA strands on the Au nanorods and CTAB-coated Te nanorods, DNA on the Au nanorods was removed by gold plating before the placement of CTAB-coated Te nanorods, as described in a prior publication.[20] The length distribution of CTAB-coated Te

nanorods ranged from 40-100 nm, similar to the result reported previously.[20] A significant advantage of this broad length distribution was that wider gaps accommodated longer Te nanorods, without impacting the formation of Au/Te/Au structures, even with Au nanorods shorter than 50 nm. This design for attaching multiple Au and Te nanorods on single DNA origami templates increased the opportunity to form at least one Au/Te/Au heterostructure. **Figure 4.5a** shows a complete Au/Te/Au/Te/Au/Te/Au structure, whereas in **Figure 4.5(b-f)**, the formation of individual Au/Te/Au structures without having all six junctions present is seen. The observed Au/Te/Au placement on DNA origami templates provided sufficient numbers of junctions to study the impact of annealing. **Figure 4.6** shows additional SEM images of Au/Te/Au structures on single DNA templates.

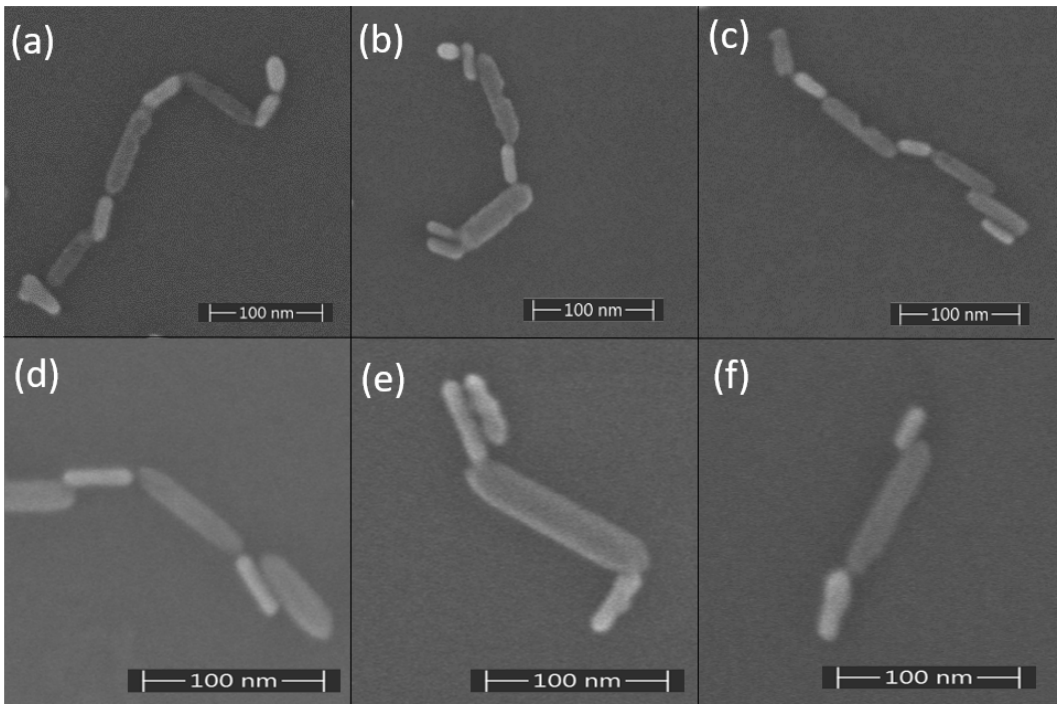

Figure 4.5 SEM images of placement of CTAB-coated Te nanorods in gaps between Au nanorods on bar DNA origami. The elongated white features are Au nanorods. The darker, longer, and wider species between Au nanorods are Te nanorods.

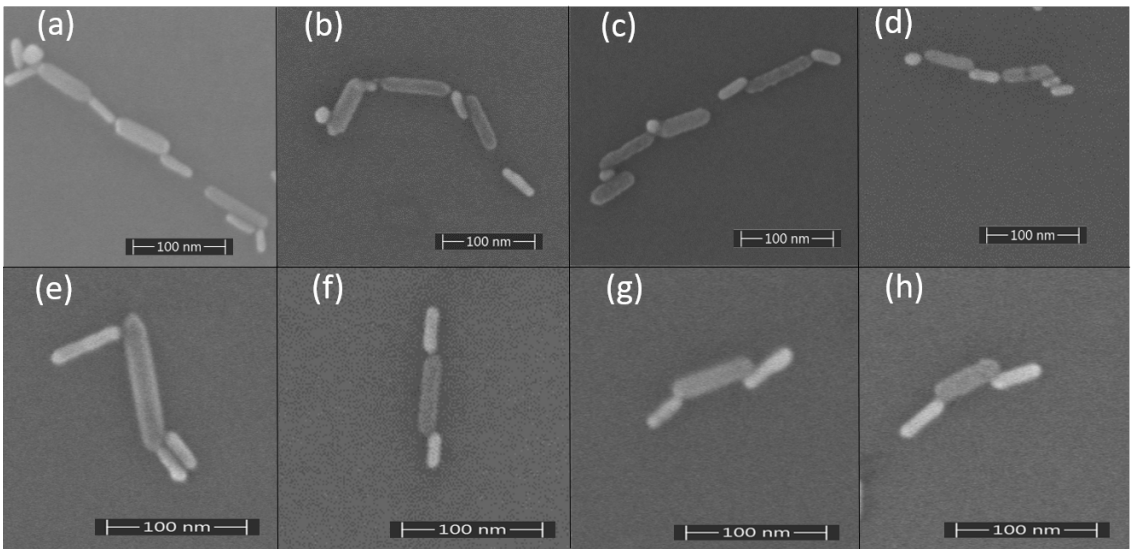

Figure 4.6 Additional SEM images of Au/Te/Au structures before PBI coating and annealing.

Polymer coating of a surface with Au nanorods on DNA origami prior to annealing helped to maintain nanorod morphology in a published report.[40] I expanded on this approach to create electrical continuity between metal and semiconductor nanorods by annealing after PBI coating. To demonstrate these effects of the polymer coating during annealing, Au/Te/Au heterostructures on DNA origami were annealed both with and without the coating. **Figure 4.7** shows SEM images of Au/Te/Au structures before and after annealing at 170 °C for 2 min without this PBI coating. **Figure 4.7(a-d)** presents Au/Te/Au heterostructures before annealing, where brighter Au nanorods and darker Te nanorods are visible; a Te nanorod is seen between the Au nanorods or nanoparticles in each panel. These same Au/Te/Au structures were imaged again after annealing at 170 °C for 2 min without a PBI film cover, as seen in **Figure 4.7(e-h)**. Annealing negatively impacted the Te nanorods, drastically altering their morphology and surface features. In the annealed Au/Te/Au structures, the Te nanorods largely evaporated. In contrast, the Au nanorods had only small decreases in length and increases in diameter. **Figure 4.8** shows additional before/after images of

annealed Au/Te/Au structures without PBI coating. Annealing Au/Te/Au structures in the absence of a polymer overlayer revealed the unstable characteristics of Te nanorods toward heat, particularly in comparison to Au nanorods.

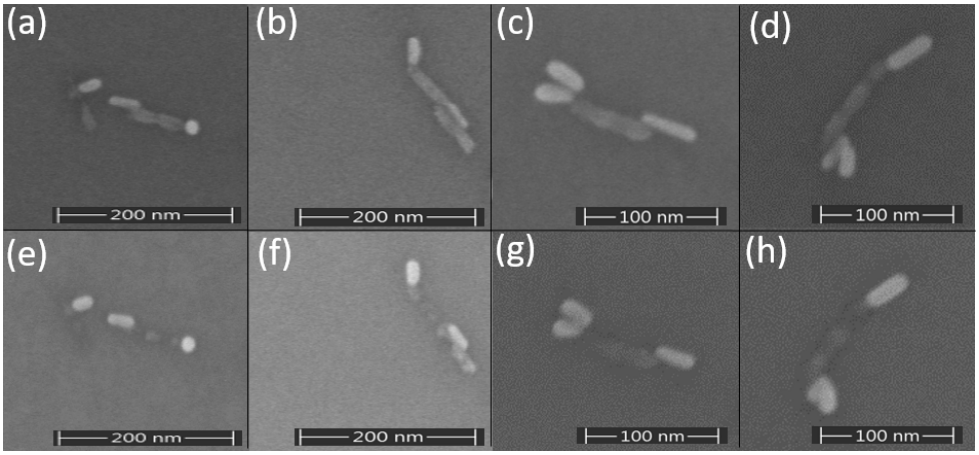

Figure 4.7 Au/Te/Au structures before and after annealing at 170 °C for 2 min without PBI coating. (a-d) SEM images of Au/Te/Au structures before annealing. (e-h) SEM images of the respective Au/Te/Au structures after annealing without the polymer coating.

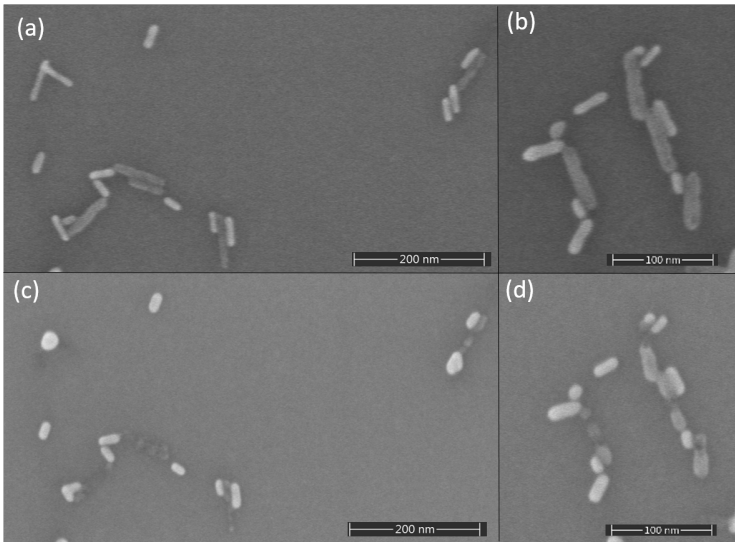

Figure 4.8 Additional SEM images of Au/Te/Au structures without PBI coating (a-b) before annealing and (c-d) after annealing at 170 °C for 2 min.

Au/Te/Au structures annealed with a PBI coating were significantly different compared with Au/Te/Au structures annealed without a PBI coating. I chose to use PBI because of its temperature stability up to 427 °C. **Figure 4.9** compares Au/Te/Au nanostructures before/after PBI coating and annealing at 170 ºC for 2 min. In each panel of **Figure 4.9(a-c)**, a darker Te nanorod is sandwiched between two brighter Au nanorods before annealing. Te nanorods with a PBI coating survived annealing at 170 ºC without significant damage, as seen in **Figure 4.9(d-f)**. However, annealing with a PBI coating resulted in some modifications in the morphology of Au nanorods; similar to the uncoated surfaces, annealed Au nanorods were shorter and wider than

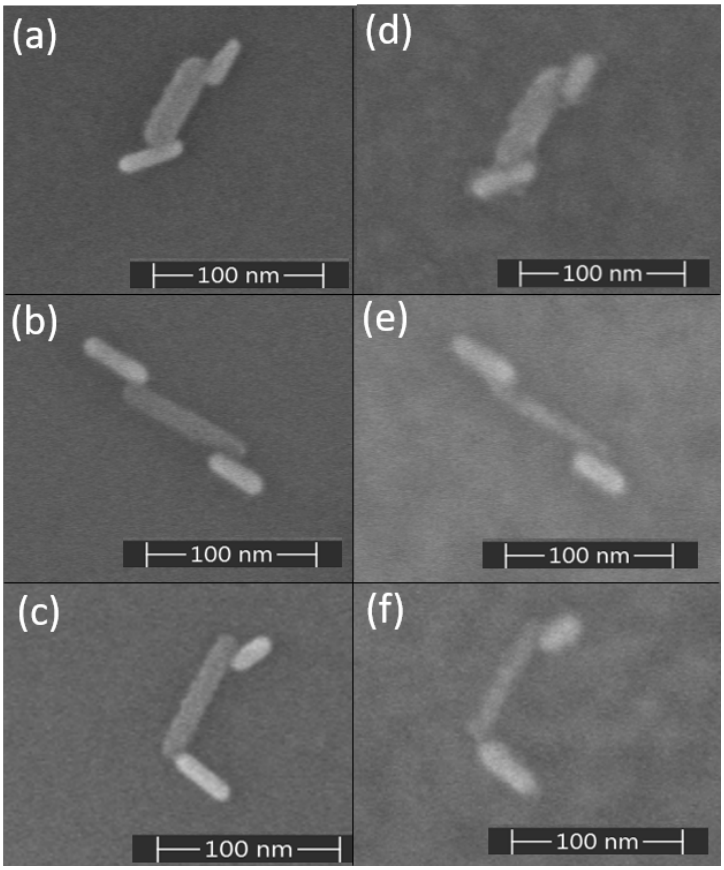

Figure 4.9 Au/Te/Au nanostructures before and after PBI coating and annealing at 170 °C for 2 min. (a-c) SEM images of Au/Te/Au structures before PBI coating and annealing. (d-f) SEM images of the respective structures after annealing at 170 ºC for 2 min with the PBI coating.

the unannealed ones. To better understand the changes in the dimensions of Au nanorods before and after annealing at 170 ºC for 2 min, an analysis of length distribution was performed. **Figure 4.10** plots Au nanorod lengths before and after annealing. Before annealing, the average length (±standard deviation) of Au nanorods (n=128) was 37 ± 7 nm. After annealing with a PBI coating, the average length (±standard deviation) of Au nanorods (n=138) decreased to 32 ± 7 nm, whereas the average length (±standard deviation) of Au nanorods after annealing without a PBI coating was 29 ± 6 nm (n=133). Annealing with or without the polymer coating shortened the length of Au nanorods.

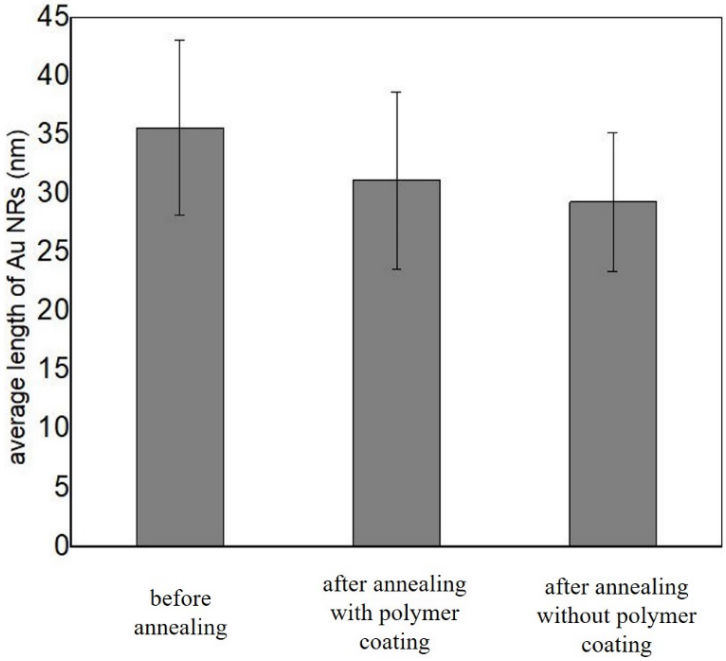

Figure 4.10 Length distribution analysis of Au nanorods before and after annealing at 170 °C for 2 min. Before annealing (n=128), after annealing with polymer coating (n=138), and after annealing without polymer (n=133). Error bars show the standard deviation.

Besides the length variation of Au nanorods, the oxidized wafer surface also experienced some modifications. **Figure 4.11** shows an SEM image of an oxidized Si wafer before and after annealing at 170 ºC for 2 min with a PBI coating, which was removed prior to the "after" image.

Before annealing, the Si wafer oxide surface was smooth with few background features, as seen in **Figure 4.11a**; however, heating with PBI polymer coating made darker sections on the oxide surface as seen in **Figure 4.11b**. These darker features or lines are likely from residual PBI on the surface that might have reacted with the oxidized surface during annealing.

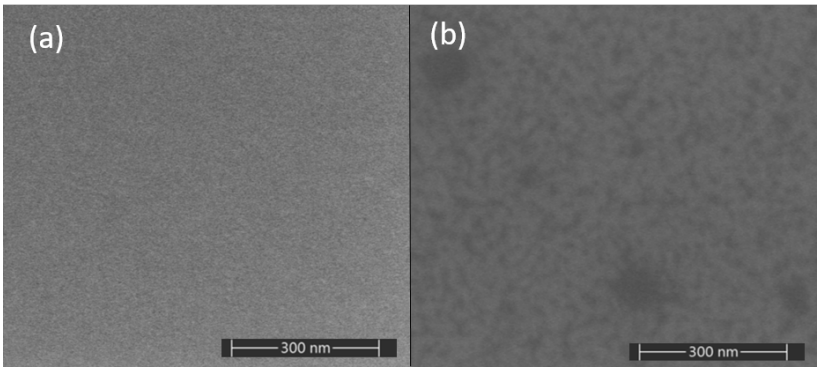

Figure 4.11 SEM images of oxidized silicon wafers (a) before annealing without PBI coating and (b) after annealing at 170 °C for 2 min with PBI coating and subsequent PBI removal.

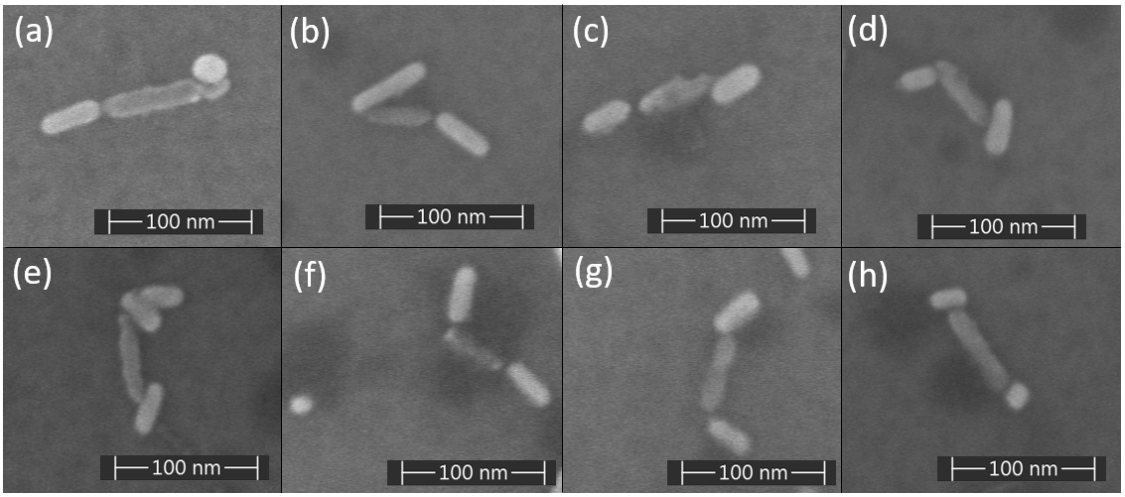

Figure 4.12 SEM images of Au/Te/Au structures annealed at 150 °C for 2 min with a PBI coating.

To determine if annealing would be critical to forming electrically connected Au/Te/Au heterojunctions, annealing experiments were performed at temperatures ranging from 150 to 230 ºC, in 10 ºC increments. Here I discuss the results from four different temperatures (150, 170, 200,

and 230 ºC), to demonstrate notable differences in the annealing experiments. **Figure 4.12** shows SEM images of Au/Te/Au structures after annealing at 150 °C for 2 min with a PBI coating. The Au/Te/Au nanostructures in **Figure 4.12** did not show any notable changes in the shape or size of Au and Te nanorods relative to unannealed assemblies (see **Figure 4.5**). Moreover, the interfacial areas between Au and Te nanorods remained disconnected after annealing. Significant changes appeared with DNA origami-templated Au/Te/Au structures after annealing at 170 ºC for 2 min with a PBI coating, as seen in **Figure 4.9** and **Figure 4.13**. Clear material movement or migration can be observed at the interfaces, which connected the Au and Te nanorods. **Figure 4.14** shows DNA origami-templated Au/Te/Au structures after annealing at 200 ºC for 2 min with a PBI coating. In these SEM images, the Te nanorods in the middle of the structures appeared unaffected by annealing, but the Au nanorods had become shorter and wider relative to their pre-annealed lengths (see **Figures 4.3** and **4.4**). Au nanorods in close proximity further started merging into larger particles, as seen in **Figure 4.14(d, f)**; however, significant interaction between Au and Te did not occur anywhere else, including their junctions. Finally, **Figure 4.15** displays Au/Te/Au structures annealed at 230 ºC for 2 min in the presence of a PBI coating. In these SEM images, Te nanorods did not exhibit a considerable morphological change; however, the Au nanorods appeared even shorter and wider than after the 200 ºC anneal. The average length (±standard deviation) of Au nanorods (n=84) after annealing at 230 °C for 2 min with a PBI coating was 25 ±5 nm. Most of the Au nanorods became increasingly spherical, and did not interface with the Te nanorods.

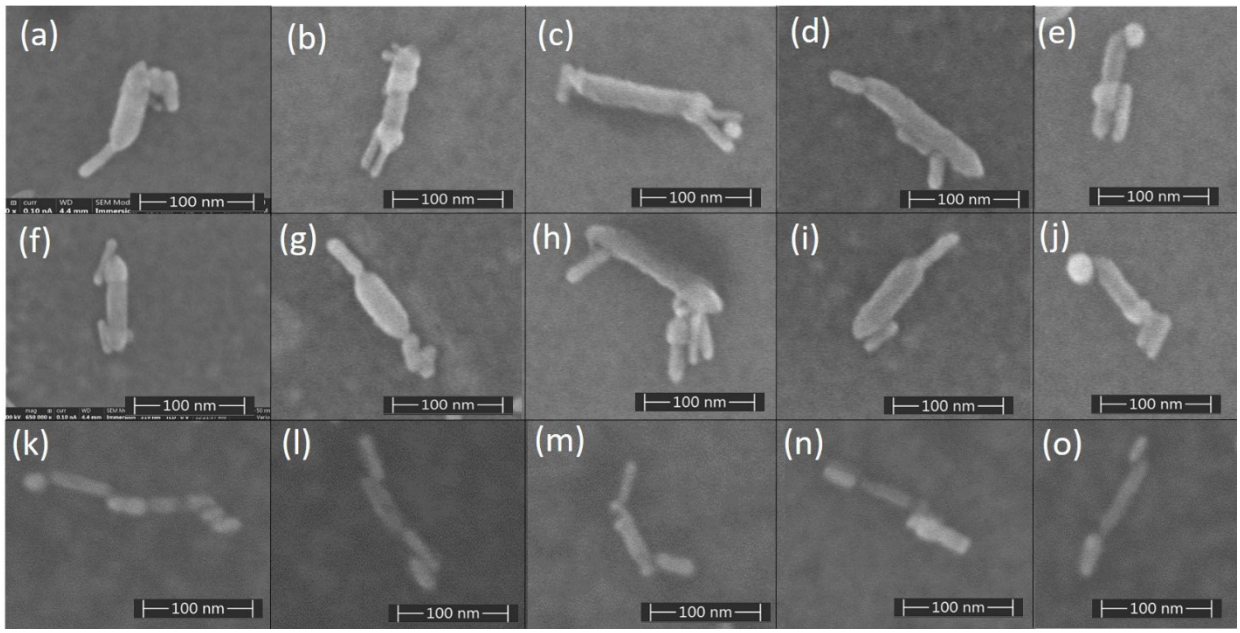

Figure 4.13 SEM images of Au/Te/Au structures annealed at 170 °C for 2 min with a PBI coating.

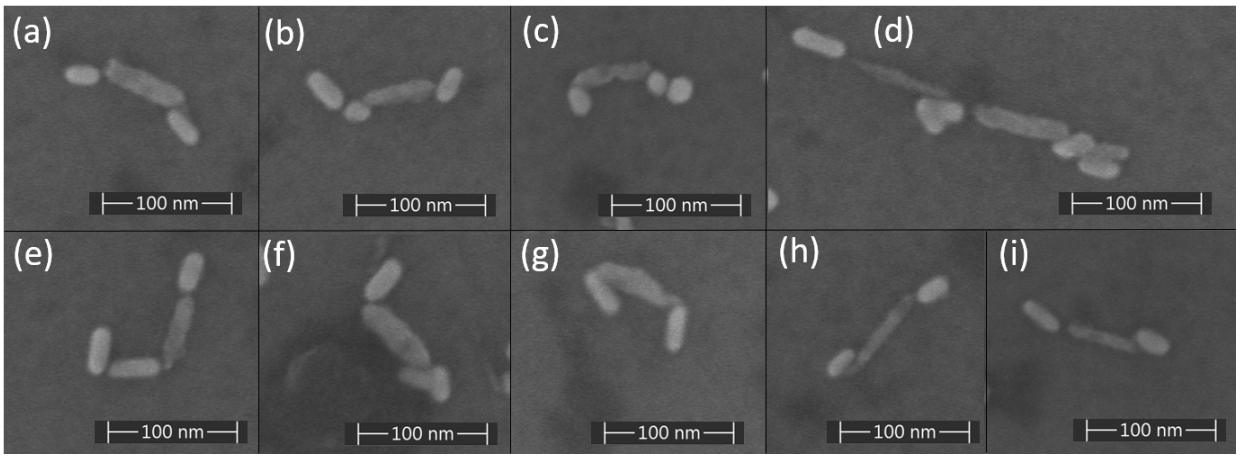

Figure 4.14 SEM images of Au/Te/Au structures annealed at 200 °C for 2 min with a PBI coating.

Analysis of these experiments at different temperatures revealed that 170 ºC was the most appropriate polymer-constrained annealing temperature to generate connected Au/Te/Au structures. My annealing data at 170 ºC are also consistent with published results which provided the explanation of atomic mobility of Au during annealing at 160-180 °C.[40] In contrast, at higher

temperatures, Au nanorods displayed less affinity to Te and started to form spherical-like shapes. Annealing for up to 10 min was also performed for PBI-coated Au/Te/Au, but the results were similar to those for a 2 min anneal, consistent with prior results.[40]

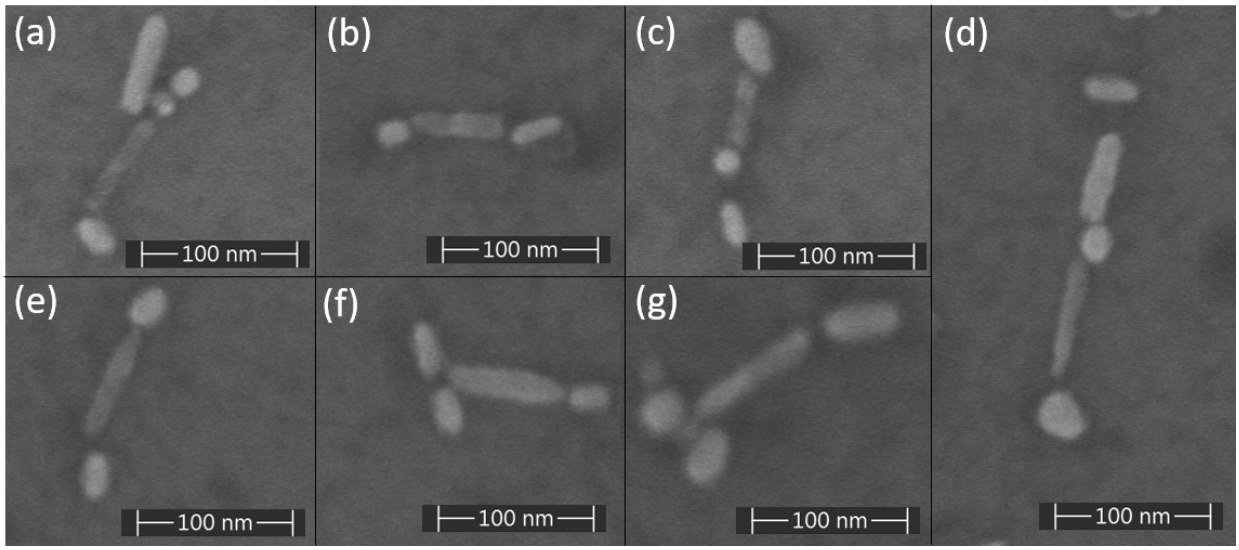

Figure 4.15 SEM images of Au/Te/Au structures annealed at 230 °C for 2 min with a PBI coating.

TEM images before and after were collected to study with higher resolution connections between Au and Te nanorods. I took TEM images of DNA origami-formed Au/Te nanostructures before and after annealing at 170 °C for 2 min with a PBI coating. In pre-annealing images in **Figure 4.16(a-d)**, the Au and Te nanorods, while in close proximity, were separate. In contrast, the TEM images in **Figure 4.16(e-h)** demonstrated Au movement onto Te nanorods during the annealing at 170 ºC for 2 min with a PBI coating. These data revealed that Au migrated into the Te nanorods when the Au and Te nanorods were positioned end-to-end; however, Au migration did not appear to occur between Au and Te nanorods that were side-by-side, even if they were in close proximity, as seen in **Figure 4.16(e)**. I hypothesize that the CTAB layer on Te nanorods contributed to end-to-end gold migration. The more compactly layered CTAB on the sides of Te

nanorods prevented gold migration, but due to higher curvature at the nanorod ends, CTAB was more loosely layered, and Au could more readily migrate onto the Te nanorods.

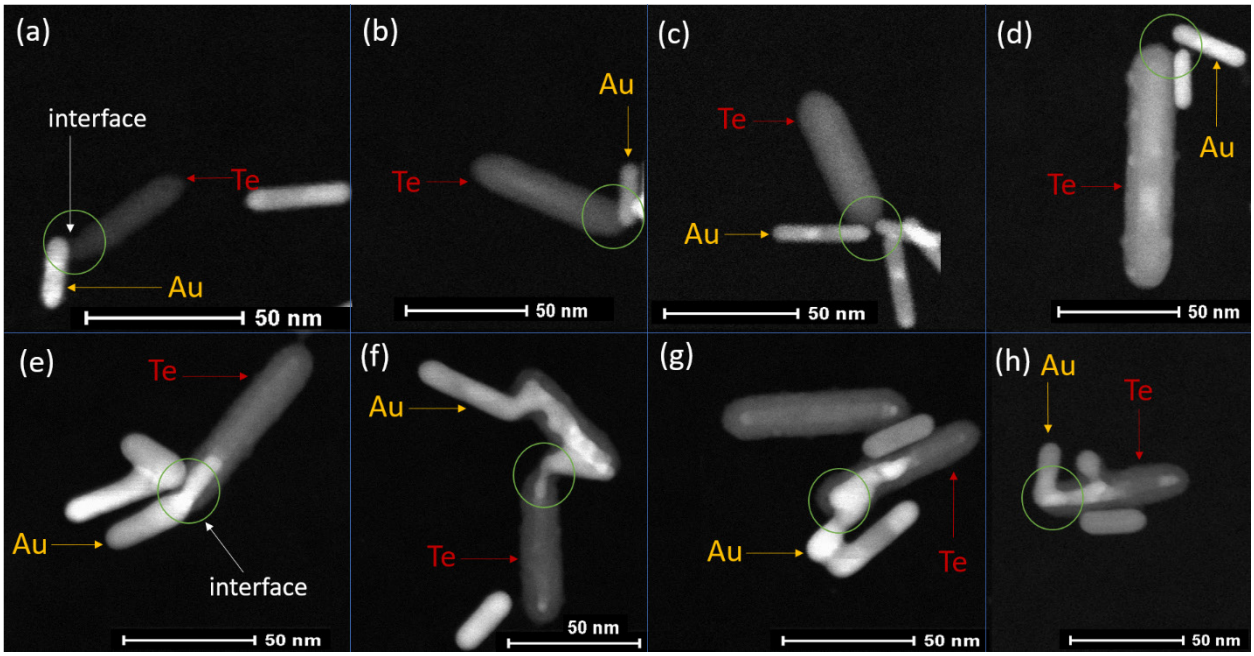

Figure 4.16 TEM images of Au and Te nanorods attached to DNA origami before and after annealing at 170 ºC with PBI coating. Green circles indicate Au/Te interfaces. (a-d) Before annealing the interfaces show limited interconnection between Au and Te nanorods. (e-h) After annealing at 170 ºC with a PBI coating, Au has clearly migrated onto the Te nanorods, creating a connection.

During TEM imaging, I exposed Au-Te nanowires to an electron beam in an attempt to collect EDX data (**Figure 4.17**). I found that electron beam exposure rapidly removed the Te; Au/Te nanowires in **Figure 4.17(a-b)** are in TEM images with initial electron beam exposure. The same structures were imaged after 15 sec **Figure 4.17(c-d)**, and after 30 sec of electron beam exposure, **Figure 4.17(e-f)**. The results showed that the Au nanorods and the Au/Te interfaces remained intact, but the Te was quickly removed, possibly indicating a phase or other structural change due to the energy of the electron beam. This phenomenon is consistent with what I observed

after annealing Au/Te/Au structures without a polymer coating (**Figures 4.7** and **4.8**), where annealing likewise caused major changes or disappearance of Te nanorods.

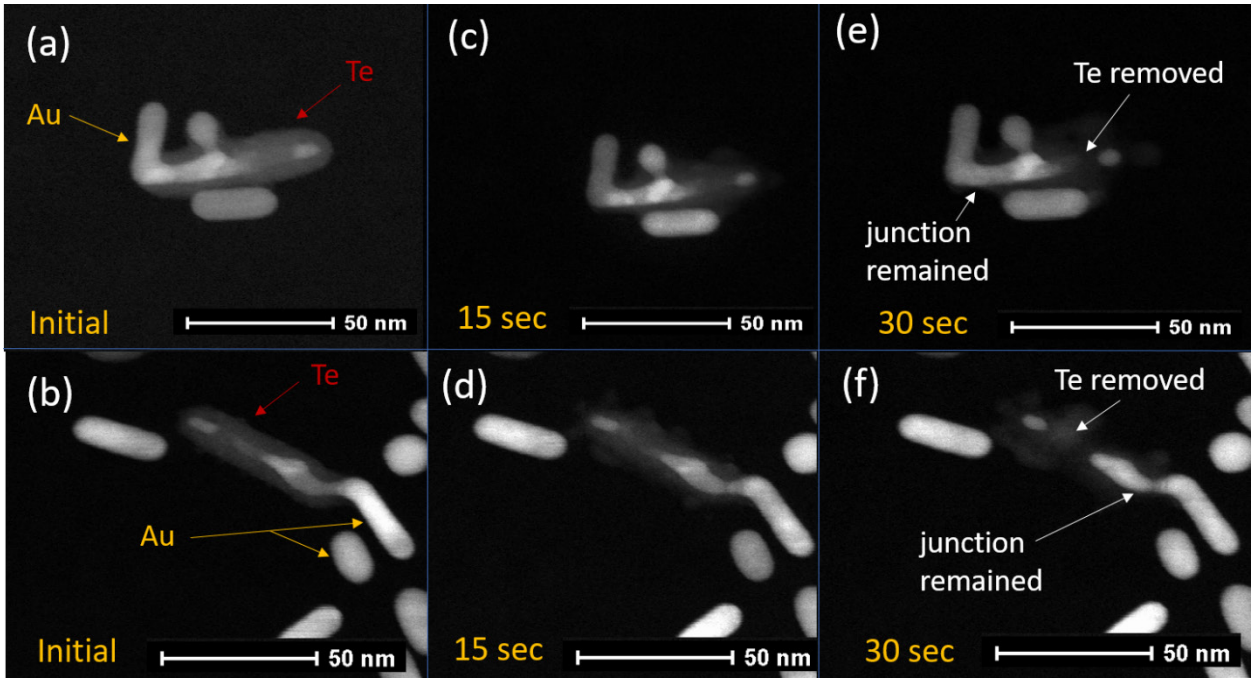

Figure 4.17 Additional TEM images of Au-Te junctions (a-b) initial image, and after (c-d) 15 sec or (e-f) 30 sec electron beam exposure.

Electrical testing of DNA origami-templated Au/Te/Au heterojunctions was essential to verify that annealing successfully created junctions. **Figure 4.18** shows SEM images of EBID connections, which make possible electrical characterization; the panels have different magnifications that show connection to Au pads and to an individual Au/Te/Au heterostructure. **Figure 4.18d** shows EBID wiring for a blank test structure that lacks a connected nanowire.

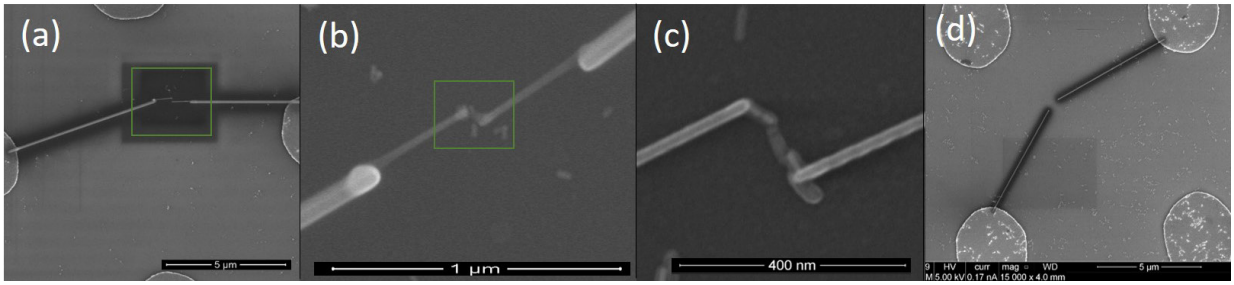

Figure 4.18 SEM images of EBID wiring. (a) Large-area view of EBID wires that linked gold pads to a Au/Te/Au structure. (b) Zoom view from the green box in (a) of EBID platinum wires connected to a Au/Te/Au structure in the middle. (c) Zoom view of the green box in (b) showing Au-Te-Au structure wired to two platinum EBID lines. (d) A blank test substrate where EBID lines were not connected to any nanostructure.

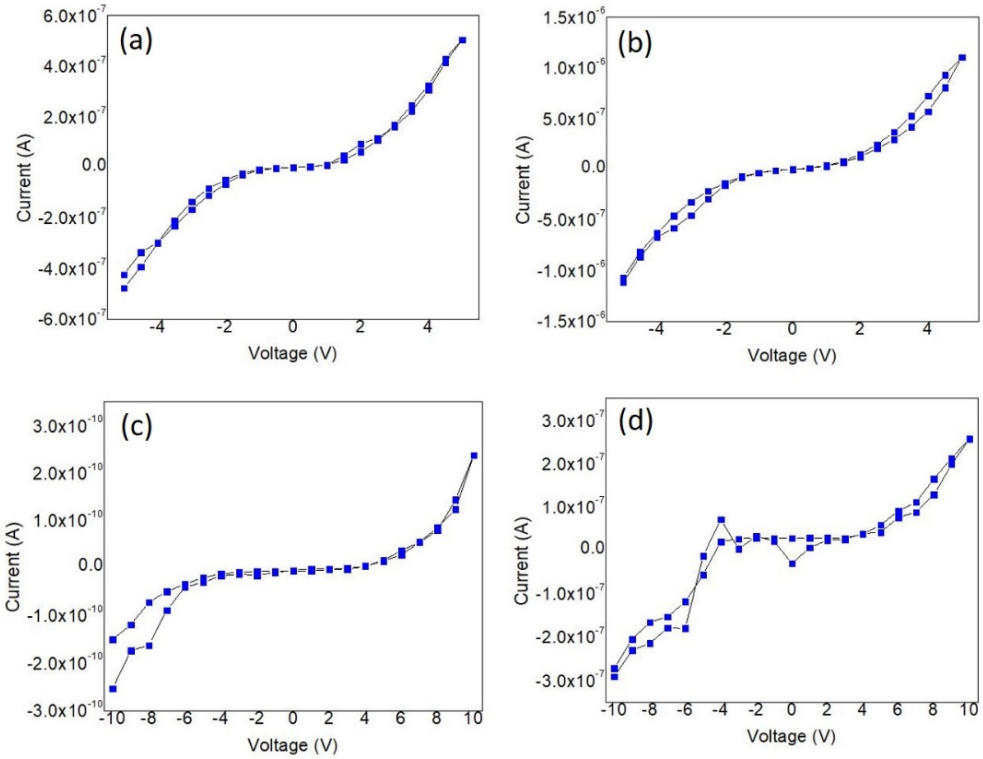

Figure 4.19 Electrical characterization of Au/Te/Au nanostructures after annealing with PBI coating at 170 °C for 2 min. Two-point I-V curves of Au/Te/Au structures measured from (a-b) -5V to +5V or (c-d) -10 V to +10 V.

Figure 4.19 shows two-point I-V curves of four representative structures. **Figure 4.19(a-b)** presents non-linear I-V curves measured from -5V to +5V. Additional I-V curves measured

from -5V to +5V are given in **Figure 4.20(a-c)**. I also collected I-V curves from -10V to +10V from different Au/Te/Au nanowires to compare to my published data with junctions formed by electroless plating.[20] My analysis of 44 structures revealed that 37% of the Au/Te/Au nanowires annealed at 170 ºC for 2 min with a PBI coating demonstrated non-linear I-V curves like those in **Figures 4.19** and **4.20(a-c)**, similar to my published results.[20] Another 44% displayed instrument noise level curves as in **Figure 4.20g**, indicating some type of discontinuity. The curves obtained from a blank test without any wire connections were consistent with these noisy curves indicating a discontinuity.

Somewhat surprisingly, linear I-V curves were collected from 19% of the annealed Au/Te/Au nanowires, as shown in **Figure 4.20(d-e)**. For comparison, an I-V curve was collected from a single Au nanorod, **Figure 4.20f**, which was also linear, as expected. I hypothesize that the non-linear and linear I-V curves obtained from annealed Au/Te/Au nanowires depended on the extent of gold migration onto Te during annealing. For example, in **Figure 4.16(e-h)**, gold migration takes place from Au to Te from one end only; for Au/Te/Au junctions, Au migration may occur from both ends. For many of the annealed Au/Te/Au nanowires, I believe that gold migration occurred from both ends, but left pure Te in the middle region, resulting in metal-semiconductor (Au-Te) junctions and non-linear I-V curves as I saw here. However, in a smaller number of annealed Au/Te/Au structure, more extensive Au migration along the Te nanorod led to a continuous Au path, resulting in linear I-V curves. I also collected I-V curves from 12 DNA origami-templated Au/Te/Au nanostructures annealed at 170 ºC for 2 min without PBI coating. Of these, 67% had noise-level I-V curves consistent with a discontinuity, as in **Figure 4.20g**. Additionally, 33% of these Au/Te/Au structures had low current, non-linear curves, as seen in **Figure 4.20(h-i)**. **Figure 4.19c** had the lowest current from annealed Au/Te/Au with a PBI coating,

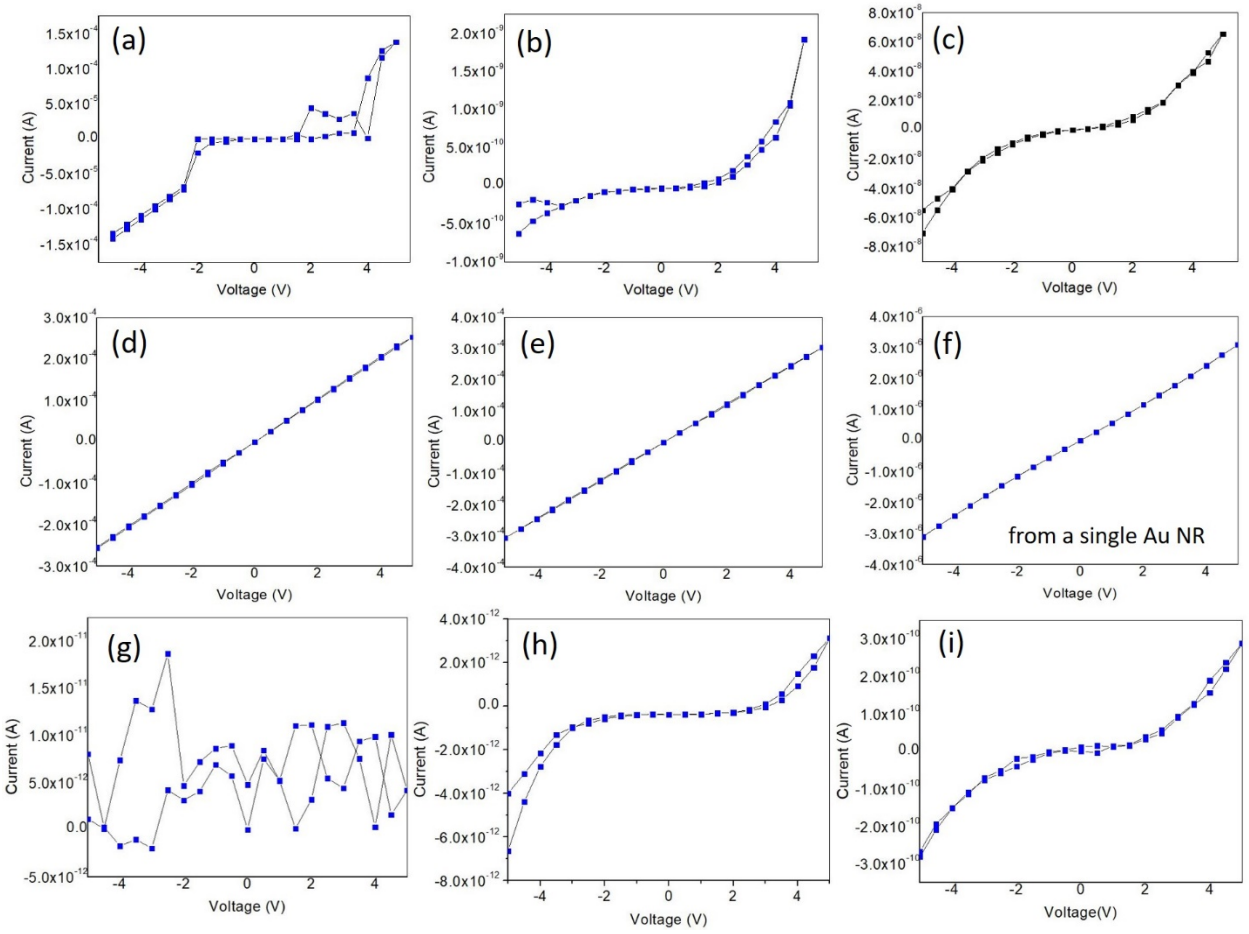

Figure 4.20 Additional I-V curves collected from EBID connected structures. (a-c) Non-linear curves obtained from PBI-constrained Au/Te/Au annealed structures. (d-e) Linear data obtained from annealed PBI-coated Au/Te/Au structures. (f) Linear data obtained from EBID connection to a single Au nanorod. (g-i) Curves obtained from Au/Te/Au structures annealed without a PBI coating. For low current I-V curves, an offset in the current measurement was manually adjusted for zero current at 0 V.

which is 3×10^{-10} A, similar to in **Figure 4.20i**, which had the highest current from annealed Au/Te/Au without a PBI coating. This comparison reveals that the current in one non-linear curve from an Au/Te/Au structure annealed without a PBI coating was as high as the lowest current measured in a non-linear curve for Au/Te/Au heterojunctions annealed with a PBI coating. These lower current, non-linear I-V curves from Au/Te/Au structures annealed without PBI may be due to tunneling of a few electrons, for example, if the Te nanorods were not removed completely

during annealing (see **Figures 4.7** and **4.8**). The shapes and currents of non-linear I-V curves are not identical for different structures (see **Figures 4.19** and **4.20**). I theorize that the variation in non-linear I-V curves and current was due to differences in physical features of the annealed Au/Te/Au nanowires, including the compactness of Au/Te junctions and impurities at the junctions.

4.5 CONCLUSION

I demonstrated the synthesis of Au/Te/Au heterostructures on single bar DNA origami via an annealing approach in association with a polymer coating. DNA origami seeded with Au and Te nanorods coated with a heat-resistant polymer and annealed at 170 ºC for 2 min resulted in electrical connections between Au and Te nanorods. The annealed Au/Te/Au nanowires were tested by two-point probe measurement after removing the PBI coating. TEM data and I-V curves indicate that the Au and Te nanorods were coupled electrically due to gold migration into Te nanorods during annealing. Annealed Au/Te/Au structures displayed both non-linear and linear I-V curves, possibly due to different extents of Au migration into Te nanorods as observed in TEM data.

Annealing metal and semiconductor nanorods assembled by DNA origami with a polymer coating is a novel approach for the fabrication of electrically connected metal-semiconductor nanostructures or heterostructures. This practice has promise as an alternative fabrication method for DNA-based nanofabrication. Such metal-semiconductor junctions or nanowires could be useful in building complex electronic components such as transistors, logic gates or integrated circuits. Conductive heterostructure formation by annealing should provide opportunities to apply physical methods in nanofabrication in addition to solution-based ones.

4.6 REFERENCES

1. Zhao, Y.; Dai, X.; Wang, F.; Zhang, X.; Fan, C.; Liu, X., Nanofabrication based on DNA nanotechnology. *Nano Today* **2019,** *26*, 123-148.

2. Hu, Q.; Li, H.; Wang, L.; Gu, H.; Fan, C., DNA Nanotechnology-Enabled Drug Delivery Systems. *Chem Rev* **2019,** *119* (10), 6459-6506.

3. Zhang, F.; Nangreave, J.; Liu, Y.; Yan, H., Structural DNA nanotechnology: state of the art and future perspective. *J. Am. Chem. Soc.* **2014,** *136* (32), 11198-211.

4. Rothemund, P. W., Folding DNA to create nanoscale shapes and patterns. *Nature* **2006,** *440* (7082), 297-302.

5. Shen, H.; Huang, X.; Min, J.; Le, S.; Wang, Q.; Wang, X.; Dogan, A. A.; Liu, X.; Zhang, P.; Draz, M. S., Nanoparticle delivery systems for DNA/RNA and their potential applications in nanomedicine. *Curr. Top. Med. Chem.* **2019,** *19* (27), 2507-2523.

6. Zhan, Y.; Ma, W.; Zhang, Y.; Mao, C.; Shao, X.; Xie, X.; Wang, F.; Liu, X.; Li, Q.; Lin, Y., DNA-based nanomedicine with targeting and enhancement of therapeutic efficacy of breast cancer cells. *ACS Appl. Mater. Interfaces* **2019,** *11* (17), 15354-15365.

7. Li, M.; Xi, N.; Wang, Y.; Liu, L., Progress in nanorobotics for advancing biomedicine. *IEEE Trans. Biomed. Eng.* **2020,** *1*, 130-147.

8. Ma, W.; Zhan, Y.; Zhang, Y.; Shao, X.; Xie, X.; Mao, C.; Cui, W.; Li, Q.; Shi, J.; Li, J., An intelligent DNA nanorobot with in vitro enhanced protein lysosomal degradation of HER2. *Nano Lett.* **2019,** *19* (7), 4505-4517.

9. Yang, Y.; Mao, G.; Ji, X.; He, Z., DNA-templated quantum dots and their applications in biosensors, bioimaging, and therapy. *J. Mater. Chem. B* **2020,** *8* (1), 9-17.

10. Wang, Y.-X.; Wang, D.-X.; Wang, J.; Du, Y.-C.; Cui, Y.-X.; Tang, A.-N.; Jiang, H.-X.; Kong, D.-M., Reversible assembly/disassembly of DNA frames and applications in logic design, ratiometric sensing and bioimaging. *Sens. Actuators B Chem.* **2021,** *330*, 129335.

11. Dai, X.; Li, Q.; Aldalbahi, A.; Wang, L.; Fan, C.; Liu, X., DNA-based fabrication for nanoelectronics. *Nano Lett.* **2020,** *20* (8), 5604-5615.

12. Vittala, S. K.; Han, D., DNA-guided assemblies toward nanoelectronic applications. *ACS Appl. Bio Mater.* **2020,** *3* (5), 2702-2722.

13. Ranasinghe, D. R.; Aryal, B. R.; Westover, T. R.; Jia, S.; Davis, R. C.; Harb, J. N.; Schulman, R.; Woolley, A. T., Seeding, Plating and Electrical Characterization of Gold Nanowires Formed on Self-Assembled DNA Nanotubes. *Molecules* **2020,** *25* (20), 4817.

14. Pearson, A. C.; Liu, J.; Pound, E.; Uprety, B.; Woolley, A. T.; Davis, R. C.; Harb, J. N., DNA origami metallized site specifically to form electrically conductive nanowires. *J. Phys. Chem. B.* **2012,** *116* (35), 10551-10560.

15. Bayrak, T.; Martinez-Reyes, A.; Arce, D. D. R.; Kelling, J.; Samano, E. C.; Erbe, A., Fabrication and temperature-dependent electrical characterization of a C-shape nanowire patterned by a DNA origami. *Sci. Rep.* **2021,** *11* (1), 1922.

16. Geng, Y.; Pearson, A. C.; Gates, E. P.; Uprety, B.; Davis, R. C.; Harb, J. N.; Woolley, A. T., Electrically conductive gold-and copper-metallized DNA origami nanostructures. *Langmuir* **2013,** *29* (10), 3482-3490.

17. Hossen, M. M.; Bendickson, L.; Palo, P. E.; Yao, Z.; Nilsen-Hamilton, M.; Hillier, A. C., Creating metamaterial building blocks with directed photochemical metallization of silver onto DNA origami templates. *Nanotechnology* **2018,** *29* (35), 355603.

18. Eskelinen, A. P.; Kuzyk, A.; Kaltiaisenaho, T. K.; Timmermans, M. Y.; Nasibulin, A. G.; Kauppinen, E. I.; Törmä, P., Assembly of single-walled carbon nanotubes on DNA-origami templates through streptavidin–biotin interaction. *Small* **2011,** *7* (6), 746-750.

19. Weichelt, R.; Ye, J.; Banin, U.; Eychmuller, A.; Seidel, R., DNA-Mediated Self-Assembly and Metallization of Semiconductor Nanorods for the Fabrication of Nanoelectronic Interfaces. *Chemistry* **2019,** *25* (38), 9012-9016.

20. Aryal, B. R.; Ranasinghe, D. R.; Westover, T. R.; Calvopiña, D. G.; Davis, R. C.; Harb, J. N.; Woolley, A. T., DNA origami mediated electrically connected metal—Semiconductor junctions. *Nano Res.* **2020,** *13* (5), 1419-1426.

21. Cui, C.; Park, D. H.; Ahn, D. J., Organic Semiconductor–DNA Hybrid Assemblies. *Adv. Mater.* **2020,** *32* (51), 2002213.

22. Petty, J. T.; Zheng, J.; Hud, N. V.; Dickson, R. M., DNA-templated Ag nanocluster formation. *J. Ame. Chem. Soc.* **2004,** *126* (16), 5207-5212.

23. Uprety, B.; Westover, T.; Stoddard, M.; Brinkerhoff, K.; Jensen, J.; Davis, R. C.; Woolley, A. T.; Harb, J. N., Anisotropic Electroless Deposition on DNA Origami Templates To Form Small Diameter Conductive Nanowires. *Langmuir* **2017,** *33* (3), 726-735.

24. Chang, P.-C.; Chang, C.-Y.; Jian, W.-B.; Yuan, C.-J.; Chen, Y.-C.; Chang, C.-C., The fabrication and application of Ni-DNA nanowire-based nanoelectronic devices. *Nano Res.* **2019,** *12* (6), 1293-1300.

25. Keren, K.; Berman, R. S.; Buchstab, E.; Sivan, U.; Braun, E., DNA-templated carbon nanotube field-effect transistor. *Science* **2003,** *302* (5649), 1380-1382.

26. Kasyanenko, N.; Qiushi, Z.; Bakulev, V.; Osolodkov, M.; Sokolov, P.; Demidov, V., DNA binding with acetate bis (1, 10-phenanthroline) silver (I) monohydrate in a solution and metallization of formed structures. *Polymers* **2017,** *9* (6), 211.

27. Ganguly, S.; Paul, S.; Yehezkeli, O.; Cha, J.; Caruthers, M. H., Boranephosphonate DNA-Mediated Metallization of Single-Walled Carbon Nanotubes. *Chem. Mater.* **2017,** *29* (5), 2239-2245.

28. Liu, D.; Park, S. H.; Reif, J. H.; LaBean, T. H., Self Assembly of DNA Nanotubes from Triple-Crossover Tiles as Templates for Conductive Nanowires. *Ann of Phar Nano Tech and Nanomedi.* **2018,** *1* (1), 5.

29. Braun, E., Eichen; Sivan, U.; Ben-Yoseph, G. *Nature* **1998,** *391*, 775-778.

30. Jia, S.; Wang, J.; Xie, M.; Sun, J.; Liu, H.; Zhang, Y.; Chao, J.; Li, J.; Wang, L.; Lin, J.; Gothelf, K. V.; Fan, C., Programming DNA origami patterning with non-canonical DNA-based metallization reactions. *Nat Commun* **2019,** *10* (1), 5597.

31. Bayrak, T.; Helmi, S.; Ye, J.; Kauert, D.; Kelling, J.; Schonherr, T.; Weichelt, R.; Erbe, A.; Seidel, R., DNA-Mold Templated Assembly of Conductive Gold Nanowires. *Nano Lett.* **2018,** *18* (3), 2116-2123.

32. Ye, J.; Helmi, S.; Teske, J.; Seidel, R., Fabrication of Metal Nanostructures with Programmable Length and Patterns Using a Modular DNA Platform. *Nano Lett.* **2019,** *19* (4), 2707-2714.

33. Helmi, S.; Ziegler, C.; Kauert, D. J.; Seidel, R., Shape-controlled synthesis of gold nanostructures using DNA origami molds. *Nano Lett* **2014,** *14* (11), 6693-6698.

34. Uprety, B.; Gates, E. P.; Geng, Y.; Woolley, A. T.; Harb, J. N., Site-specific metallization of multiple metals on a single DNA origami template. *Langmuir* **2014,** *30* (4), 1134-1141.

35. Stern, A.; Eidelshtein, G.; Zhuravel, R.; Livshits, G. I.; Rotem, D.; Kotlyar, A.; Porath, D., Highly Conductive Thin Uniform Gold-Coated DNA Nanowires. *Adv. Mater.* **2018,** *30* (26), e1800433.

36. Luo, X.; Lachance-Brais, C.; Bantle, A.; Sleiman, H. F., The assemble, grow and lift-off (AGLO) strategy to construct complex gold nanostructures with pre-designed morphologies. *Chem. Sci.* **2020,** *11* (19), 4911-4921.

37. Aryal, B. R.; Westover, T. R.; Ranasinghe, D. R.; Calvopina, D. G.; Uprety, B.; Harb, J. N.; Davis, R. C.; Woolley, A. T., Four-Point Probe Electrical Measurements on Templated Gold Nanowires Formed on Single DNA Origami Tiles. *Langmuir* **2018,** *34* (49), 15069-15077.

38. Uprety, B.; Jensen, J.; Aryal, B. R.; Davis, R. C.; Woolley, A. T.; Harb, J. N., Directional growth of DNA-functionalized nanorods to enable continuous, site-specific metallization of DNA origami templates. *Langmuir* **2017,** *33* (39), 10143-10152.

39. Mohamed, H. D. A.; Watson, S. M. D.; Horrocks, B. R.; Houlton, A., Chemical and electrochemical routes to DNA-templated rhodium nanowires. *J. Mater. Chem. C* **2015,** *3* (2), 438-446.

40. Westover, T. R.; Aryal, B. R.; Ranasinghe, D. R.; Uprety, B.; Harb, J. N.; Woolley, A. T.; Davis, R. C., Impact of Polymer-Constrained Annealing on the Properties of DNA Origami-Templated Gold Nanowires. *Langmuir* **2020,** *36* (24), 6661-6667.

41. Liu, Y.; Liu, Y.; Shen, Y., Nano-assembly and welding of gold nanorods based on DNA origami and plasmon-induced laser irradiation. *Int J Intell Robot Appl* **2018,** *2* (4), 445-453.

42. Ali, M. R.; Snyder, B.; El-Sayed, M. A., Synthesis and optical properties of small Au nanorods using a seedless growth technique. *Langmuir* **2012,** *28* (25), 9807-9815.

43. Liu, K.; Zheng, Y.; Lu, X.; Thai, T.; Lee, N. A.; Bach, U.; Gooding, J. J., Biocompatible gold nanorods: One-step surface functionalization, highly colloidal stability, and low cytotoxicity. *Langmuir* **2015,** *31* (17), 4973-4980.

44. Gautam, U. K.; Rao, C., Controlled synthesis of crystalline tellurium nanorods, nanowires, nanobelts and related structures by a self-seeding solution process. *J. Mater. Chem.* **2004,** *14* (16), 2530-2535.

CHAPTER 5: CONCLUSIONS AND OUTLOOK‡‡

Recent achievements in DNA nanotechnology involve designing and creating complex and functional DNA-based architectures in association with inorganic and organic nanomaterials for optimized fabrication. Similar to other DNA nanotechnology application fields such as medicine,[1] bio-imaging and bio-sensors,[2] bottom-up fabrication of DNA-assembled conductive nanostructures along with their electrical characterization is growing rapidly. I demonstrated fundamental steps associated with bottom-up fabrication of DNA origami-templated electronic nanowires and metal-semiconductor junctions. I further demonstrated different characterization approaches to study the electrical properties of structures on diverse DNA templates.

The programmable, precise, and predictable binding specificity of DNA molecules is making possible revolutionary changes utilizing DNA-assembled nanomaterials.[3-5] For example, DNA architectures which offer directed positioning of heterogeneous nanomaterials with customized orientations are ideal platforms to perform nanofabrication via self-assembly. Such sophisticated and ordered DNA-based nanostructures have displayed preliminary but promising applications in numerous research fields. For example, multiple material attachment to DNA provides unprecedented opportunities to fabricate conductive and functional structures or devices such as nanowires, metal-semiconductor structures, transistors, logic gates, and eventually integrated circuits in the future. Integration of photonic and electronic materials on DNA structures offers opportunities to explore biophysics and develop biosensing, plasmonic, and surface-enhanced Raman scattering sensors.[6, 7] In addition, nano-medicine and therapeutics can take

‡‡ Chapter 5 is adapted with permission from Pang, C.; Aryal, B. R.; Ranasinghe, D. R.; Westover, W. R.; Ehlert, A. E. F.; Harb, J. N.; Davis, R. C.; Woolley, A. T. Bottom-up Fabrication of DNA-templated Nanomaterials and Their Characterization. *Nanomaterials* **2021** (submitted).

advantage of DNA nanostructures by utilizing them in photothermal therapy for cancer.[8, 9] Different types of DNA templates can also serve as masks to create nanopatterns on substrates for lithography, or further act as a nano-breadboard in forming functional components or devices. Similarly, the assembly of DNA with proteins is growing as a unique research area. These protein-DNA hybrid structures may benefit synthetic biology and cellular signaling, helping to better understand protein functions.

Current progress in placing nanomaterials onto DNA templates demands innovative fabrication methodologies. To meet these needs, inspiration comes from nature's ability to form complicated biological systems by self-assembly of biomaterials. Although current achievements lack the technology to fully replicate many natural phenomena, it is possible to use them to guide the development of new techniques and skills to improve nanofabrication. Advancements associated with DNA-templated nanomaterials will keep growing by improving, providing increased knowledge and better procedures for their creation and characterization. To develop industry-friendly methods, further scientific improvements are needed in: (a) the design and self-assembly of DNA scaffolds into complex structures, (b) mechanisms of precise and controlled placement of heterogeneous nanomaterials onto DNA platforms, (c) the creation of composite and conductive networks such as integrated circuits, and (d) effective characterization techniques to ensure next-generation nanoelectronics can be fabricated using DNA. In an interdisciplinary field, these improvements require collective efforts from many scientific specialties to mitigate challenges related to alignment, precision and yields. DNA nanotechnology should be able to move beyond present issues and powerfully influence the nanoelectronic domain in the future.

5.1 FUTURE WORK

To continue the current achievements in building electronic nanocomponents, collection of gated I-V curves from DNA origami-templated Au/Te/Au nanowires or other metal-semiconductor junctions would be an important advancement. In my previous work, the templated metal-semiconductor chains of Au and Te nanorods after electrical connection displayed non-linear I-V curves, without having a conductive path at lower voltages, which may be a suitable condition for using gate voltages to turn on Au/Te/Au devices in the presence of a silicon dioxide layer as a capacitor, as shown in **Figure 5.1**. These anticipated field-effect transistors are likely to work under the influence of electric field with either enhancement or depletion mode to give I-V curves, which would mark important progress toward DNA-based nanoelectronics. To make this feasible, it is necessary to ensure that the Au/Te/Au devices retain electrical properties through a number of tests, because in my initial studies, I-V properties changed irreversibly when a gate voltage was applied.

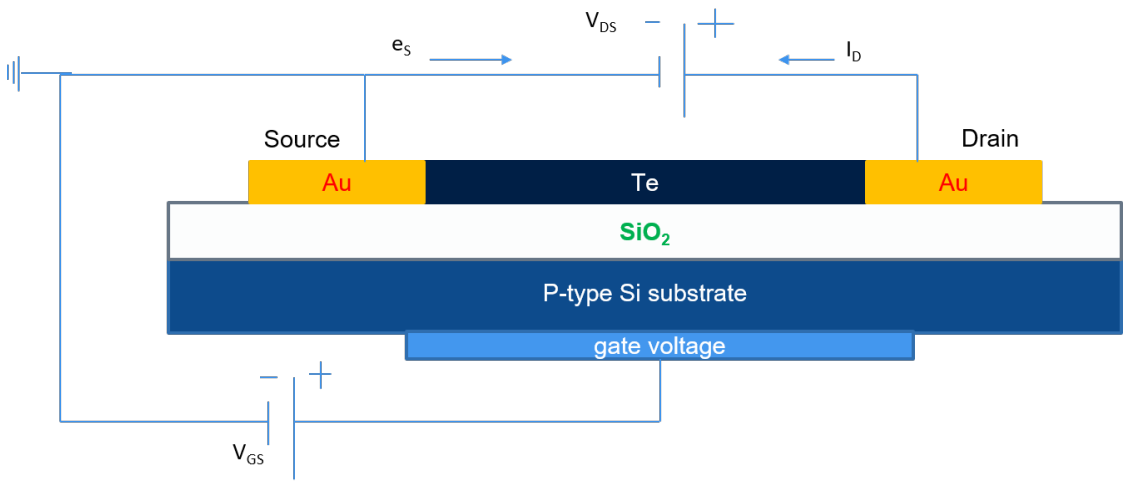

Figure 5.1 A schematic diagram of a DNA-templated field-effect transistor and setup for collecting gated I-V curves.

Successful demonstration of field-effect transistor devices will be a key step toward the study and testing of different logic gates, which are basic building blocks of digital electronic circuits, on DNA origami. It is still early to predict the possible setup and parameters needed to demonstrate DNA-supported logic gates; however, some logic gate systems such as NAND, AND or OR could be promising to study. Such logic gates would provide a basis for DNA-enabled computers, a next level achievement in nanoelectronics.

5.2 REFERENCES

1. Campolongo, M. J.; Tan, S. J.; Xu, J.; Luo, D., DNA nanomedicine: Engineering DNA as a polymer for therapeutic and diagnostic applications. *Adv. Drug Delivery Rev.* **2010,** *62* (6), 606-616.

2. Yang, Y.; Mao, G.; Ji, X.; He, Z., DNA-templated quantum dots and their applications in biosensors, bioimaging, and therapy. *J. Mater. Chem. B* **2020,** *8* (1), 9-17.

3. Bian, X.; Zhang, Z.; Xiong, Q.; De Camilli, P.; Lin, C., A programmable DNA-origami platform for studying lipid transfer between bilayers. *Nat. Chem. Biol.* **2019,** *15* (8), 830-837.

4. Zhao, Y.; Dai, X.; Wang, F.; Zhang, X.; Fan, C.; Liu, X., Nanofabrication based on DNA nanotechnology. *Nano Today* **2019,** *26*, 123-148.

5. Zhang, G.; Surwade, S. P.; Zhou, F.; Liu, H., DNA nanostructure meets nanofabrication. *Chem. Soc. Rev.* **2013,** *42* (7), 2488-96.

6. Kühler, P.; Roller, E.-M.; Schreiber, R.; Liedl, T.; Lohmüller, T.; Feldmann, J., Plasmonic DNA-origami nanoantennas for surface-enhanced Raman spectroscopy. *Nano Lett.* **2014,** *14* (5), 2914-2919.

7. Zhan, P.; Wen, T.; Wang, Z. G.; He, Y.; Shi, J.; Wang, T.; Liu, X.; Lu, G.; Ding, B., DNA Origami Directed Assembly of Gold Bowtie Nanoantennas for Single-Molecule Surface-Enhanced Raman Scattering. *Angew. Chem. Int. Ed. Engl.* **2018,** *57* (11), 2846-2850.

8. Ma, V. P.; Salaita, K., DNA Nanotechnology as an Emerging Tool to Study Mechanotransduction in Living Systems. *Small* **2019,** *15* (26), e1900961.

9. Zhan, Y.; Ma, W.; Zhang, Y.; Mao, C.; Shao, X.; Xie, X.; Wang, F.; Liu, X.; Li, Q.; Lin, Y., DNA-based nanomedicine with targeting and enhancement of therapeutic efficacy of breast cancer cells. *ACS Appl. Mater. Interfaces* **2019,** *11* (17), 15354-15365.

APPENDIX A: SCAFFOLD AND STAPLE STRAND SEQUENCES

(All sequences are given 5' to 3')

Single-stranded scaffold DNA: M13mp18 viral DNA, total bases sequences 7249

Staple sequences: Sequences in blue font have a protruding poly(A)$_{10}$ for DNA-coated Au nanorod capture.

(A) 'Plus' design

TGAACGGTCGCGTCTGGCCTTCCTGGGATGTG

AAGCCTGGGCCAGCTGGCGAAAGGGTAGCCAGAAAAAAAAAA

ATGCTGATGCAACCAAGTACCG

TACTGGTAACCGTTCCAGTAAGCGTAAATATT

GCCCGAAACAGTCAGGACGTTGGGAGAAACAC

TAACAATTAAGAAGATGATGAAACCTAAAATA

TTTGGAACAAGAGTCCACTATTAAAGCTGTTT

GCACAGACAATTATAATCCTGA

TTGAGTAAAAGCCAGAATGGAAAGAATTATCA

TACTTAGCCGGGAGAGGCTTTT

CCGTCACCTAGAAAATTCATATGGGTTTAACG

AATGCCACATCAACGTAACAAAGCGGAACAAC

CATTTTTGATTTCAACGCAAGGATCGTTCTAG

TTAATTTCATCGGAACGAGGGTAGCTTTTGCG

AATAACATGCTATTTTGCACCCAGAATTCTGT

GCAAAAGAAGTTTAGCTATATT

GCAAATCAGAATTGAGTTAAGCCCAACGGAAT

ACCTTTTACCCTTAGAATCCTTGAGCGTTAAAAAAAAAAAAA

ACATTAATAGGGCGATCGGTGCGGGAGTAACA

AATGCGCGTTCCTGATTATCAGATGAAGGGTT

AGAACCGCGGCGGATAAGTGCCGTATTTTCAGAAAAAAAAAA

CCGGAACCAGTATAGCCCGGAATATCAGAACCAAAAAAAAAA

TTACCGAAAACAAGCAAGCCGTTTCAAGAACG

GAGCAAGAAATCATTACCGCGCCCAATCAATA

CAAAGCGCGAAACCTGTCGTGCCACTGAGAGA

GAAAAGGTATGGTCAATAACCTGTTTTGCCAG

ATTACGCAAGCACCGTAATCAGTAACCCTCAGAAAAAAAAAA

CGCCTGATGCTTCTGTAAATCGTCTTACTAGA

CTGATTGCCCTTCACCGCCTGGCCGCTGCATT

GATTGACCTTAATGCCGGAGAGGGTGCGGGAG

GCCTGAGAAACATTAAATGTGAGCGCCTCTTCAAAAAAAAAA

TTCATTTGGGGAAATATTTAAA

TTTGAGAGGATTCTCCGTGGGAACTGCGCAAC

ATCACCATCGCATCGTAACCGTGCAGCCAGCT

TTTGACCCGCGCATAGGCTGGCTGATGCAGAT

ACCCAAAATGCCTTTAGCGTCAGACCACCCTCAAAAAAAAAA

GGATCGTCCTCAGAACCGCCACCCGGTGTATCAAAAAAAAAA

CCGCCTGCATCCTTTGCCCGAACGGTAACAGTAAAAAAAAAA

CAGAAAACATACCACATTCAACTAACCTTCATAAAAAAAAAA

CGAAAGACAGCAACTTTAATCA

AATGCAGAAACACCGGAATCATAAGCTATTAAAAAAAAAAAA

TTATTAGCAGATAGCCGAACAAAGTAGCTATC

ATTATTACACCCTGACTATTATAGTAATTGCT

CAGCCATATTACAACCGATTGA

CTTTCCAGTAAGAAACGATTTTTTTTTACCAG

GATTAGTTAAAAACAGGGAAGCGCAAAGAAAC

TTACCCAATACGAAGGCACCAACCGCTTGATA

CATTATACGACTTCAAATATCGCGGATTAGAG

TTTCATCTCGAGCATGTAGAAACCAATAGCAA

ATCGGCTGCTTTTTCAAATATATTGGTCTGAG

GGATTTTGGAATTGCGAATAATAAATCGCCTG

AAGAGCAATACTGCGGAATCGTCAATTCTGCG

CTTTCGAGTAGCATTCCACAGACATATTCTGA

ATTACCGCCAGCCATTGCAACAGGGAGCCAGC

GAGGAAGTAAGGCTTGCCCTGACGAAGAAAAA

ATCGTAGGAACAATGAAATAGCAATTACCAGA

GGTTTAACTAGATTAAGACGCTGATGGTTTGA

ACCAGTCACACGACCAGTAATAAAACATCGCC

CTGCAAGGTACGAGCCGGAAGCATTCAAAAGA

AGGAAACCTCGGCATTTTCGGTCAAGCCACCAAAAAAAAAAA

GAGGATCCCCGACCGTCTATCA

AAGAGAAGCCAGAACCACCACCAGTGAAACCA

AGGAAGGTTATAAACATCAAGA

AGCCGCCAGATTAGGATTAGCGGGATGTACCGAAAAAAAAAA

ATTAAAAAAAACCACCAGAAGGAGTGCACGTA

AGCATTAAGATTTAGTTTGACCATACTGGATA

TAACATCACTTGCCTGAGTAGAAGTCAATATC

TAAGAATAACGCGCCTGTTTATCAAACCTCCCAAAAAAAAAA

TAGATGGGCAATATGATATTCAACAAAAATTT

CGAGCTTCCTTATGCGATTTTAAGGAGATGGT

CCTCATTACAGTGCCCGTATAAACTGTCGTCTAAAAAAAAAA

AGGCTTGCCAGAGCCACCACCCTCCGAGAGGGAAAAAAAAAA

GCCACCCTAGGGAGTTAAAGGCCGCAACGGCT

CTAAGAACTTGAGCGCTAATATCAGACTCCTT

AACTAAAGCTAAACAACTTTCAACCAGGAGTGAAAAAAAAAA

CGATAGCTGTCAGATGAATATACATTATTAAT

GAAATCGGCAAAATCCCTTATAAAAAAGTGTAAAAAAAAAAA

GGGAGGGAAGGTCATACATGGCAAAAAAAAAA

AATAGTGAATAAAGAAATTGCGTAATTTTGCG

CCAACTTTAACGGAGATTTGTATCTTTTTTCA

GTCTGAAATGGATTATTTACATTGAGCAGAAG

AGAACCTATTTTTAACCTCCGGCTAAAGAACG

CAAAAACATCGCATTAAATTTTTGACGACGGC

TAACACTGTGCGCCGACAATGACAAAATACGT

AATGAATCCCGCTTCTGGTGCCGGCGTTGGTG

ATCAAGTTGAACTGGCATGATTAAGAGAGATA

AATCCAAAAGCCTAATTTGCCAGTATTTAGGC

AGCAAATGGACTTTACAAACAATTAACGGATT

CTTTCATCGTCTGGAGCAAACAAGATAAAGCCAAAAAAAAAA

TTCCGGCAGGCCAACGCGCGGGGAGGCAACAG

CAGTACCACACCCTCAGAGCCACCGCGACAGA

ACATAACGCCCCCTCAAATGCTTTGAAGTTTC

ACAGAGGCGTAGTAAATTGGGCTTAACTGGCT

TTCCAGACATCTCCAAAAAAAAGGGCGCGAAA

TAGCAAGGAAGGTGGCAACATATAATTAGACGAAAAAAAAAA

TCATCATAAACTGATAGCCCTAAAAGGGACAT

CGCCAAAGTTATTCATTAAAGGTGCGCAGTCTAAAAAAAAAA

AAGTATTAAAAAATCTAAAGCATCAGAACAAT

TTATCCTGGAAAATAGCAGCCTTTATTTTGTC

TTTAAAAGGAGGTGAGGCGGTCAGGCTCAATC

AAGCCTTTCGGATGGCTTAGAGCTTCAGAAGC

ACCCACAAGATATAGAAGGCTTATATCCCATC

GTACCGCCACCACCCTCAGCAG

CCGATAGTAGTTTCGTCACCAGTAGACTCCTC

GCCGTCAAAATATCAAACCCTCAAAACTCAAA

TGAGTAATAACTCCAACAGGTCAGTTTTAATT

GTATCGGCCTCTGGGCGCCAGG

GTGGTTTTTCTTTTCACCAGTGAGACGGAGGCGGT

CAGACCAGCCAGCGATTATACCAACTCCAAAA

GCGTCCAACACTATCATAACCCTCCGAACTGA

CCCCCTGCCTTGATATTCACAAACGAATTAGA

GAAAGCGTAAGAATACGTG

TATGCAACTAAAGCTAAATCGGTTAGGTCATTAAAAAAAAAA

CCAGACGAGTTTAGTATCATATGCGTGAGTGA

ATATGTACTTTAACCAATAGGAACCGCCAGGG

TTCATCAAATTTTTGAATGGCTATTCTGACCT

ACACAACACGATTAAGTTGGGTAAGCCATCAA

GAAAAGTAAGCGTTTGCCATCT

TTTCGCAAGGCATCAATTCTACTAAAAAGCCC

ATTCCATATTAGCAAAATTAAGCAAGAATCGA

TTAGAACCTAATTGCTCCTTTTGAAAGAGGAA

GCCAGCAAACCACGGAATAAGTTTACAGAGAG

GTTATATAATACTTCTGAATAATGGATGGCAA

GCTATTACGGTGCCTAATGAGTGAGTGGTTCCAAAAAAAAAA

ACCGTACTAAATCACCGGAACCAGTAGCCCCC

GATTCAAAAGGGGACGACGACA

CAGTGAATTTCCATTAAACGGGTAACAACCAT

CGAGAAAATCTTTCCTTATCATTCTTATTTTC

TCGCGCAGACATAAATCAATATATGTTATACA

CGTTGAAAGTTAGTAAATGAATTTTCAGTGCCAAAAAAAAAA

AGCAGGCGAAAATCCTGTTTGATGGCTAACTC

CATACATACCGGAAACGTCACCAAAGCCGCCG

CCAGCATTAGTATTAAGAGGCTGACAAACTAC

AGTTAGCGTAATTGTATCGGTTTACACTCATC

AAACAAAATTATATTTAACAAC

CGATTGGCCTATTTCGGAACCTATGCCCTCAT

GACGGAAAACAAAAGGGCGACATTTTTATCCC

GACTTGCGAACTGAACACCCTGAAAGAAAATAAAAAAAAAAA

ATAGCCCGAGATAGGGTTGAGTGTACAATTCC

TTGTTTGGATTACTATATGTAA

TTAATTTTCATCGGGAGAAACAATCGACAACTAAAAAAAAAA

TTGTGAATTACAAAGCGAACCA

GCCAACATGTATACAAAATAAA

CGTTTTCAGAGGAAACGCAATAATAATAATAA

GCAGACGGTGTCGAAATCCGCGACAAAGGAAC

TCTACGTTTTGCATCAAAAAGATTTAAGAGGT

AGTACCTTCTCATATATTTTAAATACAGTCAA

CACTCATCGAGGCCCTTTTTAA

TTTTCCCAAAATTGTTATCCGCTCTGTTCCAG

TCTTTAGGTGGCAAATCAACAGTTATTAGTAA

AAAGCGGAAATAAAACGAACTAACTGCTCATT

AATACCGAGAACAAGAAAAATAATCCGGTATT

AGTGAGAATAGCTGCTCCATGT

GAACCTCATAGATAATACATTTGATTACAAAA

CTGAATTTATAAGTTTTAACGGGGTCTGTATGAAAAAAAAAA

AACATGAAGACAGGAGGTTGAGGCATTACCAT

GAATATAAGACCCTGTAATACTTTTAGCTATT

CATTGAATCCAAAAGGAATTACGAACGGTGTA

CAGAACGATTTGAGGACTAAAGACGGTCGCTG

GTTTGAGGGTGAGAAAGGCCGGAGGCAATGCC

TTTTGATGATAAGTTTCAGCGGAAAAAAAAAA

ACAATCAAGACTTGAGCCATTTGGAAATAAATAAAAAAAAAA

TGGTCAGTAGCACTAACAACTAATTCAATTAC

ATAAATTGTCAATCATAAGGGAACGTTTACCA

AAACAGAAATTTATCAAAATCATATTAGTTAA

AGGGGGTATAAAAACCAAAATAGCAACGAGGC

GAAACAGTAGGCGAATTATTCATTAGATTAGA

GTTAAAATGGAAGATTGTATAAGCCGCGAGCT

AAATAATTAATCGTAAAACTAGCACAGGCAAG

AGGTCTTTAGGTAGAAAGATTCATGATATTCA

ATAACCTTTGCTTTGAATACCAAGGGATTTAG

GACTCCAACGTCAAAGGGCGAAAAGGTACCGA

GCTCGAATAGCTTGCATGCCTGCAAATATTTT

CTGAGCAATCATTTGAATTACCTTGCTCAACA

ATAAAACATTTGAGTAACATTATCGATTTTCA

TTGCGTATAGGAAGATCGCACTCCATCTGCCA

GGAGAATTGGAGGTTTTGAAGCCTGTTCAGCTAAAAAAAAAA

TGTTGGGATGCGTTGCGCTCACTGTTTGCCCC

CTGATAAAGTAATGGGATAGGTCAAAACCAGG

TCATGGAAATACCTACATTTTGACTATTAACAAAAAAAAAAA

CAAAGTACGAAAGAGGACAGATGAGGCATAGT

ATACTTCTTTGGAAAGGAATTG

GGTATTAAAATCCAATCGCAAGACTAGGTTGG

TTGTAAACGTTGGTCGACTCTA

AATTCTTACGACAAAAGGTAAAGTCTACAATT

TTTCATAATCACAGGAGGTTTAAAAAAAAAAA

GCAAAGAATAACAGTTGATTCCCATAAATATT

CGCCCACGAGCCCAATAGGAACCCGTTTTGCTAAAAAAAAAA

CTATCGGCCTTGCTGGTAATATCCACCTTGCT

CTAATTTATCTGACCTAAATTTAAGAAGAGTC

GAACAAAGTACCGAACGAACCACCGCAGATTC

TAAAGTACCCAGTATAAAGCCAACTTTTAATG

AGAGGCATTAATTGAGAATCGCCAATTACATT

GTTGCAGCAAGCGGTCCACGCTGGCCCGCTTT

GTAGGGCTTTTCGAGCCAGTAATAACGAGCGT

GACGACGAATAGTAAAATGTTTAGTAGATACA

ATTTAGGAGAGAATGACCATAAATGTTTTAAAAAAAAAAAAA

AAAAGCCTCGACAATAAACAACATTAAATCAA

TCTGGCCAACAGAGATAGAACCCTTAGTCTTT

AACGAGTACATCCAATAAATCATATGTCAATC

CAAGAGTAAAAGAATACACTAAAATCAGCTTG

CCAGTCGGCATTCGCCATTCAGGCAAACGGCG

TAAGTCCTCCGTGTGATAAATAAGAAACATAG

GAGGGTAAGCGAGGCGTTTTAGCGACAATAGA

TCGATAGCGTATGTTAGCAAACGTCAAAGTCA

AAGAGGCAATCTTGACAAGAACCGCAGTTGAGAAAAAAAAAA

GGATAGCACATAACCGATATATTCTTTTTCAT

GGAGCCTTTAACGATCTAAAGTTTAGTTAATGAAAAAAAAAA

AGACTACCCCATATCAAAATTATTCGGAATTA

TCAAAAATAATCTTACCAACGCTAAGAGAATA

ACCCGTCGATCTACAAAGGCTATCGTACCAAA

CAGTGCCATCGTAATCATGGTCATAGAACGTG

TTGATATAGCCTCCCTCAGAGCCGCTGTAGCG

TCAGAGCATAAAGTACGGTGTCTGAAACAGTTAAAAAAAAAA

AACGCCTGGTGAATTTCTTAAACATAAAACGA

AACATTATTGCTGTAGCTCAACATCAAAAATC

CGTATTAAAACAGTGCCACGCTGAAAAAACGCAAAAAAAAAA

GCTCATTTCCCGGTTGATAATCAGATAGTAGT

GCAAAGACAATCACCAGTAGCACCAGGTCAGA

GACCGGAAGCAGTGTAGGTAAA

CCTGTGTGGTCACGACGTTGTAAATTAAATCA

(B) 'Cross' design

TGAACGGTCGCGTCTGGCCTTCCTGGGATGTG

AAGCCTGGGCCAGCTGGCGAAAGGGTAGCCAGAAAAAAAAAA

ATGCTGATGCAACCAAGTACCG

TACTGGTAACCGTTCCAGTAAGCGTAAATATT

GCCCGAAACAGTCAGGACGTTGGGAGAAACAC

TAACAATTAAGAAGATGATGAAACCTAAAATA

TTTGGAACAAGAGTCCACTATTAAAGCTGTTT

GCACAGACAATTATAATCCTGA

TTGAGTAAAAGCCAGAATGGAAAGAATTATCA

TACTTAGCCGGGAGAGGCTTTT

CCGTCACCTAGAAAATTCATATGGGTTTAACG

AATGCCACATCAACGTAACAAAGCGGAACAACAAAAAAAAAA

CATTTTTGATTTCAACGCAAGGATCGTTCTAGAAAAAAAAAA

TTAATTTCATCGGAACGAGGGTAGCTTTTGCG

AATAACATGCTATTTTGCACCCAGAATTCTGT

GCAAAAGAAGTTTAGCTATATT

GCAAATCAGAATTGAGTTAAGCCCAACGGAATAAAAAAAAAA

ACCTTTTACCCTTAGAATCCTTGAGCGTTAAA

ACATTAATAGGGCGATCGGTGCGGGAGTAACA

AATGCGCGTTCCTGATTATCAGATGAAGGGTTAAAAAAAAAA

AGAACCGCGGCGGATAAGTGCCGTATTTTCAG

CCGGAACCAGTATAGCCCGGAATATCAGAACC

TTACCGAAAACAAGCAAGCCGTTTCAAGAACG

GAGCAAGAAATCATTACCGCGCCCAATCAATAAAAAAAAAAA

CAAAGCGCGAAACCTGTCGTGCCACTGAGAGA

GAAAAGGTATGGTCAATAACCTGTTTTGCCAG

ATTACGCAAGCACCGTAATCAGTAACCCTCAGAAAAAAAAAA

CGCCTGATGCTTCTGTAAATCGTCTTACTAGA

CTGATTGCCCTTCACCGCCTGGCCGCTGCATT

GATTGACCTTAATGCCGGAGAGGGTGCGGGAG

GCCTGAGAAACATTAAATGTGAGCGCCTCTTC

TTCATTTGGGGAAATATTTAAA

TTTGAGAGGATTCTCCGTGGGAACTGCGCAAC

ATCACCATCGCATCGTAACCGTGCAGCCAGCTAAAAAAAAAA

TTTGACCCGCGCATAGGCTGGCTGATGCAGATAAAAAAAAAA

ACCCAAAATGCCTTTAGCGTCAGACCACCCTC

GGATCGTCCTCAGAACCGCCACCCGGTGTATC

CCGCCTGCATCCTTTGCCCGAACGGTAACAGT

CAGAAAACATACCACATTCAACTAACCTTCAT

CGAAAGACAGCAACTTTAATCA

AATGCAGAAACACCGGAATCATAAGCTATTAA

TTATTAGCAGATAGCCGAACAAAGTAGCTATC

ATTATTACACCCTGACTATTATAGTAATTGCT

CAGCCATATTACAACCGATTGA

CTTTCCAGTAAGAAACGATTTTTTTTTACCAG

GATTAGTTAAAAACAGGGAAGCGCAAAGAAACAAAAAAAAAA

TTACCCAATACGAAGGCACCAACCGCTTGATA

CATTATACGACTTCAAATATCGCGGATTAGAG

TTTCATCTCGAGCATGTAGAAACCAATAGCAAAAAAAAAAAA

ATCGGCTGCTTTTTCAAATATATTGGTCTGAGAAAAAAAAAA

GGATTTTGGAATTGCGAATAATAAATCGCCTG

AAGAGCAATACTGCGGAATCGTCAATTCTGCGAAAAAAAAAA

CTTTCGAGTAGCATTCCACAGACATATTCTGA

ATTACCGCCAGCCATTGCAACAGGGAGCCAGC

GAGGAAGTAAGGCTTGCCCTGACGAAGAAAAAAAAAAAAAAA

ATCGTAGGAACAATGAAATAGCAATTACCAGA

GGTTTAACTAGATTAAGACGCTGATGGTTTGA

ACCAGTCACACGACCAGTAATAAAACATCGCC

CTGCAAGGTACGAGCCGGAAGCATTCAAAAGA

AGGAAACCTCGGCATTTTCGGTCAAGCCACCAAAAAAAAAAA

GAGGATCCCCGACCGTCTATCA

AAGAGAAGCCAGAACCACCACCAGTGAAACCA

AGGAAGGTTATAAACATCAAGA

AGCCGCCAGATTAGGATTAGCGGGATGTACCGAAAAAAAAAA

ATTAAAAAAAACCACCAGAAGGAGTGCACGTA

AGCATTAAGATTTAGTTTGACCATACTGGATA

TAACATCACTTGCCTGAGTAGAAGTCAATATCAAAAAAAAAA

TAAGAATAACGCGCCTGTTTATCAAACCTCCC

TAGATGGGCAATATGATATTCAACAAAAATTT

CGAGCTTCCTTATGCGATTTTAAGGAGATGGT

CCTCATTACAGTGCCCGTATAAACTGTCGTCT

AGGCTTGCCAGAGCCACCACCCTCCGAGAGGG

GCCACCCTAGGGAGTTAAAGGCCGCAACGGCT

CTAAGAACTTGAGCGCTAATATCAGACTCCTTAAAAAAAAAA

AACTAAAGCTAAACAACTTTCAACCAGGAGTG

CGATAGCTGTCAGATGAATATACATTATTAAT

GAAATCGGCAAAATCCCTTATAAAAAAGTGTA

GGGAGGGAAGGTCATACATGGC

AATAGTGAATAAAGAAATTGCGTAATTTTGCG

CCAACTTTAACGGAGATTTGTATCTTTTTTCA

GTCTGAAATGGATTATTTACATTGAGCAGAAG

AGAACCTATTTTTAACCTCCGGCTAAAGAACGAAAAAAAAAA

CAAAAACATCGCATTAAATTTTTGACGACGGCAAAAAAAAAA

TAACACTGTGCGCCGACAATGACAAAATACGTAAAAAAAAAA

AATGAATCCCGCTTCTGGTGCCGGCGTTGGTGAAAAAAAAAA

ATCAAGTTGAACTGGCATGATTAAGAGAGATAAAAAAAAAAA

AATCCAAAAGCCTAATTTGCCAGTATTTAGGC

AGCAAATGGACTTTACAAACAATTAACGGATT

CTTTCATCGTCTGGAGCAAACAAGATAAAGCCA

TTCCGGCAGGCCAACGCGCGGGGAGGCAACAG

CAGTACCACACCCTCAGAGCCACCGCGACAGAAAAAAAAAAA

ACATAACGCCCCCTCAAATGCTTTGAAGTTTC

ACAGAGGCGTAGTAAATTGGGCTTAACTGGCT

TTCCAGACATCTCCAAAAAAAAGGGCGCGAAA

TAGCAAGGAAGGTGGCAACATATAATTAGACG

TCATCATAAACTGATAGCCCTAAAAGGGACAT

CGCCAAAGTTATTCATTAAAGGTGCGCAGTCT

AAGTATTAAAAAATCTAAAGCATCAGAACAAT

TTATCCTGGAAAATAGCAGCCTTTATTTTGTCAAAAAAAAAA

TTTAAAAGGAGGTGAGGCGGTCAGGCTCAATC

AAGCCTTTCGGATGGCTTAGAGCTTCAGAAGCAAAAAAAAAA

ACCCACAAGATATAGAAGGCTTATATCCCATC

GTACCGCCACCACCCTCAGCAG

CCGATAGTAGTTTCGTCACCAGTAGACTCCTC

GCCGTCAAAATATCAAACCCTCAAAACTCAAA

TGAGTAATAACTCCAACAGGTCAGTTTTAATT

GTATCGGCCTCTGGGCGCCAGG

GTGGTTTTTCTTTTCACCAGTGAGACGGAGGCGGT

CAGACCAGCCAGCGATTATACCAACTCCAAAA

GCGTCCAACACTATCATAACCCTCCGAACTGA

CCCCCTGCCTTGATATTCACAAACGAATTAGAAAAAAAAAAA

GAAAGCGTAAGAATACGTG

TATGCAACTAAAGCTAAATCGGTTAGGTCATT

CCAGACGAGTTTAGTATCATATGCGTGAGTGA

ATATGTACTTTAACCAATAGGAACCGCCAGGG

TTCATCAAATTTTTGAATGGCTATTCTGACCT

ACACAACACGATTAAGTTGGGTAAGCCATCAA

GAAAAGTAAGCGTTTGCCATCT

TTTCGCAAGGCATCAATTCTACTAAAAAGCCCAAAAAAAAAA

ATTCCATATTAGCAAAATTAAGCAAGAATCGA

TTAGAACCTAATTGCTCCTTTTGAAAGAGGAA

GCCAGCAAACCACGGAATAAGTTTACAGAGAGAAAAAAAAAA

GTTATATAATACTTCTGAATAATGGATGGCAA

GCTATTACGGTGCCTAATGAGTGAGTGGTTCC

ACCGTACTAAATCACCGGAACCAGTAGCCCCC

GATTCAAAAGGGGACGACGACA

CAGTGAATTTCCATTAAACGGGTAACAACCAT

CGAGAAAATCTTTCCTTATCATTCTTATTTTC

TCGCGCAGACATAAATCAATATATGTTATACAAAAAAAAAAA

CGTTGAAAGTTAGTAAATGAATTTTCAGTGCC

AGCAGGCGAAAATCCTGTTTGATGGCTAACTC

CATACATACCGGAAACGTCACCAAAGCCGCCG

CCAGCATTAGTATTAAGAGGCTGACAAACTAC

AGTTAGCGTAATTGTATCGGTTTACACTCATCAAAAAAAAAA

AAACAAAATTATATTTAACAAC

CGATTGGCCTATTTCGGAACCTATGCCCTCAT

GACGGAAAACAAAAGGGCGACATTTTTATCCC

GACTTGCGAACTGAACACCCTGAAAGAAAATA

ATAGCCCGAGATAGGGTTGAGTGTACAATTCC

TTGTTTGGATTACTATATGTAA

TTAATTTTCATCGGGAGAAACAATCGACAACT

TTGTGAATTACAAAGCGAACCA

GCCAACATGTATACAAAATAAA

CGTTTTCAGAGGAAACGCAATAATAATAATAA

GCAGACGGTGTCGAAATCCGCGACAAAGGAAC

TCTACGTTTTGCATCAAAAAGATTTAAGAGGTAAAAAAAAAA

AGTACCTTCTCATATATTTTAAATACAGTCAAAAAAAAAAAA

CACTCATCGAGGCCCTTTTTAA

TTTTCCCAAAATTGTTATCCGCTCTGTTCCAG

TCTTTAGGTGGCAAATCAACAGTTATTAGTAA

AAAGCGGAAATAAAACGAACTAACTGCTCATTAAAAAAAAAA

AATACCGAGAACAAGAAAAATAATCCGGTATT

AGTGAGAATAGCTGCTCCATGT

GAACCTCATAGATAATACATTTGATTACAAAA

CTGAATTTATAAGTTTTAACGGGGTCTGTATG

AACATGAAGACAGGAGGTTGAGGCATTACCAT

GAATATAAGACCCTGTAATACTTTTAGCTATT

CATTGAATCCAAAAGGAATTACGAACGGTGTAAAAAAAAAAA

CAGAACGATTTGAGGACTAAAGACGGTCGCTG

GTTTGAGGGTGAGAAAGGCCGGAGGCAATGCC

TTTTGATGATAAGTTTCAGCGG

ACAATCAAGACTTGAGCCATTTGGAAATAAAT

TGGTCAGTAGCACTAACAACTAATTCAATTACAAAAAAAAAA

ATAAATTGTCAATCATAAGGGAACGTTTACCA

AAACAGAAATTTATCAAAATCATATTAGTTAAAAAAAAAAA

AGGGGGTATAAAAACCAAAATAGCAACGAGGC

GAAACAGTAGGCGAATTATTCATTAGATTAGA

GTTAAAATGGAAGATTGTATAAGCCGCGAGCT

AAATAATTAATCGTAAAACTAGCACAGGCAAG

AGGTCTTTAGGTAGAAAGATTCATGATATTCA

ATAACCTTTGCTTTGAATACCAAGGGATTTAG

GACTCCAACGTCAAAGGGCGAAAAGGTACCGA

GCTCGAATAGCTTGCATGCCTGCAAATATTTT

CTGAGCAATCATTTGAATTACCTTGCTCAACAAAAAAAAAA

ATAAAACATTTGAGTAACATTATCGATTTTCA

TTGCGTATAGGAAGATCGCACTCCATCTGCCA

GGAGAATTGGAGGTTTTGAAGCCTGTTCAGCT

TGTTGGGATGCGTTGCGCTCACTGTTTGCCCC

CTGATAAAGTAATGGGATAGGTCAAAACCAGG

TCATGGAAATACCTACATTTTGACTATTAACA

CAAAGTACGAAAGAGGACAGATGAGGCATAGTAAAAAAAAAA

ATACTTCTTTGGAAAGGAATTG

GGTATTAAAATCCAATCGCAAGACTAGGTTGG

TTGTAAACGTTGGTCGACTCTA

AATTCTTACGACAAAAGGTAAAGTCTACAATTAAAAAAAAAA

TTTCATAATCACAGGAGGTTTA

GCAAAGAATAACAGTTGATTCCCATAAATATTAAAAAAAAAA

CGCCCACGAGCCCAATAGGAACCCGTTTTGCT

CTATCGGCCTTGCTGGTAATATCCACCTTGCT

CTAATTTATCTGACCTAAATTTAAGAAGAGTC

GAACAAAGTACCGAACGAACCACCGCAGATTC

TAAAGTACCCAGTATAAAGCCAACTTTTAATGAAAAAAAAAA

AGAGGCATTAATTGAGAATCGCCAATTACATT

GTTGCAGCAAGCGGTCCACGCTGGCCCGCTTT

GTAGGGCTTTTCGAGCCAGTAATAACGAGCGT

GACGACGAATAGTAAAATGTTTAGTAGATACA

ATTTAGGAGAGAATGACCATAAATGTTTTAAA

AAAAGCCTCGACAATAAACAACATTAAATCAA

TCTGGCCAACAGAGATAGAACCCTTAGTCTTT

AACGAGTACATCCAATAAATCATATGTCAATCAAAAAAAAAA

CAAGAGTAAAAGAATACACTAAAATCAGCTTG

CCAGTCGGCATTCGCCATTCAGGCAAACGGCG

TAAGTCCTCCGTGTGATAAATAAGAAACATAG

GAGGGTAAGCGAGGCGTTTTAGCGACAATAGA

TCGATAGCGTATGTTAGCAAACGTCAAAGTCA

AAGAGGCAATCTTGACAAGAACCGCAGTTGAG

GGATAGCACATAACCGATATATTCTTTTTCAT

GGAGCCTTTAACGATCTAAAGTTTAGTTAATG

AGACTACCCCATATCAAAATTATTCGGAATTA

TCAAAAATAATCTTACCAACGCTAAGAGAATAAAAAAAAAAA

ACCCGTCGATCTACAAAGGCTATCGTACCAAA

CAGTGCCATCGTAATCATGGTCATAGAACGTG

TTGATATAGCCTCCCTCAGAGCCGCTGTAGCG

TCAGAGCATAAAGTACGGTGTCTGAAACAGTT

AACGCCTGGTGAATTTCTTAAACATAAAACGA

AACATTATTGCTGTAGCTCAACATCAAAAATC

CGTATTAAAACAGTGCCACGCTGAAAAAACGC

GCTCATTTCCCGGTTGATAATCAGATAGTAGTAAAAAAAAAA

GCAAAGACAATCACCAGTAGCACCAGGTCAGAAAAAAAAAAA

GACCGGAAGCAGTGTAGGTAAA

CCTGTGTGGTCACGACGTTGTAAATTAAATCAAAAAAAAAAA

(C) 'C' design

TGAACGGTCGCGTCTGGCCTTCCTGGGATGTG

AAGCCTGGGCCAGCTGGCGAAAGGGTAGCCAG

ATGCTGATGCAACCAAGTACCG

TACTGGTAACCGTTCCAGTAAGCGTAAATATTAAAAAAAAAA

GCCCGAAACAGTCAGGACGTTGGGAGAAACAC

TAACAATTAAGAAGATGATGAAACCTAAAATA

TTTGGAACAAGAGTCCACTATTAAAGCTGTTT

GCACAGACAATTATAATCCTGA

TTGAGTAAAAGCCAGAATGGAAAGAATTATCA

TACTTAGCCGGGAGAGGCTTTT

CCGTCACCTAGAAAATTCATATGGGTTTAACG

AATGCCACATCAACGTAACAAAGCGGAACAAC

CATTTTTGATTTCAACGCAAGGATCGTTCTAG

TTAATTTCATCGGAACGAGGGTAGCTTTTGCGAAAAAAAAAA

AATAACATGCTATTTTGCACCCAGAATTCTGT

GCAAAAGAAGTTTAGCTATATT

GCAAATCAGAATTGAGTTAAGCCCAACGGAAT

ACCTTTTACCCTTAGAATCCTTGAGCGTTAAA

ACATTAATAGGGCGATCGGTGCGGGAGTAACA

AATGCGCGTTCCTGATTATCAGATGAAGGGTT

AGAACCGCGGCGGATAAGTGCCGTATTTTCAG

CCGGAACCAGTATAGCCCGGAATATCAGAACCAAAAAAAAAA

TTACCGAAAACAAGCAAGCCGTTTCAAGAACG

GAGCAAGAAATCATTACCGCGCCCAATCAATA

CAAAGCGCGAAACCTGTCGTGCCACTGAGAGA

GAAAAGGTATGGTCAATAACCTGTTTTGCCAGAAAAAAAAAA

ATTACGCAAGCACCGTAATCAGTAACCCTCAG

CGCCTGATGCTTCTGTAAATCGTCTTACTAGA

CTGATTGCCCTTCACCGCCTGGCCGCTGCATT

GATTGACCTTAATGCCGGAGAGGGTGCGGGAG

GCCTGAGAAACATTAAATGTGAGCGCCTCTTC

TTCATTTGGGGAAATATTTAAA

TTTGAGAGGATTCTCCGTGGGAACTGCGCAAC

ATCACCATCGCATCGTAACCGTGCAGCCAGCT

TTTGACCCGCGCATAGGCTGGCTGATGCAGAT

ACCCAAAATGCCTTTAGCGTCAGACCACCCTC

GGATCGTCCTCAGAACCGCCACCCGGTGTATCAAAAAAAAAA

CCGCCTGCATCCTTTGCCCGAACGGTAACAGT

CAGAAAACATACCACATTCAACTAACCTTCAT

CGAAAGACAGCAACTTTAATCA

AATGCAGAAACACCGGAATCATAAGCTATTAAAAAAAAAAAA

TTATTAGCAGATAGCCGAACAAAGTAGCTATCAAAAAAAAAA

ATTATTACACCCTGACTATTATAGTAATTGCT

CAGCCATATTACAACCGATTGA

CTTTCCAGTAAGAAACGATTTTTTTTTACCAGAAAAAAAAAA

GATTAGTTAAAAACAGGGAAGCGCAAAGAAAC

TTACCCAATACGAAGGCACCAACCGCTTGATA

CATTATACGACTTCAAATATCGCGGATTAGAGAAAAAAAAAA

TTTCATCTCGAGCATGTAGAAACCAATAGCAA

ATCGGCTGCTTTTTCAAATATATTGGTCTGAGAAAAAAAAAA

GGATTTTGGAATTGCGAATAATAAATCGCCTGAAAAAAAAAA

AAGAGCAATACTGCGGAATCGTCAATTCTGCG

CTTTCGAGTAGCATTCCACAGACATATTCTGA

ATTACCGCCAGCCATTGCAACAGGGAGCCAGCAAAAAAAAAA

GAGGAAGTAAGGCTTGCCCTGACGAAGAAAAA

ATCGTAGGAACAATGAAATAGCAATTACCAGAAAAAAAAAAA

GGTTTAACTAGATTAAGACGCTGATGGTTTGA

ACCAGTCACACGACCAGTAATAAAACATCGCCAAAAAAAAAA

CTGCAAGGTACGAGCCGGAAGCATTCAAAAGA

AGGAAACCTCGGCATTTTCGGTCAAGCCACCAAAAAAAAAAA

GAGGATCCCCGACCGTCTATCA

AAGAGAAGCCAGAACCACCACCAGTGAAACCA

AGGAAGGTTATAAACATCAAGA

AGCCGCCAGATTAGGATTAGCGGGATGTACCG

ATTAAAAAAAACCACCAGAAGGAGTGCACGTAAAAAAAAAA

AGCATTAAGATTTAGTTTGACCATACTGGATA

TAACATCACTTGCCTGAGTAGAAGTCAATATCAAAAAAAAAA

TAAGAATAACGCGCCTGTTTATCAAACCTCCC

TAGATGGGCAATATGATATTCAACAAAAATTT

CGAGCTTCCTTATGCGATTTTAAGGAGATGGTAAAAAAAAAA

CCTCATTACAGTGCCCGTATAAACTGTCGTCT

AGGCTTGCCAGAGCCACCACCCTCCGAGAGGG

GCCACCCTAGGGAGTTAAAGGCCGCAACGGCTAAAAAAAAAA

CTAAGAACTTGAGCGCTAATATCAGACTCCTT

AACTAAAGCTAAACAACTTTCAACCAGGAGTGAAAAAAAAAA

CGATAGCTGTCAGATGAATATACATTATTAATAAAAAAAAAA

GAAATCGGCAAAATCCCTTATAAAAAAGTGTA

GGGAGGGAAGGTCATACATGGC

AATAGTGAATAAAGAAATTGCGTAATTTTGCGAAAAAAAAAA

CCAACTTTAACGGAGATTTGTATCTTTTTTCA

GTCTGAAATGGATTATTTACATTGAGCAGAAGAAAAAAAAAA

AGAACCTATTTTTAACCTCCGGCTAAAGAACG

CAAAAACATCGCATTAAATTTTTGACGACGGC

TAACACTGTGCGCCGACAATGACAAAATACGT

AATGAATCCCGCTTCTGGTGCCGGCGTTGGTG

ATCAAGTTGAACTGGCATGATTAAGAGAGATA

AATCCAAAAGCCTAATTTGCCAGTATTTAGGC

AGCAAATGGACTTTACAAACAATTAACGGATTAAAAAAAAAA

CTTTCATCGTCTGGAGCAAACAAGATAAAGCC

TTCCGGCAGGCCAACGCGCGGGGAGGCAACAG

CAGTACCACACCCTCAGAGCCACCGCGACAGA

ACATAACGCCCCCTCAAATGCTTTGAAGTTTC

ACAGAGGCGTAGTAAATTGGGCTTAACTGGCTAAAAAAAAAA

TTCCAGACATCTCCAAAAAAAAGGGCGCGAAA

TAGCAAGGAAGGTGGCAACATATAATTAGACG

TCATCATAAACTGATAGCCCTAAAAGGGACATAAAAAAAAAA

CGCCAAAGTTATTCATTAAAGGTGCGCAGTCTAAAAAAAAAA

AAGTATTAAAAAATCTAAAGCATCAGAACAATAAAAAAAAAA

TTATCCTGGAAAATAGCAGCCTTTATTTTGTC

TTTAAAAGGAGGTGAGGCGGTCAGGCTCAATCAAAAAAAAAA

AAGCCTTTCGGATGGCTTAGAGCTTCAGAAGC

ACCCACAAGATATAGAAGGCTTATATCCCATC

GTACCGCCACCACCCTCAGCAG

CCGATAGTAGTTTCGTCACCAGTAGACTCCTC

GCCGTCAAAATATCAAACCCTCAAAACTCAAA

TGAGTAATAACTCCAACAGGTCAGTTTTAATTAAAAAAAAAA

GTATCGGCCTCTGGGCGCCAGG

GTGGTTTTTCTTTTCACCAGTGAGACGGAGGCGGT

CAGACCAGCCAGCGATTATACCAACTCCAAAA

GCGTCCAACACTATCATAACCCTCCGAACTGA

CCCCCTGCCTTGATATTCACAAACGAATTAGA

GAAAGCGTAAGAATACGTG

TATGCAACTAAAGCTAAATCGGTTAGGTCATT

CCAGACGAGTTTAGTATCATATGCGTGAGTGAAAAAAAAAAA

ATATGTACTTTAACCAATAGGAACCGCCAGGG

TTCATCAAATTTTTGAATGGCTATTCTGACCT

ACACAACACGATTAAGTTGGGTAAGCCATCAA

GAAAAGTAAGCGTTTGCCATCT

TTTCGCAAGGCATCAATTCTACTAAAAAGCCCAAAAAAAAAA

ATTCCATATTAGCAAAATTAAGCAAGAATCGA

TTAGAACCTAATTGCTCCTTTTGAAAGAGGAA

GCCAGCAAACCACGGAATAAGTTTACAGAGAG

GTTATATAATACTTCTGAATAATGGATGGCAA

GCTATTACGGTGCCTAATGAGTGAGTGGTTCC

ACCGTACTAAATCACCGGAACCAGTAGCCCCCAAAAAAAAAA

GATTCAAAAGGGGACGACGACA

CAGTGAATTTCCATTAAACGGGTAACAACCAT

CGAGAAAATCTTTCCTTATCATTCTTATTTTC

TCGCGCAGACATAAATCAATATATGTTATACA

CGTTGAAAGTTAGTAAATGAATTTTCAGTGCC

AGCAGGCGAAAATCCTGTTTGATGGCTAACTC

CATACATACCGGAAACGTCACCAAAGCCGCCG

CCAGCATTAGTATTAAGAGGCTGACAAACTAC

AGTTAGCGTAATTGTATCGGTTTACACTCATC

AAACAAAATTATATTTAACAAC

CGATTGGCCTATTTCGGAACCTATGCCCTCAT

GACGGAAAACAAAAGGGCGACATTTTTATCCCAAAAAAAAAA

GACTTGCGAACTGAACACCCTGAAAGAAAATA

ATAGCCCGAGATAGGGTTGAGTGTACAATTCC

TTGTTTGGATTACTATATGTAA

TTAATTTTCATCGGGAGAAACAATCGACAACTAAAAAAAAAA

TTGTGAATTACAAAGCGAACCA

GCCAACATGTATACAAAATAAA

CGTTTTCAGAGGAAACGCAATAATAATAATAA

GCAGACGGTGTCGAAATCCGCGACAAAGGAAC

TCTACGTTTTGCATCAAAAAGATTTAAGAGGT

AGTACCTTCTCATATATTTTAAATACAGTCAA

CACTCATCGAGGCCCTTTTTAA

TTTTCCCAAAATTGTTATCCGCTCTGTTCCAG

TCTTTAGGTGGCAAATCAACAGTTATTAGTAA

AAAGCGGAAATAAAACGAACTAACTGCTCATT

AATACCGAGAACAAGAAAAATAATCCGGTATT

AGTGAGAATAGCTGCTCCATGT

GAACCTCATAGATAATACATTTGATTACAAAAAAAAAAAAAA

CTGAATTTATAAGTTTTAACGGGGTCTGTATGAAAAAAAAAA

AACATGAAGACAGGAGGTTGAGGCATTACCAT

GAATATAAGACCCTGTAATACTTTTAGCTATT

CATTGAATCCAAAAGGAATTACGAACGGTGTA

CAGAACGATTTGAGGACTAAAGACGGTCGCTG

GTTTGAGGGTGAGAAAGGCCGGAGGCAATGCCAAAAAAAAAA

TTTTGATGATAAGTTTCAGCGG

ACAATCAAGACTTGAGCCATTTGGAAATAAATA

TGGTCAGTAGCACTAACAACTAATTCAATTAC

ATAAATTGTCAATCATAAGGGAACGTTTACCA

AAACAGAAATTTATCAAAATCATATTAGTTAA

AGGGGGTATAAAAACCAAAATAGCAACGAGGCAAAAAAAAAA

GAAACAGTAGGCGAATTATTCATTAGATTAGAAAAAAAAAA

GTTAAAATGGAAGATTGTATAAGCCGCGAGCTAAAAAAAAAA

AAATAATTAATCGTAAAACTAGCACAGGCAAG

AGGTCTTTAGGTAGAAAGATTCATGATATTCA

ATAACCTTTGCTTTGAATACCAAGGGATTTAGAAAAAAAAAA

GACTCCAACGTCAAAGGGCGAAAAGGTACCGA

GCTCGAATAGCTTGCATGCCTGCAAATATTTT

CTGAGCAATCATTTGAATTACCTTGCTCAACA

ATAAAACATTTGAGTAACATTATCGATTTTCAAAAAAAAAAA

TTGCGTATAGGAAGATCGCACTCCATCTGCCA

GGAGAATTGGAGGTTTTGAAGCCTGTTCAGCT

TGTTGGGATGCGTTGCGCTCACTGTTTGCCCC

CTGATAAAGTAATGGGATAGGTCAAAACCAGG

TCATGGAAATACCTACATTTTGACTATTAACA

CAAAGTACGAAAGAGGACAGATGAGGCATAGT

ATACTTCTTTGGAAAGGAATTG

GGTATTAAAATCCAATCGCAAGACTAGGTTGG

TTGTAAACGTTGGTCGACTCTA

AATTCTTACGACAAAAGGTAAAGTCTACAATT

TTTCATAATCACAGGAGGTTTA

GCAAAGAATAACAGTTGATTCCCATAAATATT

CGCCCACGAGCCCAATAGGAACCCGTTTTGCTAAAAAAAAAA

CTATCGGCCTTGCTGGTAATATCCACCTTGCTAAAAAAAAAA

CTAATTTATCTGACCTAAATTTAAGAAGAGTC

GAACAAAGTACCGAACGAACCACCGCAGATTCAAAAAAAAAA

TAAAGTACCCAGTATAAAGCCAACTTTTAATG

AGAGGCATTAATTGAGAATCGCCAATTACATT

GTTGCAGCAAGCGGTCCACGCTGGCCCGCTTT

GTAGGGCTTTTCGAGCCAGTAATAACGAGCGT

GACGACGAATAGTAAAATGTTTAGTAGATACAAAAAAAAAAA

ATTTAGGAGAGAATGACCATAAATGTTTTAAA

AAAAGCCTCGACAATAAACAACATTAAATCAA

TCTGGCCAACAGAGATAGAACCCTTAGTCTTT

AACGAGTACATCCAATAAATCATATGTCAATC

CAAGAGTAAAAGAATACACTAAAATCAGCTTG

CCAGTCGGCATTCGCCATTCAGGCAAACGGCG

TAAGTCCTCCGTGTGATAAATAAGAAACATAGAAAAAAAAAA

GAGGGTAAGCGAGGCGTTTTAGCGACAATAGA

TCGATAGCGTATGTTAGCAAACGTCAAAGTCA

AAGAGGCAATCTTGACAAGAACCGCAGTTGAG

GGATAGCACATAACCGATATATTCTTTTTCAT

GGAGCCTTTAACGATCTAAAGTTTAGTTAATG

AGACTACCCCATATCAAAATTATTCGGAATTAAAAAAAAAAA

TCAAAAATAATCTTACCAACGCTAAGAGAATA

ACCCGTCGATCTACAAAGGCTATCGTACCAAA

CAGTGCCATCGTAATCATGGTCATAGAACGTG

TTGATATAGCCTCCCTCAGAGCCGCTGTAGCG

TCAGAGCATAAAGTACGGTGTCTGAAACAGTT

AACGCCTGGTGAATTTCTTAAACATAAAACGA

AACATTATTGCTGTAGCTCAACATCAAAAATC

CGTATTAAAACAGTGCCACGCTGAAAAAACGCAAAAAAAAAA

GCTCATTTCCCGGTTGATAATCAGATAGTAGT

GCAAAGACAATCACCAGTAGCACCAGGTCAGA

GACCGGAAGCAGTGTAGGTAAA

CCTGTGTGGTCACGACGTTGTAAATTAAATCA

(D) Bar DNA origami design

AAACGCAAAACGGGTAAAATACGTACCCTGACAAAAAAAAAA

ACCGTGCAAAAGGTGGCATCAATTTTTCTGTAAAAAAAAAA

TAAGAGAATAATAAAAGGGACATTCTGGCCAAAAAAAAAAA

TTAAATCCTTTGACGAGCACGTATAACGTGCAAAAAAAAAA

AACCAGAGACTCTAGAGGATCCCCGGGTACAAAAAAAAAA

ATCTAAAGAGTTAATTTCATCTTCAGCGACAG

CCCACGCACTTGAGCCATTTGGGAGTTTAGT

ATCATAACCTTCACCGCCTGGCCCTGAGAG

AGGAATTGCATCGGCATTTTCGGTCAATCGCAAAAAAAAAA

AGAGATAAATGAACGGTGTACAGACGCCAA

AGGCGAATTAGAACCTACCATATCAAAATTAAAAAAAAAAA

GCGCTAGGGCGCTGGCAAGTGTAGAAAAAAAAAA

ATAGCAAGGATATTCACAAACAATACATAAA

GATCGTCAGGGAGGGAAGGTAACTTAATTG

GAAACCAAAAGAACTCAAACTATCGGCCTTG

AAATATCGAATTCGTAATCATGGTCATAGCTGAAAAAAAAAA

CTGTCCATATCGAGAACAAGCAAGAAATAGCA

GGATTAGAGGCCAGTGCCAAGCTTGCATGCC

ATAGCAAGGCCAGAATCCTGAGAAGTGTTTT

AAAATTAATGATGGCAATTCATCAATATAATAAAAAAAAAA

AGAATCGCCGTGGCACAGACAATATTTTTGA

ATTACCTTGCGGAATTATCATCATATTCCTG

CGAGCTGATCTGCCAGTTTGAGGGGACGACGAAAAAAAAAAA

CCTGTAGAAACATTATGACCCTGTGTACCGT

CTAATAGACATAGGTCTGAGAGACACCGGAAAAAAAAAAAA

TTTTTCTTATAGCGAGAGGCTTTTCCATGT

ATAGCTATCGGAACGAGGCGCAGAGACGATAA

TCAATATAATTTTGCGGAACAAAGAAACCAC

AAGTCAGGGCTGACCTTCATCAGGAATACCAAAAAAAAAAA

ATTGTGTCAGATAGCCGAACAAAGTTTCCTT

TGAATTTAAGAACCGCCACCCTCAATATTTTA

TAATATTTGCCTGAGTAATGTGTAGTACCGAAAAAAAAAA

AAACCAAATTCACCAGTGAGACGGGCAACAG

AACCAGGCCTGCGAACGAGTAGACACGTTGAAAAAAAAAA

TTATTACGTACACTAAAACACTCACCCTCAAA

AGTGCCCGACCAGGCGGATAAGTAACCGTTAAAAAAAAAA

AAAAAGATGTGAAATTGTTATCCGCTCACAAAAAAAAAAAA

CAGAAGGATTTTAATGGAAACAGATAAATCC

ACATTCAAGAAAATCCTGTTTGATGGTGGTTAAAAAAAAAA

CCGGTATTCGATTAAAGGGATTTTAGACAGG

ATTTTAAGTCCAACGTCAAAGGGCGAAAAACCGTCTATCAAAAAAAAAAA

TACTTCTAAGAACGGGTATTAAATTAAGAA

GGCTTTTGCGTACTCAGGAGGTTTAGGTAAAGAAAAAAAAAA

CCACCCTCCCGTTCCAGTAAGCGTAAGAAAACAAAAAAAAAA

CGGAACGACAAAGACAAAAGGGCCAACATGTAAAAAAAAAA

TTTCCTGTTAAGAGGAAGCCCGAACAGAGGCTAAAAAAAAAA

ACATGTTTCGCTATTACGCCAGCTGGCGAAAG

ATTTGAGGCTGAGAAGAGTCAATACTCAGAACAAAAAAAAAA

AAAATCACTGCTAAACAACTTTCTGGGGCGAAAAAAAAAA

TTCCACACTCAGAAGCAAAGCGGGAGGAAGTAAAAAAAAAA

CCCCAGCGAGAACTGGCATGATTCAAGAAAA

TGCGCAACGTTTCATTCCATATAAAAAGGAGC

CGGTCACGCGTCTTTCCAGAGCCTATTTATCAAAAAAAAAA

TATTAAGAGGCCTATCAGGTCAAAAAAAAAAA

TTTGCACGTACCAAGTTACAAAATGAGTAACAAAAAAAAAA

GGAACAAACAAAGAATTAGCAAAGCCCTCA

AATGCAATTGTTAAAATTCGCATTAAATTTT

CTGATTGCCCCTCGTTTACCAGACCGGTCAAT

TACAACGGCGAGGAAACGCAATAAAGCATGTA

CCTTATTTGAGAATAGAAAGGATGGTCAATAAAAAAAAAA

CTAGCTGAATGTCAATCATATGTACCCCGGTTAAAAAAAAAA

AGAGAATAACAAAGCTGCTCATTCTAATAAAAAAAAAAAAA

TACAAAGGTGAGACTCCTCAAGAGAACCTATTATTCTGCTTTTACAAAAAAAAA

AA

CATAAATCCCTGGGGTGCCTAATGAGTGAGCAAAAAAAAAA

CAGGAGGCCTAAGAACGCGAGGCGCCTGAACAAAAAAAAAAA

AACGCCAGGTCATTTTTGCGGATAACCATCG

GGAAATTAGGGAGTTAAAGGCCGCACAGGTCA

ACATTATCTGTGAGTGAATAACCTCAGACGA

TGTACCAACCAGCTTTCATCAACATTAAATGT

CAGCAAAGCCGACAATGACAACGGCTTAGA

CGCGCTTATTTTATCCTGAATCTTTTGTTTAAAAAAAAAAA

AACGGTACCAAATCAGATATAGAAATATCAG

ACAATTCTGAAAACATAGCGATACAGAGCC

ATACATACGCACCAACCTAAAACGAGAATGACAAAAAAAAAA

GAGGACAGCCCACAAGAATTGAGCGCGCCCA

TGTCACATAAAGACTTTTTCATATTGCATCAAAAAAAAAA

ACAGAGATCAGAGGCATTTTCGATATGGTTTAAAAAAAAAA

TATGGTTGAAGATTAGTTGCTATTCTTTACAGAAAAAAAAAA

CAGCGGAGAGCGTTTGCCATCTTTTATATAACAAAAAAAAAA

CTTGACAAAGAATTAACTGAACACTTTTAGCAAAAAAAAAA

GATAATCACATCAATATGATATTCGCCGTCGAAAAAAAAAAA

AAATAAACAGCCATATTAATTTGCCAGTTACAAAAAAAAAAA

GGAAGGGTTATTCATTTCAATTACCTGGTAATAAAAAAAAAA

TTAACCTCAATATCTTTAGGAGCACTAACAAAAAAAAAAAA

GGCCTCTTTAAATATGCAACTAAACTTGCTTT

GATTATTTGTCCAGACGACGACAATAAAAGAAAAAAAAAA

AATTTAGGAGAACCCTTCTGACCTGAAAGCGAAAAAAAAAA

GCCCTAACGTTATACAAATTCTTTATCACC

AAGACAAACTCAATCAATATCTGGTCAGTTGGAAAAAAAAAA

CATTGACGTTTCGTCACCAGTAAAATCGGT

AACGCCTGAACCACCACCAGAGCCTTCCCTT

AAACTAGCTAAATTAATGCCGGAGCGGGGTTTAAAAAAAAAA

TCAAACCGAACGCGAGAAAACTTACTGTAGAAAAAAAAAA

CGCACTCCACGCAAATTAACCGTTGTAGCAA

AGTAGTATTGGTGTAGATGGGCGCATCGTAAAAAAAAAAA

CGAACTAACCGAGATAGGGTTGAGTGTTGTTAAAAAAAAAA

AAGGAATTCAAGCGGTCCACGCTGGTTTGCCC

CGCGTTTTCGAATAATAATTTTTTTTTAGTTTAAAAAAAAAA

CCGAACGTTCGCTATTAATTAATTGCCGCCAG

CTGGTAATCCATCCTAATTTACGTAACGGAA

ATTCAAAAGCAAATATTTAAATTGTAAACGTAAAAAAAAAA

TACTTAGCCTTACCGAAGCCCTTTCCAAGTAC

TTTAGACTAATGAATCGGCCAACGCGCGGGGA

CGAGCTCGCGTTTTAATTCGAGCTGACAGCATAAAAAAAAAA

TCCCAATTAAAGCGCCATTCGCCATTCAGGC

GAACCTCCGTTAGAATCAGAGCGGGAGCTAAAAAAAAAAAAA

ACGACCAGTATAAAGTACCGACAAGTTTATTTAAAAAAAAAA

CTATTTCGGAAGGATTAGGATTAGAGGGTAGCAAAAAAAAAA

AAAGCCATAGTCTTTAATGCGCGAACTGATA

ACGTCAAACCCTGACGAGAAACACCAGTCAGGAAAAAAAAAA

TTGAGGACATCAATAGAAAATTCAGCCAGTAAAAAAAAAAAA

CCGAAATCATCAGTTGAGATTTAAGAGTAATAAAAAAAAAA

CCAGTTTGGAAGAAAAATCTACGTAGTGAATAAAAAAAAAAA

ACGTTGGGAACAAGAGTCCACTATTAAAGAAAAAAAAAAA

ATTTTCATGTGAGGCCACCGAGTAAAAGAGT

AGGTCACGGCATTAACATCCAATATTGTCGTCAAAAAAAAAA

ATAAAGCCAACAACCCGTCGGATTCTCCGTG

AAGTTTTATATAAGTATAGCCCGAGACAGTAAAAAAAAAA

TCTGGAATGTTGGGAAGGGCGATCGGTGCG

GAGGGTTGAACGGGGTCAGTGCCTTCGCGCAGAAAAAAAAAA

TATTTTTAGAATCGATGAACGGTAATCGTAAAAAAAAAAA

GGGGATGGCTGAATATAATGCTGTGATACCG

GTCACCGATAACCGATATATTCGGCTCCTTTT

AACCTGTTGCCTCAGGAAGATCGCACTCCAGAAAAAAAAAA

TAGTTAGCTCAGAGCCACCACCCTGCTTAGAT

TGTTAAATTTTTTAGAACCCTCATGAACCGCC

ATCAAAATTTAGAGCCGTCAATAGATAATACAAAAAAAAAA

TGTATCACATGATACAGGAGTGTACTGAGCAAAAAAAAAAA

TAACTCACAACAGTTCAGAAAACGAAAGAGGCAAAAAAAAAA

TCGGGAGATCAGGTTTAACGTCAGATGAATATACAAAAAAAAAA

ATCATATGAACATCGCCATTAAAAATACCGAA

AAGTAAGCGAAATCCGCGACCTGCTGCAAAAG

AAAGATTCGGCAAAATCCCTTATAAATCAAAAAAAAAAAAA

GCTTAATTTGCTGCAAGGCGATTAAGTTGGGT

AGGCGGTCCGTTAAATAAGAATATTACCATT

TTTGCGGGCAAAAATAATTCGCGTCTGGCCTT

AATAATAAGAACCGAACTGACCAAGCAACACT

CAGTATCGTAGCTATATTTTCATTAACAGTTTAAAAAAAAAA

GGCTTGCATTCATTAAAGGTGAATACCAGTAT

CTAACGAGCTGCGCGTAACCACCACACCCGCAAAAAAAAAA

TGCCACGCGTTTGAAATACCGACTGAAACCA

CATAAGGGAGCAAGAAACAATGCCGTTTTT

CGAGGTGACGGAAACGTCACCAACGTGTGAT

AGAATCCTGACAACTCGTATTAAATCCTTTGC

TTGCCTGAGAGTCTGGAGCAAACAAGGAGAGATCAAAAAAAAAA

CCATTGCATAGATAAGTCCTGAAAAGACTCC

GTAGTAAAAAATAAGAAACGATTTTACCAACGAAAAAAAAAA

GTAGATTTAACAATAACGGATTCCCCCCTGCAAAAAAAAAA

TGGGATTTCGGAACCAGAGCCACCTACCTTTAAAAAAAAAA

CGAACCACTTACTAGAAAAAGCCTATTAGAGC

TATAATCACGTAGGAATCATTACTTAAGCCC

AATCATAACAGCAGAAGATAAAACAGAGGTG

CTTTAATAGCACCGTAATCAGTTGACCTAA

CGCCACCCGTAACGATCTAAAGTTAATCATACAAAAAAAAAA

CTACGAAGATAAAGGTGGCAACATATAAACAAAAAAAAAAAA

AAGTTTTGTTGCGTATTGGGCGCCAGGGTGG

TAAGAATACATATTTAACAACGCGACATTCAAAAAAAAAAAA

ATAGTTGCATCACCAGTAGCACCAAACACCGG

GTAAATCGTATTAATTTTAAAAGTTTGAGTA

AAAAGAACAGTATGTTAGCAAAGCCTGTTTAAAAAAAAAA

TATATGTACAGTTGAAAGGAATTGAGGAAGGAAAAAAAAAA

AAAATCTCTTGCCTTTAGCGTCAGTTTCAAATAAAAAAAAAA

AGCAAGGCATTTCTTAAACAGCTTAGCTCA

ACCGATTGACCCTCAGCAGCGAAATCAAAGCGAAAAAAAAAA

GCTTTGAATAAAACAGAAATAAAGAAATTGCAAAAAAAAAA

GAGGCGGTCCAGAGGGGGTAATACCTGATAA

CATGTTCTTTGACGCTCAATCGTCTGAAATGAAAAAAAAAA

TTATCTAACGGCTTAGGTTGGGTTCATAATCAAAAAAAAAA

AGAATAGCCGGAACAACATTATTACCCAAAAAAAAAAAAA

ATCATTGTGAATTACCTTTAATTTCAACTTTAAAAAAAAAA

TACCCAAAATTATACCAAGCGCGTGCGGAA

CCAGCTTTGATACATTTCGCAAAACAACTAAAAAAAAAAAA

CTGAGTAGTCAATAATCGGCTGTCTTACCAGA

ATTTAATGTGAGAGCCAGCAGCAAATGAAAA

TTTCCTCCGACTTGCGGGAGGTTAGCGCATAAAAAAAAAA

TAAGACGATTTAGAAGTATTAGACTTTACAA

ATAAAAACAGCTCATTTTTTAACCAATAGG

TCAACGTAACATAAAAACAGGGATTGAAGCCAAAAAAAAAA

TAGACGGGGAACCGGATATTCATTACAGGTAGAAAAAAAAAA

CCGCCTCCACGTTAGTAAATGAATCTACTAATAAAAAAAAAA

AATCAAGTCAAAAAAAAGGCTCCACAGTTGAT

AAATAAGGAGTATTAACACCGCCTGCAACAG

ATCATTCCTTGATTAGTAATAACATCACTTGC

TCATTAAAGAGCCACCACCCTCATACGCAAGG

AGGAAACAGATTTGTATCATCGGTAAAATG

GTGTAAAGAAAAATCAGGTCTTTAATGCCAAAAAAAAAAA

TTGTATAAGGGTGAGAAAGGCCGGGAATAGGAAAAAAAAAA

TGCTCAGTTATAAACAGTTAATGGCCTGATTAAAAAAAAAA

CCGCTTTCAATATTCATTGAATCCTCTTTGAC

TTCCATTAAGACACCACGGAATAAAAGGTAAAAAAAAAAAA

GAGCGAGTTCAGAGCATAAAGCTCAAACTAC

ACCTACATAGCTAATGCAGAACGCCGTAGAAAAAAAAAAAAA

AGTTGCAGACGAGGCATAGTAAGACTTTGAAA

ATCAACAAACAGGAAAAACGCTCATGGAAATAAAAAAAAAA

CATAGGCTAGGGTAATTGAGCGCTAGGCTTAT

AGTAACAGTACAAACATGAAAGAAAAAAAAAA

ATAATATCATCCAGAACAATATTACCGCCAG

GCCACCAGTAGCATTCCACAGACAATTAAGCA

GACCATTACCGGCACCGCTTCTGGTGCCGGAAAAAAAAAA

ATATTTTCATCACCTTGCTGAACCTCAAATAAAAAAAAAAA

ATTATCAGATTACATTTAACAATTGCAGTCTC

CTGCATTGGATAGCGTCCAATACAAACAAAG

TTGGCCTTCCCAATAGGAACCCATAATACT

AGGCAAGGCGGCGGATTGACCGTAATGGGATAAAAAAAAAAA

ACGTGGACAACTGGCTCATTATACCAGAACGAAAAAAAAAAA

AAAACGACGAGTACCTTTAATTGTCGCTGA

AACGCCATAGAAGCCTTTATTTCATTTCAGGG

AAAGAAGAGTTTGGATTATACTTCTGAATAATAAAAAAAAAA

TCGATAGCTGTATCGGTTTATCAGGTACGGTG

TGCAGGTCCCGGAAGCAAACTCCATTTTGCGG

GATAAGAGGGTTTTCCCAGTCACGACGTTGT

CAAATCAAAATGCTGATGCAAATCCATAGCCCAAAAAAAAAA

CCAATCCTTGGGCTTGAGATGGTTATGCGAAAAAAAAAA

TCGTCATACAGTCGGGAAACCTGTCGTGCCAG

CAAATCACGAAAAGCCCCAAAAACAGGAAGAAAAAAAAAAA

TATTATAGAACATACGAGCCGGAAGCATAAAAAAAAAAAAA

ACCCTCAGCCAGAATGGAAAGCTCATTTGA

ATGGCTATACGCTCAACAGTAGGGATATTGAC

AGCTACAAATGCGCCGCTACAGGGCGCGTACAAAAAAAAAA

AGTAATTCTACATTGGCAGATTCACCAGTCACAAAAAAAAAA

TGCTTTAATTAATTGCGTTGCGCTCACTGC

CAGCAGGCCTAATGCAGATACATAACCAGGCG

TTTCCAGCTCAGAGCCGCCACCGTGAATTTAAAAAAAAAA

ACCAGCGCGGGTAGCAACGGCTAAGACTTCAAAAAAAAAA

CCTGATTTGATGAAACAAACATCCATACATAAAAAAAAAA

AGGCTTGAATGAAAATAGCAGCTTGCACCCAAAAAAAAAA

AACACTGAAGGAGGTTGAGGCAGGTTGCTTCTAAAAAAAAAA